Die approbierte Originalversion dieser Dissertation ist an der Hauptbibliothek der Technischen Universität Wien aufgestellt (http://www.ub.tuwien.ac.at).

The approved original version of this thesis is available at the main library of the Vienna University of Technology (http://www.ub.tuwien.ac.at/englweb/).

TECHNISCHE UNIVERSITÄT WIEN
Vienna University of Technology

DISSERTATION

Analog Filters in Nanometer CMOS

ausgeführt zum Zwecke der Erlangung des akademischen Grades
eines Doktors der technischen Wissenschaften unter der Leitung von

Univ. Prof. Dr.-Ing. Horst Zimmermann
am Institute of Electrodynamics, Microwave and Circuit Engineering

eingereicht an der Technischen Universität Wien
Fakultät für Elektrotechnik und Informationstechnik

von

DI Heimo Uhrmann
Matrikelnummer: 9825910
Landstraße 3
2003 Leitzersdorf

Wien, im Oktober 2011

Abstract

Analog filters are an essential function block in analog circuit design. They are embedded in analog-to-digital converters to eliminate the effect of aliasing and in digital-to-analog converters to remove higher frequency components. This work presents analog filters for radio frequency frontends, another task for filters. Two applications of radio frequency front-ends are targeted, one for a transmit path in a software defined radio and another for a receiving chain of a direct conversion DVB-H receiver. The filters are designed in 65 nm CMOS technology to operate in a system on chip, where many digital function blocks are implemented as well. Design limits of new technologies are considered and solved.

The first filter structure is an element of the transmit path in a software defined radio system. The transmit path uses a current-steering DAC and a current-mode mixer. A voltage-mode filter would need a current-to-voltage and a voltage-to-current transformation. In order to save power dissipation and chip area, current-mode filters are investigated. Three different current-mode 3rd-order Butterworth low-pass filters are presented with a switchable -3 dB cut-off frequency. The overall filters are based on cross-coupled current mirror integrators and first-order low-pass filters. The first differential filter is implemented by using one fully differential current-mode integrator and two first-order low-pass filters. Experimental results show -3 dB cut-off frequencies of 1.12 MHz and 4.46 MHz at a power consumption of 12.36 mW at 1.2 V supply voltage. The filter gain is -0.93 dB and the 3rd-order input intercept point is 1.8 mA_p. The filter has a dynamic range of 77.2 dB and a figure of merit of 2115 at the -3 dB cut-off frequency of 1.12 MHz. The second filter is a fully differential current-mode filter realized with current-mode integrators only. The -3 dB cut-off frequencies are 1 MHz and 4 MHz and the gain is 0.9 dB. The filter consumes 12 mW at a supply voltage of 1.2 V. At 1 MHz the dynamic range results in 77.3 dB and the figure of merit is 2258.9. The third current-mode filter is a low-voltage design which uses the strategy of capacitance multiplication. The filter -3 dB cut-off frequencies are 1 MHz and 4 MHz and the filter gain is 4 dB. The power consumption is 9.6 mW at only 1 V supply voltage. At the frequency setting of 1 MHz the 3rd-order input intercept point is 1.7 mA_p, the dynamic range is 73.8 dB, and the figure of merit is 3873. Capacitor saving techniques lead to an enlargement of the effective capacitance up to 30% at constant area needed for the capacitors. All filters are successfully implemented and experimentally verified. In a comparison to the state-of-the-art of current-mode filters good values for the figure of

merit and dynamic range are achieved, despite of the new technology.

The second filter implementation is used in a receiving path of a direct conversion DVB-H receiver. The direct conversion receiver contains a passive mixer, whose output signal is amplified and filtered with a 1st-order Butterworth operational amplifier RC low-pass filter. Therefore three different multi-stage feed-forward operational amplifiers with a large gain-bandwidth product for operational amplifier RC low-pass filters are introduced. The first operational amplifier is a four-stage feed-forward design and has a gain of 58 dB, a gain-bandwidth product of 1 GHz, and the phase margin is 62° at a load of 2 × 5 pF in parallel to 10 kΩ. The power consumption is 11.4 mW at 1.2 V supply voltage and the figure of merit is 1052 $\frac{MHz \cdot pF}{mA}$. The first-order low-pass filter using this operational amplifier is implemented with a tunable -3 dB cut-off frequency range from 3.5 MHz to 4.5 MHz. The filter has a DC gain of 38 dB, a dynamic range of 57.2 dB and a figure of merit of 143945. The second operational amplifier is a four-stage multiple feed-forward operational amplifier with a DC gain of 68 dB and a gain-bandwidth product of 1 GHz. The phase margin is 60° and the power consumption is 11.5 mW at a load of 2 × 4 pF in parallel to 10 kΩ. The figure of merit is 833 $\frac{MHz \cdot pF}{mA}$. The first-order low-pass filter made with this operational amplifier has a DC gain of 40 dB and a -3 dB cut-off frequency of 4 MHz. The dynamic range is 62.7 dB and the figure of merit is 54744. The third operational amplifier is a three-stage feed-forward design. A peculiarity of this operational amplifier is the supply voltage of 2.5 V in a 65 nm CMOS technology. A higher supply voltage is needed for a higher output signal swing and lower distortion and intermodulation products. Cascoding prevents the transistors from over-voltage breakdown. The power consumption is 14.6 mW and the DC gain is 89 dB. The gain-bandwidth product is 1.1 GHz. Driving a load of 2 × 1 pF the operational amplifier has a phase margin of 53.3° and a figure of merit of 367 $\frac{MHz \cdot pF}{mA}$. The high-voltage operational amplifier in 1st-order low-pass configuration is inserted in a mixer filter combination. The mixer filter combination has an overall gain of 24 dB and a base-band bandwidth of 4 MHz. The mixer and the filter are supplied with 2.5 V and have a current consumption of 12.7 mA. A 3rd-order input intercept point of +10 dBm and a noise figure of 16.1 dB is achieved. The operational amplifiers were successfully implemented in 65 nm CMOS. Due to the limited supply voltage multi-stage designs were investigated. The comparison to the state-of-the-art of operational amplifiers shows good results despite the limiting CMOS technology. High gain-bandwidth products could be achieved. The realized 1st-order Butterworth operational amplifier RC low-pass filters have only moderate performance, using a standard figure of merit, due to the desired filter-order and distortion specifications. The high-voltage passive mixer filter combination, where the high-voltage operational amplifier is used, shows a good linearity, represented by the very good 3rd-order input intercept point.

Kurzfassung

Analoge Filter sind wichtige Funktionsbausteine in der analogen Schaltungstechnik. Sie sind Bestandteil von Analog-Digital Konvertern, um Aliasing Effekte zu verringern, und von Digital-Analog Konvertern, um höhere Spektralanteile im Frequenzband zu dämpfen. Diese Arbeit präsentiert analoge Filter für Sende- und Empfangsteile zur drahtlosen Informationsübertragung, eine andere wichtige Anwendung von Filtern. Es werden zwei Anwendungsfälle von Funk Front-Ends behandelt. Die erste Filterapplikation ist in einem Sendepfad eines Software Defined Radio Systems integriert, die andere ist Bestandteil eines Empfangspfads eines DVB-H Empfängers. Die Filter sind in 65 nm CMOS implementiert, um sie in einer System on Chip Lösung einzusetzen, in der viele digitale Funktionsblöcke ebenfalls enthalten sind.

Die erste Filterstruktur ist ein Element in einem Sendepfad in einem Software Defined Radio System. Im Empfangspfad wird ein current-steering DAC und ein current-mode Mischer verwendet. Voltage-mode Filter würden eine Strom-Spannungskonversion und eine Spannungs-Stromkonversion benötigen. Um Verlustleistung und Chipfläche zu minimieren werden current-mode Filter untersucht. Drei verschiedene current-mode Butterworth Tiefpassfilter 3. Ordnung mit einer umschaltbaren -3 dB Grenzfrequenz werden präsentiert. Die Filter basieren auf kreuzgekoppelten Integratoren und Tiefpassfiltern 1. Ordnung aus Stromspiegeln. Der erste differentielle Filter besteht aus einem volldifferentiellen current-mode Integrator und zwei Tiefpassfilter 1. Ordnung. Messergebnisse zeigen -3 dB Grenzfrequenzen von 1.12 MHz und 4.46 MHz bei einem Leistungsverbrauch von 12.36 mW und einer Versorgungsspannung von 1.2 V. Die Filterverstärkung ist -0.93 dB und der Input Intercept Point der 3. Ordnung liegt bei 1.8 mA_p. Der Filter hat einen Dynamikbereich von 77.2 dB und einen Gütefaktor von 2115 bei der Grenzfrequenz von 1.12 MHz. Der zweite Filter ist ein volldifferenzieller current-mode Filter, der nur mittels current-mode Integratoren realisiert ist. Die -3 dB Grenzfrequenzen sind 1 MHz und 4 MHz und die Filterverstärkung beträgt 0.9 dB. Der Leistungsverbrauch beträgt 12 mW bei einer Versorgungsspannung von 1.2 V. Bei der Grenzfrequenz von 1 MHz zeigt der Filter einen Dynamikbereich von 77.3 dB und einen Gütefaktor von 2258.9. Der dritte current-mode Filter ist ein Design mit niedriger Versorgungsspannung, der zusätzlich eine Strategie zur Kapazitätsmultiplikation beinhaltet. Die -3 dB Grenzfrequenzen sind wiederum 1 MHz und 4 MHz und die Filterverstärkung beträgt 4 dB. Der Leistungsverbrauch ist 9.6 mW bei einer Versorgungsspannung von 1 V. Der Filter hat bei der Bandbreite von 1 MHz einen Input Intercept Point der 3. Ordnung von

1.7 mA_p, einen Dynamikbereich von 73.8 dB und einen Gütefaktor von 3873. Strategien zum Einsparen von Kapazitäten erreichen eine Vergrößerung der effektiven Kapazität bis zu 30% bei konstanter Chipfläche. Alle Filter wurden erfolgreich implementiert und experimentell getestet. In einem Vergleich zu dem State-of-the-Art von current-mode Filtern werden, trotz des Einsatzes von Nanometer CMOS Technologien, gute Werte für Gütefaktoren und Dynamikbereich erzielt.

Die zweite Filtertopologie ist Bestandteil eines direct conversion DVB-H Empfängers. Der Empfänger besteht aus einem passiven Mischer, dessen Ausgangssignal mittels Operationsverstärker RC Butterworth Tiefpassfilter 1. Ordnung verstärkt und gefiltert wird. Dafür werden drei verschiedene mehrstufige vorwärtsgekoppelte Operationsverstärker mit hohem Verstärkungsbandbreiteprodukt für den Einsatz in Operationsverstärker RC Butterworth Tiefpassfiltern 1. Ordnung vorgestellt. Der erste Operationsverstärker besteht aus vier Stufen inklusive Vorwärtskopplung und hat eine Verstärkung von 58 dB, ein Verstärkungsbandbreiteprodukt von 1 GHz und eine Phasenreserve von 62° bei einer Last von 2×5 pF parallel zu 10 kΩ. Der Leistungsverbrauch ist 11.4 mW bei einer Versorgungsspannung von 1.2 V und der Gütefaktor ist 1052 $\frac{MHz \cdot pF}{mA}$. Der mit diesem Operationsverstärker implementierte Tiefpassfilter 1. Ordnung ist mit einer abstimmbaren -3 dB Grenzfrequenz realisiert. Der Frequenzbereich reicht von 3.5 MHz bis 4.5 MHz. Der Filter hat eine Verstärkung von 38 dB, einen Dynamikbereich von 57.2 dB und einen Gütefaktor von 143945. Der zweite Operationsverstärker besitzt vier Stufen und eine mehrfache Vorwärtskopplung. Dadurch wird eine Verstärkung von 68 dB und ein Verstärkungsbandbreiteprodukt von 1 GHz erreicht. Die Phasenreserve beträgt 60° und der Leistungsverbrauch 11.5 mW bei einer Last von 2×4 pF parallel zu 10 kΩ. Der Gütefaktor beträgt 833 $\frac{MHz \cdot pF}{mA}$. Der Tiefpassfilter 1. Ordnung mit diesem Operationsverstärker hat eine Verstärkung von 40 dB und eine -3 dB Grenzfrequenz von 4 MHz. Der Dynamikbereich ist 62.7 dB und der Gütefaktor beträgt 54744. Der dritte Operationsverstärker besteht aus drei Stufen und einer Vorwärtskopplung. Die Besonderheit an diesem Operationsverstärker ist die Versorgungsspannung von 2.5 V in 65 nm CMOS Technologie. Eine erhöhte Versorgungsspannung ist notwendig um einen größeren Ausgangssignalhub und weniger Verzerrungen und Intermodulationen zu erhalten. Kaskoden verhindern die Zerstörung der einzelnen Transistoren durch Überspannung. Der Leistungsverbrauch ist 14.6 mW und die Verstärkung ist 89 dB. Das Verstärkungsbandbreiteprodukt ist 1.1 GHz bei einer Last von 2×1 pF. Der Operationsverstärker hat eine Phasenreserve von 53.3° und einen Gütefaktor von 367 $\frac{MHz \cdot pF}{mA}$. Der Operationsverstärker ist als Tiefpass 1. Ordnung eingesetzt in einer Mischer-Filter Kombination. Diese hat als Ganzes eine Verstärkung von 24 dB und eine Bandbreite im Basisband von 4 MHz. Mischer und Filter sind mit 2.5 V versorgt und benötigen 12.7 mA Strom. Die Mischer-Filter Kombination erreicht einen Input Intercept Point der 3. Ordnung von +10 dBm und eine Rauschzahl von 16.1 dB. Die Operationsverstärker wurden erfolgreich in 65 nm CMOS implementiert. Aufgrund der niedrigen Versorgungsspannung, die den Einsatz von Kaskoden erschwert, wurden mehrstufige Schaltungen untersucht. Ein Vergleich zum State-of-the-Art zeigt gute Eigenschaften der Operationsverstärker, trotz der Einschränkungen durch die 65 nm CMOS Technologie. Die implementierten Butterworth Tiefpässe 1. Ordnung

haben nur mäßige Gütefaktoren aufgrund des spezifizierten Tiefpasses 1. Ordnung und der Verzerrungsanforderungen. Die passive Mischer-Filter Kombination für eine Versorgungsspannung von 2.5 V, in der der Hochvolt-Operationsverstärker eingesetzt wird, erreicht eine gute Linearität, die durch den hohen Input Intercept Point der 3. Ordnung repräsentiert wird.

Acknowledgement

I want to thank my colleagues from the Institute of Electrodynamics, Microwave and Circuit Engineering at Vienna University of Technology for valuable discussions and their support. Special thanks go to Franz Schlögl, Robert Kolm, and Kurt Schweiger for many hints and advice.

I thank Andreas Bertl, Thomas Hartig, and Lukas Dörrer from Infineon Technologies Austria AG for technical support and constructive advice and Andreas Mikula for his administrative support.

I am deeply grateful to Univ. Prof. Dr.-Ing. Horst Zimmermann for making this work possible, his advice and assistance. Special thanks go also to Univ. Prof. Dr. Martin Gröschl from the Institute of Applied Physics for the co-examination of the thesis.

This work was partially funded by Infineon Technologies Austria AG and by the Austrian Federal Ministry for Transport, Innovation, and Technology in the FIT-IT projects Soft-RoC and M2RX via FFG.

Finally I am deeply indebted to my parents and my wife Sonja for never-ending encouragement.

Contents

Abstract **I**

Kurzfassung **III**

Acknowledgement **VII**

Nomenclature **XII**

1 Introduction **1**

2 Butterworth Filters **3**
2.1 Filter Classification 3
2.1.1 Analog - and Digital Filters 3
2.1.2 Active - and Passive Filters 4
2.1.3 Lumped - and Distributed Filters 5
2.2 Analog Filter Types 5
2.2.1 Low-Pass Filter 6
2.2.2 High-Pass Filter 6
2.2.3 Band-Pass Filter 7
2.2.4 Band-Stop Filter 7
2.2.5 All-Pass Filter 8
2.2.6 Equalization Filter 8
2.3 Filter Approximation 8
2.3.1 Butterworth Filter 9
2.3.2 Chebyshev or Equiripple Filters 11
2.3.3 Inverse Chebyshev Filter 12
2.3.4 Elliptic or Cauer Filter 12
2.3.5 Bessel Filter 12

3 CMOS Technology **13**
3.1 System on Chip (SoC) 13
3.1.1 Scaling in Digital CMOS Technology - a Retrospection 14
3.1.2 Scaling in Digital CMOS Technology - Today 15
3.1.3 Challenges of Scaling with Respect to Analog Circuits 16

3.2 65 nm CMOS Technology 18

4 Current-Mode Filters **25**
4.1 Current-Mode Technique 25
4.2 Filter Characterization 26
4.3 Motivation 29
4.4 State-of-the-Art 31
4.5 Realization of Current-Mode Filters 35
4.5.1 A 3rd-Order Current-Mode Continuous-Time Low-Pass Filter Using a Chip Area Saving Strategy 35
4.5.2 A Chip Area Saving 3rd-Order Current-Mode Continuous-Time Low-Pass Filter with Virtual Ground Regulation 47
4.5.3 A 3rd-Order Low-Voltage Current-Mode Continuous-Time Low-Pass Filter Using Capacitance Multiplication and Virtual Ground Regulation 56
4.6 Comparison to the State-of-the-Art 66

5 Operational Amplifier RC Low-Pass Filter **71**
5.1 Motivation 71
5.2 Operational Amplifiers - An Overview 74
5.3 Characterization of Operational Amplifiers 75
5.4 Challenges for Operational Amplifier Design in Nanometer CMOS 76
5.5 State-of-the-Art of Operational Amplifiers 77
5.6 State-of-the-Art of Voltage-Mode Filters 80
5.7 Realization of Operational Amplifiers and Operational Amplifier Filters . 82
5.7.1 A Four-Stage Feed-Forward Operational Amplifier 82
5.7.2 A First-Order Operational Amplifier RC Low-Pass Filter Using the Four-Stage Feed-Forward Operational Amplifier 88
5.7.3 A Four-Stage Multiple Feed-Forward Operational Amplifier 92
5.7.4 A First-Order Operational Amplifier RC Low-Pass Filter Using the Four-Stage Multiple Feed-Forward Operational Amplifier . . . 98
5.7.5 Three-Stage High-Voltage Operational Amplifier in 65 nm CMOS at 2.5 V Supply Voltage 102
5.7.6 Mixer and Filter Combination Using the Three-Stage High-Voltage Operational Amplifier 107
5.8 Comparison to State-of-the-Art of Operational Amplifiers 109
5.9 Comparison to State-of-the-Art of Voltage-Mode Filters 114

6 Conclusion **119**

Bibliography **121**

Curriculum Vitae **133**

Nomenclature

C_L	Load capacitance
C_{OX}	Gate oxide capacitance
CMFB	Common-mode feedback
CMRR	Common-mode rejection ratio
dBc	Decibels relative to the carrier
DR	Dynamic range
DVB-H	Digital video broadcast - handheld
DVB-T	Digital video broadcast - terrestrial
f_c	-3 dB cut-off frequency
f_T	Transit frequency
FOM	Figure of merit
g_m	Transconductance
g_{DS}	Output conductance
g_m	Transconductance
GBW	Gain-bandwidth product
HD3	3rd-order harmonic distortions
I_{dsat}	Saturation current
IIP3	Input third-order intercept point
IM3	3rd-order intermodulations
IP3	3rd-order intercept point
L	Gate length

LP	Low-power
N	Filter order
NF	Noise figure
OFDM	Orthogonal frequency division multiplex
OIP3	Output third-order intercept point
opamp	Operational amplifier
P	Power Consumption
PM	Phase margin
PSRR	Power supply rejection ratio
Q	Quality factor
rms	Root mean square
SDR	Software defined radio
SF	Scaling factor
SNR	Signal-to-noise ratio
SoC	System on Chip
STI	Shallow trench isolation
t_{OX}	Oxide thickness
THD	Total harmonic distortions
TV	Television
U_{DS}	Drain-source voltage
U_{GD}	Gate-drain voltage
U_{GS}	Gate-source voltage
UMTS	Universal mobile telecommunication system
V_{TH}	Threshold voltage
W	Channel width
WCDMA	Wideband Code Division Multiple Access

Chapter 1

Introduction

Analog circuits have still a right to exist in a society that is shaped by the digital revolution. The digital advance is driven by various trends of market and economy [CSB92]. High-performance multimedia systems allow a colorful and high-resolution presentation of digital contents while simultaneously navigating and interacting with this medium. In telecommunication and high-speed communication systems the data volume and speed is rising rapidly while the receiving terminals have to process the incoming data stream in time. Computer systems become faster in terms of higher clock speed and contain a huge amount of data storage in order to provide enough performance, which is necessary to execute the growing number of resource intensive application in a convenient time.

These few examples give an impression on the progress in digital CMOS design. The development of low-power CMOS technologies is mainly forced by power dissipation, manufacturing costs, and speed performance [GGH97]. During the last decades these requirements are mostly obtained by the technological progress of scaling of the device feature sizes to the nanometer domain. Scaling has a significant impact on the density of digital circuits [Fot99]. A larger number of transistors per chip-area increase the functionality and lower the fabrication costs. Another benefit of shrinking structure sizes is the reduction of the parasitic transistor capacitances. Smaller parasitic capacitances cause thus lower dynamic power dissipation in digital logic. The shortest available channel length ensures the maximum performance [San98]. However scaling induces undesirable and challenging effects as well [Vit90]. Short channel MOSFET transistors suffer from the so-called short channel effects. These are, among other things, velocity saturation, hot electrons, and impact ionization. The breakdown of the transistors is another issue. The scaling of the minimum feature sizes require the lowering of the supply voltage due to the rising electrical fields inside the transistor. A high electrical field, which is inversely proportional to the distance, can destroy the transistor. The lowering of the supply voltage has a power saving effect in digital logic. Power saving in digital applications provokes lower costs for cooling and longer battery life-time for

handheld devices. Summarizing, the ongoing downscaling of digital CMOS technology pushes the development stimulus in economy and science.

Unfortunately, the world where digital systems operate has an analog manner and, thus, interfaces between analog and digital blocks have to be created. An interfacing block may be an analog-digital or a digital-analog converter, an amplifier, an I/O buffer, an analog filter, or a radio frequency (rf) front-end for a communication channel. From an economical point of view it is favorable to integrate all analog and digital system blocks into a mixed-signal system on one chip. Although the analog part is not the essential core of such a mixed-signal system, it has a great impact on the overall system performance. The process of scaling affects the performance of the MOS transistors in analog circuitry severely [GD05]. Nevertheless analog system design in digital CMOS is a good possibility for low precision analog processing considering some limitations. One of the major challenges is the low supply voltage, which is limiting the maximum signal swing. The increasing 1/f noise at small structure sizes worsens this challenge. Errors due to device mismatch are inversely proportional to the device sizes as well [Bul00]. Additional gate leakage due to reduced gate oxide thickness has a considerable magnitude [ANvLT05]. The downscaling of CMOS transistors has some advantages for analog circuits, of course [HBHK95]. For example, the transit frequency of the transistors is rising due to the smaller parasitic capacitances, comparable to digital logic design.

For the purpose of a power and cost saving device, system on chip solutions are desirable. In this work analog continuous-time filters for radio frequency front-ends are presented as an element in a system on chip. Analog continuous-time filters are sometimes preferable in contrast to switched-capacitor filters or digital filters because of the possibility for high-frequency operation and low power dissipation [Tsi94]. Many passive discrete-component filter structures are known, which use the inductor as an important element [Tsi01]. Integrated inductors are difficult to realize due to the bad quality factor and large chip area. Inductors can be substituted by the use of active analog continuous-time filters, which use an active element, resistors, and capacitors. Active elements may be operational amplifiers or transconductance amplifiers. Integrated analog filter design in nanometer CMOS faces many technological restrictions, for example the limited dynamic range and matching [CMRB95]. The low signal swing, caused by the low supply voltage and the constant noise level, decreases the dynamic range of analog filters at a constant current dissipation. Additionally varying device parameters due to mismatch cause a non-constant frequency response. The use of an active tuning system may correct those errors.

This work considers above mentioned issues and is structured as follows. Chapter 2 deals with the characteristics of Butterworth filters. The used nanometer CMOS technology is described in chapter 3. During the last years a variety of active continuous-time filters were presented in literature. Chapter 4 discusses current-mode filters for software defined radio applications and chapter 5 presents operational amplifier filters for digital video broadcast - handheld terminals.

Chapter 2

Butterworth Filters

A filter is a general term. It is used to separate desired parts from unwanted parts of an original set. In an electrical point of view filters have a variety of duties. Filters are used to cut a particular range of the frequency spectrum of an electrical quantity out of the overall frequency spectrum to retrieve the interesting information out of the plenty of information channels and noise. They can be used as equalizers or matched filter in transmission channels in order to compensate distortions caused by the transmission channel itself. Filters can also be employed for smoothing purposes at the output of digital-to-analog converters [Lam79]. This chapter deals with the characterization of filters, it gives an overview of some analog filters and describes the Butterworth-filter approach in more detail.

2.1 Filter Classification

Due to the diversity of filters many classifications of electronic filters are possible. Some are described in a short overview [DSF99].

2.1.1 Analog - and Digital Filters

Electronic filters are distinguished in analog and digital filters. Analog filters have a long tradition in analog circuit design and communication systems and can be grouped in electric and electronic filters, sampled data filters, and electromechanic filters. Electric and electronic filters are realized by using resistors (R), capacitors (C), inductors (L), and active elements like operational amplifiers or g_m-cells. Analog filters process analog continuous-time input signals in real-time and transform it according to the filter transfer

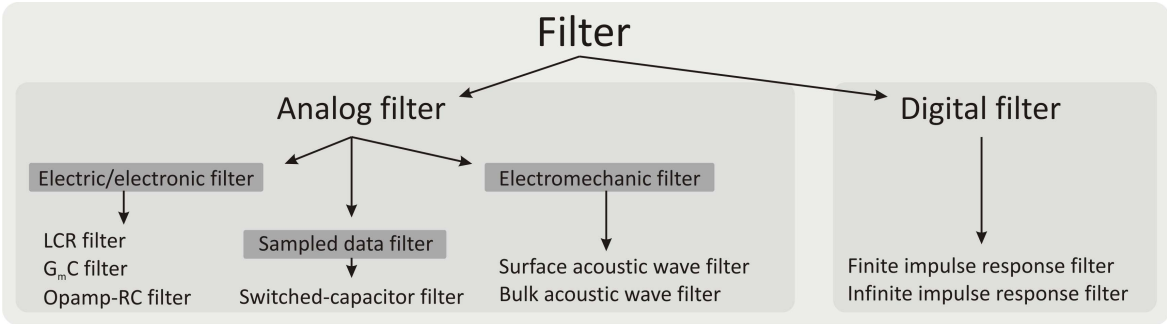

Figure 2.1: Classification of filters - overview

function. Examples for analog electric/electronic continuous-time filters are LCR-filters, g_mC-filters, or operational amplifier-RC filters.

Sampled data filters sample the input signal by using a Sample-and-Hold stage on the input before processing the signal. The input signal is quantized at discrete time steps but the signal remains analog. Because of the sampling of the input signal these filters are discontinuous in time. However, sampled data filters belong to the group of analog filters. The switched-capacitor filter is a well known member of the sampled data filters.

Electromechanic filters convert the electrical signal into a mechanical (acoustic) wave which propagates over a ceramic or a crystal and then finally convert it back to the electrical domain. The combination of two electro-acoustic transformers and the signal delay on the crystal perform the filtering operation. Well known representatives of electromechanic filters are surface acoustic wave filters (SAW filter) or bulk acoustic wave filters (BAW filter).

Digital filters emerged since the development of computers and grew rapidly. Digital filters can be realized in hardware or software. They are characterized by sampled, time discrete input- and output signals. Sampled and time-discrete signals represent periodical series of discrete pulses, which represent the signal waveform. The sampled discrete pulses are discrete values due to the finite resolution of the digital number representation. Examples for digital filters are the finite impulse response filter (FIR) and infinite impulse response filter (IIR). Figure 2.1 shows an overview of the filter classification scheme.

2.1.2 Active - and Passive Filters

A passive filter is defined formally in the following way:

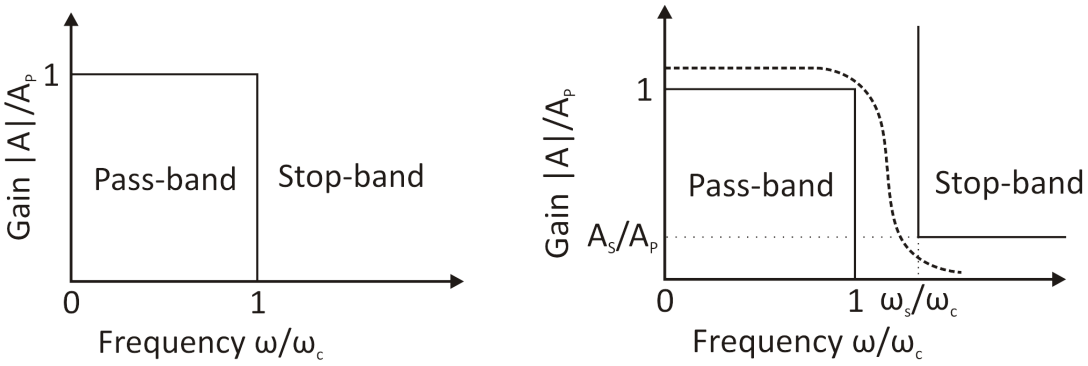

(a) Ideal low-pass filter

(b) Specification of a real low-pass filter

Figure 2.2: Amplitude-frequency response

> A filter is passive, if the total energy supplied to the filter is nonnegative at any instant of time.

All other filters than passive filters are active filters.

A more common characterization of a passive filter is defined regarding the used elements. A filter is classified as passive, if only passive elements are applied. The basic passive elements are resistors (R), capacitors (C), and inductors (L). If any other active elements are used, such as transistors or amplifiers, a filter is an active filter.

2.1.3 Lumped - and Distributed Filters

Lumped filters or lumped networks are circuits whose elements (e.g.: R, C, L) are concentrated within their physical devices. The electrical and physical properties of the devices are defined at their terminals and the component connections are small compared to the wavelength of the highest signal frequencies, which are applied to the filter. Distributed filters are networks where the physical dimensions of the elements are in the same range of the signal wavelengths.

2.2 Analog Filter Types

Filters divide the frequency spectrum in different bands and, hence, shape the transfer characteristic of the filter. Stop-bands denominate frequency ranges which block accor-

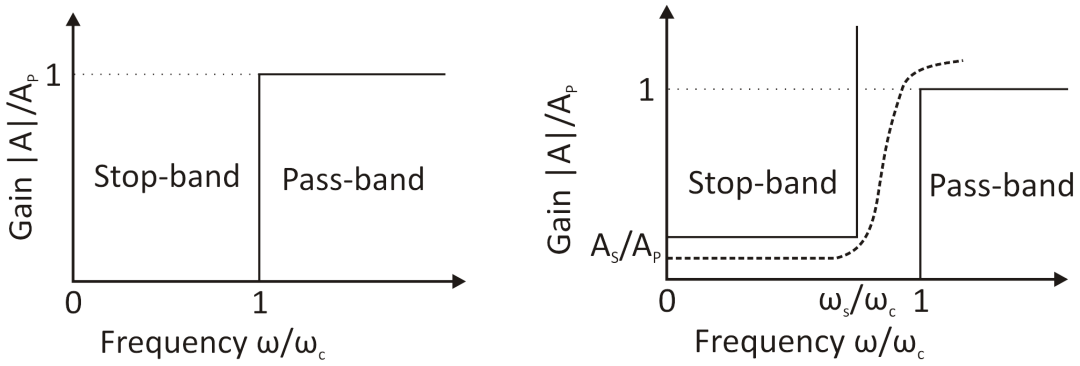

(a) Ideal high-pass filter

(b) Specification of a real high-pass filter

Figure 2.3: Amplitude-frequency response

dant signal fractions from the signal applied at the input. In contrast to this, pass-bands are frequency ranges, which forward the in-band residing input signal frequency fractions to the output. The allocation of the stop-bands and pass-bands specifies the type of the filter. Feasible filter types are the low-pass filter, the high-pass filter, the band-pass filter, the band-stop filter, the all-pass filter and or the equalization filter [Bah96].

2.2.1 Low-Pass Filter

An ideal low-pass filter exhibits a pass-band from dc, i.e. 0 $\frac{rad}{s}$, to the cut-off frequency ω_c whereas the signal is amplified by a gain of A_P. The stop-band starts directly at ω_c and reaches up to infinity with a signal gain of zero. Figure 2.2(a) shows an ideal low-pass filter. In reality filter transfer functions can only approximate the ideal filter transfer characteristics. Figure 2.2(b) shows a general low-pass specification including an example of a filter transfer function (dashed line). The pass-band reaches from dc to the cut-off frequency ω_c with a gain of A_p. In reality filters are not able to switch between pass-band and stop-band abruptly and, hence, the stop-band starts at $\omega_s > \omega_c$ at a gain of A_s. The span from ω_c to ω_s is called transmission-band. The width of the transmission-band $\omega_s - \omega_c$ indicates the selectivity of the filter.

2.2.2 High-Pass Filter

An ideal high-pass filter is depicted in figure 2.3(a). All signal frequencies in the stop-band are blocked. The stop-band ranges from dc to the cut-off frequency ω_c. All frequencies greater than ω_c pass the filter at a gain of A_p. A specification of a feasible

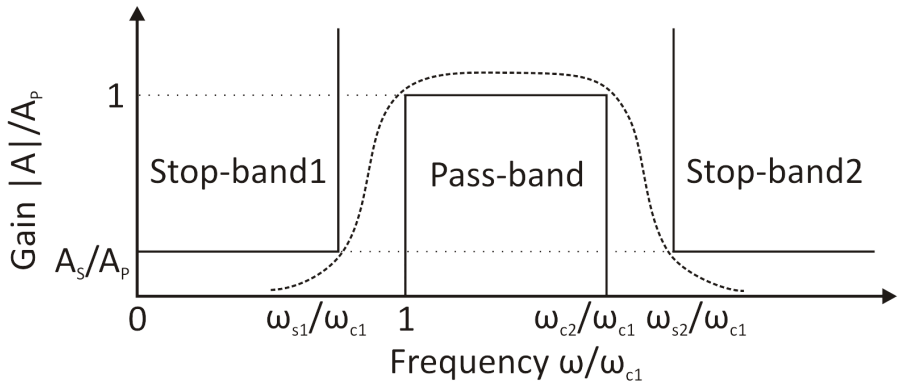

Figure 2.4: Specification of a band-pass filter

high-pass filter in reality is shown in 2.3(b). The stop-band extends from zero to ω_s, the pass-band from ω_c to infinity and the transition-band is located between ω_s and ω_c.

2.2.3 Band-Pass Filter

A band-pass filter, as depicted in figure 2.4, forwards a specified bundle of wavelengths from ω_{c1} to ω_{c2} having a gain of A_P. The two stop-bands *Stop-band1* and *Stop-band2* cover frequencies from zero to ω_{s1} and ω_{s2} to infinity, respectively. The gain of the two stop-bands is denoted by A_s. An exemplary frequency response is plotted in figure 2.4 (dashed line).

2.2.4 Band-Stop Filter

In contrast to the band-pass filter, a band-stop filter or notch filter eliminates a frequency band from ω_{s1} to ω_{s2}. The rejected band resides between the two pass-bands *Pass-band1* and *Pass-band2*, which are located between zero and ω_{s1} and ω_{s2} and infinity, respectively. Figure 2.5 depicts an example of a band-stop filter specification, A_s and A_p are the corresponding gains for the stop-band and the pass-bands.

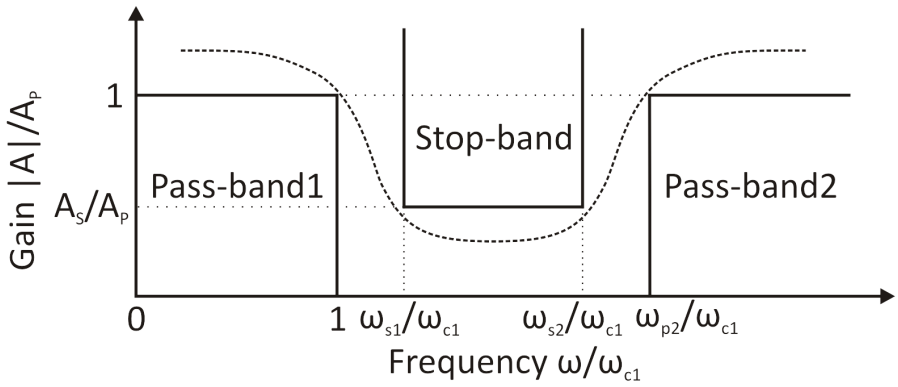

Figure 2.5: Specification of a band-stop filter

2.2.5 All-Pass Filter

All-pass filters forward all wavelengths from zero to infinity equally without any amplitude attenuation. The characteristic filter property concerns the phase response. The propagation delay of the signal depends on the frequency. All-pass filters are mainly used for phase error correction of transmission channels.

2.2.6 Equalization Filter

Equalization filters or equalizers are used for the correction of an uneven frequency response characteristic for smoothing purposes of signals or systems. The transfer function is different from the above considered and is often only usable for one special case of distorted signal.

2.3 Filter Approximation

A physical realization of an ideal filter transfer function is impossible. Hence, a frequency scheme is given, which is dependent on many system parameters and trade-offs. Within this frequency scheme the real filter transfer function has to be located. Important selection criteria are for example a fast transmission from the pass-band to the stop-band or a minimum of filter distortion. The closer the ideal filter transfer function is approximated, the greater is the effort regarding number of elements, power consumption or costs. De-

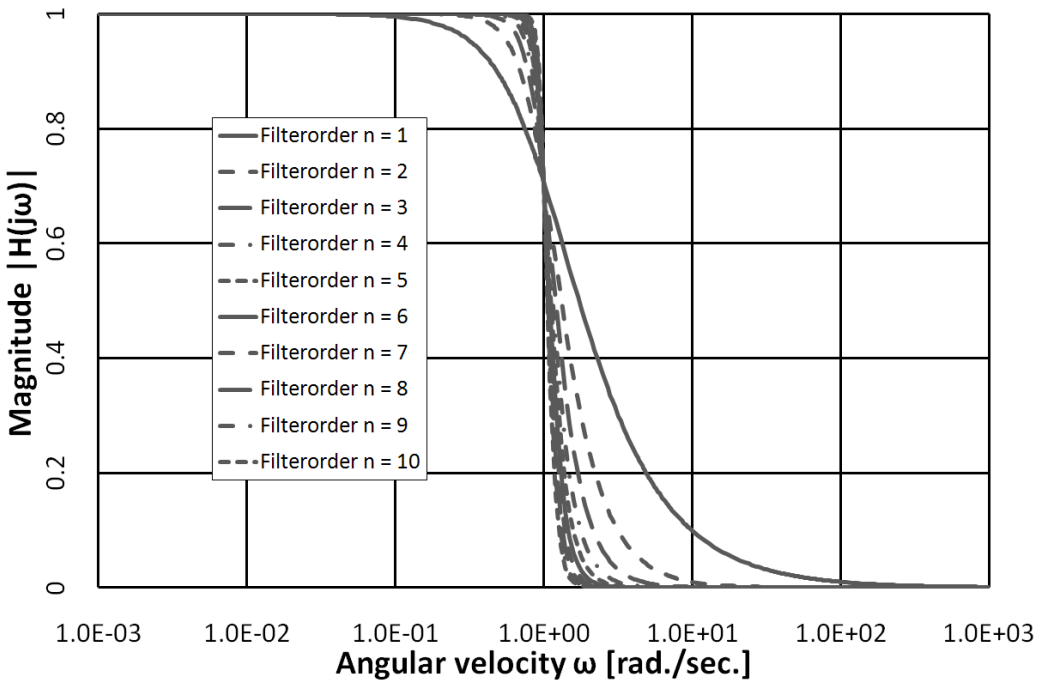

Figure 2.6: Magnitude functions of normalized Butterworth low-pass filters of first-order to 10th-order

pending on the latitudes various approximations for the ideal filter transfer functions are realizable. Important and popular approximation functions are Butterworth approximations, which are explained in more detail, Chebyshev and inverse Chebyshev approximations, elliptic or Cauer approximations, and Bessel approximations.

2.3.1 Butterworth Filter

The Butterworth filter was first described by Stephen Butterworth and is nowadays popular and often used. The Butterworth filter approximation is demonstrated on the normalized low-pass Butterworth filter. High-pass, band-pass, and band-stop filters can be realized by using the appropriate transformation [Lam79].

The normalized Butterworth function of Nth-order is given by

$$|H(j\omega)|^2 = \frac{1}{1+\omega^{2N}}. \tag{2.1}$$

In equation 2.1 ω denotes the angular velocity and $N = 1, 2, \ldots$ the filter-order. The

magnitude response $|H(j\omega)|$ of a first-order to a 10th-order normalized Butterworth low-pass is visualized in figure 2.6. A rising filter order (N $\rightarrow \infty$) results in a better approximation to the ideal low-pass filter (see figure 2.2(a)). The pass-band and the stop-band coincide longer with the ideal transfer function, simultaneously the transition-band becomes narrower. To comply with the filter specifications an appropriate filter-order N of the Butterworth low-pass filter is necessary.

The Butterworth low-pass filter has some important characteristics:

- The magnitude function of a Butterworth low-pass filter is monotonically decreasing for $\omega > 0$ and the maximum of $|H(j\omega)|$ is at $\omega = 0$.
- A Nth-order Butterworth low-pass filter has a maximally flat magnitude function. The maximal flatness of a Butterworth low-pass filter is defined by

$$\frac{d^{(k)}|H(j\omega)|}{d\omega} = 0 \quad \Bigg|_{\omega=0} \qquad \forall k = 1 \quad \ldots \quad 2n-1. \tag{2.2}$$

  The first 2n-1 derivations of $|H(j\omega)|$ of an Nth-order Butterworth filter at $\omega = 0$ are equal to zero.
- A Butterworth filter shows an overshoot in the step response in the time domain, which worsens at rising filter-order N.

The phase characteristics of a Butterworth low-pass filter is given by

$$\Phi(\omega) = arg[H(j\omega)]. \tag{2.3}$$

Each pole adds -90° phase lag. The phase responses of Butterworth low-pass filters from the order N = 1 to 10 is depicted in figure 2.7.

The distribution of the poles and zeros in the s-plane are characteristic for filters and can also be used for filter identification. A normalized Butterworth low-pass filter has its poles in the left half plane on the circumference of the unity circle with the centre in the point of origin of the s-plane. The poles are spread equidistant over the half circle in the left half s-plane. The location of the poles s_k of $H(s)$ in the left half plane can be calculated by

$$\begin{aligned} s_k = \sigma_k + j\omega_k &= e^{j\frac{(2k+N-1)\pi}{2N}} \\ &= \cos(\frac{2k+N-1}{2N}\pi) + j\sin(\frac{2k+N-1}{2N}\pi), \qquad k = 1 \ldots N. \end{aligned} \tag{2.4}$$

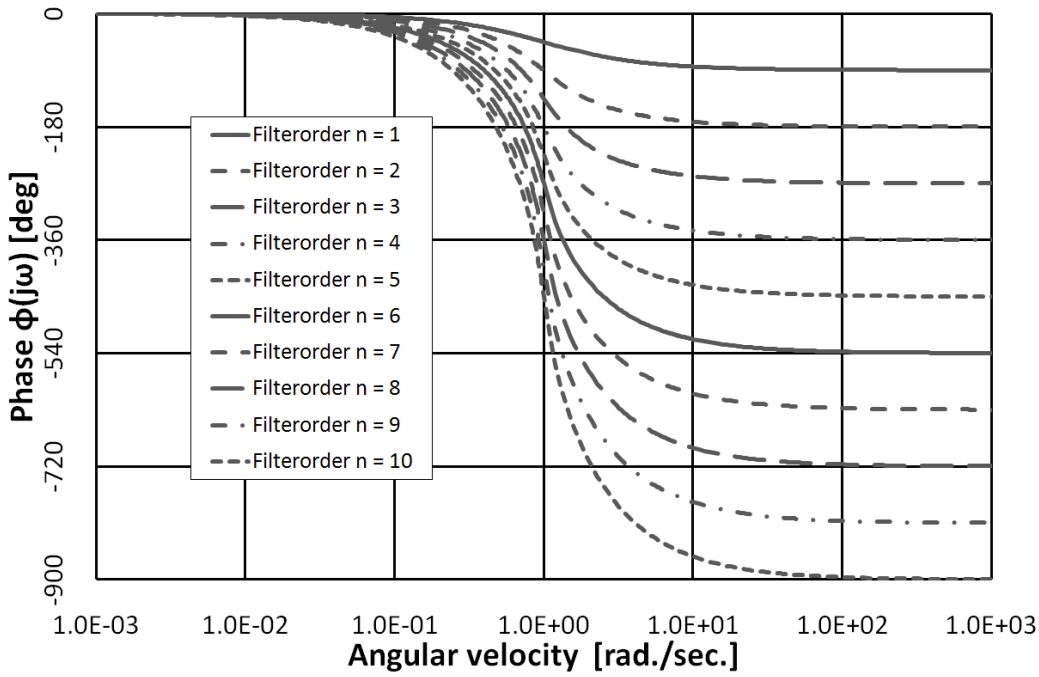

Figure 2.7: Phase characteristics of normalized Butterworth low-pass filters of first-order to 10th-order

In equation 2.4 N is the filter order of the Butterworth filter and k is the number of poles. In case of an even filter order no real pole is existent, an odd filter order has exactly one real pole.

2.3.2 Chebyshev or Equiripple Filters

Chebyshev filters offer a frequency response that approximates the ideal low-pass filter more precisely than a Butterworth filter. The transfer function has only poles and lack of any finite zeros. The pass-band of a Chebyshev filter exhibits a pass-band ripple, which ranges between two constant values. The ripple amplitude can be adjusted freely. The ripple amplitude is direct proportional to the filter slope in the transition-band (filter selectivity) and the overshoot of the step response in the time domain. The greater the pass-band ripple, the higher the filter selectivity and the overshoot. The number of ripples depends on the order N of the filter. For frequencies greater than the cut-off frequency the filter has a monotonically decreasing magnitude function similar to Butterworth filters.

2.3.3 Inverse Chebyshev Filter

The inverse Chebyshev filter has complementary properties of the Chebyshev filter concerning the magnitude response. In the pass-band the magnitude function is monotonically decreasing for $\omega > 0$ and the equiripple appears in the stop-band. The filter selectivity is not so high as in Chebyshev filters. The zeros in the filter transfer function bring an additional realization effort.

2.3.4 Elliptic or Cauer Filter

Elliptic filters have an equal ripple in the pass- and in the stop-band. Therefore elliptic filter is also called double Chebyshev filter. The two ripples are individually adjustable. The transition between pass-band and stop-band show a high filter selectivity. The sharp filter edge is realized by a transfer function using a balanced combination of poles and zeros. The magnitude function of an elliptic filter is the best approximation of the ideal low-pass filter compared to Butterworth and Chebyshev filters.

2.3.5 Bessel Filter

In contrast to Butterworth or Chebyshev filters, which approximate the magnitude function of an ideal low-pass filter, the Bessel Filter approximates the phase response. Hence, the Bessel filter is also called maximally flat group delay filter. In the pass-band the Bessel filter has a distortion free transmission and keeps the group delay constant. The constant group delay in the pass-band results in a step response, which shows no overshoot. The filter selectivity is not as good as in Butterworth filter structures. The filter order N is the only parameter to adjust a normalized Bessel filter. The value of N defines the phase and the magnitude response. The higher the filter order, the larger the frequency range with constant group delay and the higher the filter selectivity.

Chapter 3

CMOS Technology

3.1 System on Chip (SoC)

Over the last decades electronic devices arise everywhere in our society. These devices combine many standards, applications, and features and are met in low-cost high-volume markets very often. Portability is of particular importance as well. Hence there is the need to develop small-sized, energy saving, and competitive systems in order to improve the sales volume.

System on Chip (SoC) is a strategy which combines all parts that are relevant for the system operation, on one chip. Hardly any other parts are necessary for a correct system functionality. A SoC is an overall system with a high level of integration, but it cannot be seen as a simple composition of existing digital, analog, and mixed-signal circuit components. The integration into a SoC implicates innovative approaches in order to find a system design tradeoff, which concerns cost-efficiency, dimensions, and power consumption [RH04].

A major cost impact is the used process technology [Dia04]. A system on chip design always aims to use the cheapest process technology, which is currently deep sub-micron and nanometer CMOS technology. Moreover the digital part of a SoC is the major part, analog circuits have a small but important supporting role. Several interfaces of the SoC have an analog manner, such as input/output ports, analog-to-digital converters, digital-to-analog converters, and radio frequency (rf) front-ends. Although additional process steps for improvements in analog circuit design are available, these process steps are expensive and hence penalize the overall product. In SoC designs standard digital CMOS is commonly used.

3.1.1 Scaling in Digital CMOS Technology - a Retrospection

The CMOS technology underlies a persistent evolution to smaller structure sizes, which is also called scaling. Historically, the common practice of scaling is known as constant field scaling [Fot99]. This strategy keeps the electrical field in the channel of the MOSFET constant while simultaneously reducing the physical dimensions. The channel length L, channel width W, and oxide thickness t_{OX} are reduced by the factor SF. This results in a MOSFET area divided by SF^2 and the parasitic capacitances are divided by SF. The supply voltage and the threshold voltage are graduated by the factor SF to keep the constraint of a constant electrical field. The channel doping is increased by SF. This scaling technique is efficient for improving performance and reducing chip area. Nevertheless technology scaling brings some difficulties.

Scaling Supply - and Threshold Voltages The dynamic power consumption in digital circuits is caused by currents during the switching operations and by charging of the load capacitances. Hence, the dynamic power consumption is directly depending on the supply voltage, since a low supply voltage allows a saving in dynamic power consumption [CSB92]. At constant field scaling the lowering of the supply voltage involves the reduction of the threshold voltage. A low threshold voltage raises the static power consumption, when the transistor is turned off due to leakage currents. The threshold voltage level is adjusted by taking care of the maximal acceptable level of the off-state power consumption.

Gate Oxide Thickness A small gate oxide thickness enhances the transistor performance and in constant field scaling the thickness is also reduced according to SF. However, the extent of the gate oxides is only a few atom layers where quantum-mechanical effects have to be considered [HH08]. The gate leakage currents raise exponentially at decreasing t_{OX} and the tunnel currents can cause a damage of the gate oxide.

Short Channel Transistors Short channels are desirable for fast transistor switching operations, due to the shorter time for the current from source to drain. However, there are some disadvantages:

- High sub-threshold currents occur in off-state transistors. Even at $U_{GS} < V_{TH}$ a current is flowing from source to drain. The currents are generated by punch-through and drain induced barrier lowering (DIBL) [HH08].
- Surface scattering cause a reduction of the mobility of the electrons [Hau96].
- The velocity saturation lowers the mobility of the carriers of transistors in saturation [PKH91].

- High electric fields in the pinch-off region cause the generation of electron-hole pairs due to impact ionization. The electrons migrate to the drain, the holes move to the substrate in the form of a parasitic substrate current. The body potential is raised and the threshold voltage is lowered due to the body effect again causing a rising of the channel current [WP97].
- Hot electrons appear at the existence of high electric fields. High energy electrons migrate into the gate oxide and charge the gate oxide and degrade transistor performance and lifetime [Nin00].

Channel Doping The short channel effects can be extenuated by increasing the channel doping, but cause other transistor influences. Important factors are the slower carrier mobility and band-to-band tunneling [HH08].

3.1.2 Scaling in Digital CMOS Technology - Today

The scaling strategy in deep-submicron and nanometer technologies is different to constant field scaling due to many limitations and parasitic effects. The improvement of the transistor performance relies basically on the gate-length, the gate-oxide thickness, and the source-drain junction scaling [CCC+08]. Scaling of these parameters are mainly driven by power optimization, performance maximization, and device reliability.

Power optimization Reducing the power supply voltage is an effective method to reduce the power dissipation, because subthreshold currents and gate leakage are dependent on the supply voltage [CCC+08]. However, there is a limit of scaling the supply voltage, which is the threshold voltage (V_{TH}) of the transistors. A low V_{TH} leads to increasing subthreshold currents and increases the static power dissipation. In order to limit the overall power consumption the threshold voltage is not scaled by SF, it remains larger. For transistor speed issues a sufficient gate overdrive voltage should exist. Therefore the supply voltage is not scaled by SF. For power and performance optimization multi threshold voltage transistors are used. According to the requirements, thin -, regular -, or thick gate oxide transistors are available, at the drawback of needing additional masks for chip processing. The threshold voltage depends on the operating temperature as well. The power dissipation and the thermal emission are of great interest because of the temperature dependent threshold voltage and the raising number of transistors per chip. Counteractions are cooling, dynamic frequency scaling, voltage-island design technique or adaption of the threshold voltage by the back-gate bias [Iwa06].

Performance maximization The progress in transistor speed has slowed down during the downscaling of CMOS technology. Main reasons are the short-channel effects and some parasitic elements, which do not scale. In digital circuits the performance increases by lowering the capacitance and increasing the transistor saturation currents. At first the saturation current was increased by scaling the oxide thickness and the threshold voltage. As this was not possible anymore due to leaking currents the saturation current was increased by strained silicon techniques, channel oriented design, or silicon on insulator. This improves the performance of the MOSFET without scaling the gate oxide thickness [TCG+05]. High-k dielectric gates with metal gates may resume the scaling of the gate insulator thickness. Another important factor for transistor speed is the capacitance. Scaling reduces the gate capacitance and the overlap capacitance. However, the gate-to-contact capacitance and the fringing capacitance, which do not scale, will have a major impact on the total capacitance [CCC+08].

Device reliability Scaling, in particular scaling of the gate dielectric, affects the reliability of the transistors. Important reliability stress effects are [LYWM09]

- gate insulator time-dependent breakdown, due to insulator trapped charge during high-field stress,
- hot carrier injection, because of high electric fields,
- negative bias temperature instability in PMOS devices, due to interface traps from high gate voltage and high temperature, and
- electromigration, due to defects in conductive materials.

In order to maintain low failure rates at an increasing chip complexity new chip materials have to be evaluated and the design rules have to be adapted [McP07].

3.1.3 Challenges of Scaling with Respect to Analog Circuits

Besides the major digital part, analog circuits are necessary in SoC applications. The effects of scaling affect analog circuits severely. An outline of challenges and benefits is given.

Transistor Speed and Gain Major effect of scaling in digital circuits is the improvement of speed and packing density. Analog circuits benefit from the increasing speed as well. Parasitic capacitances are reduced and the gate resistance is increased due to the gate length scaling and layout optimizations. The transit frequency of the transistors (f_T) and the maximum oscillation frequency increase with ongoing scaling. The transistor

speed and the transistor intrinsic gain are in direct competition. High speed transistors lead to a low output resistance and in a low intrinsic gain. Both can be improved by increasing V_{TH} or decreasing U_{GS} to operate in moderate inversion. However, moderate inversion is accompanied with a drop of f_T and oscillation frequency [MJR+04].

Supply Voltage and Signal Headroom Digital circuits benefit from a small supply voltage and have a reduced power consumption and increased logic speed. In analog circuits a reduced supply voltage leads to a small signal range and a limited signal headroom and may cause a larger layout area. Newer technologies may induce an increased power consumption [MJR+04]. At a constant power consumption the performance deteriorates when newer technologies are used because of their lower supply voltage [ANvLT05]. By lowering the supply voltage of analog circuits the power dissipation has to be increased to keep a constant circuit performance. The increase of power becomes more relevant as the supply voltage is in the range of the threshold voltage V_{TH}. Low V_{TH} devices are sometimes available for analog circuits but cannot be used in the digital domain due to the subthreshold currents. The limited signal range and signal headroom demand accurate analog designs and a good noise performance to maintain the signal-to-noise ratio (SNR) and dynamic range.

Low-Frequency Noise Flicker noise or 1/f noise is generated by the fluctuation of the total number of carriers and the fluctuation of the mobility of the carriers in the transistor channel [LKC+06]. It attains increasing observance in analog design due to the shrinking feature sizes in CMOS technology. 1/f noise increases inversely proportional to the gate area and has a considerable amount in deep submicron CMOS technology. A common expression of the 1/f-noise density is given in [San06]:

$$d\overline{v^2} = \frac{KF_F}{WLC_{OX}^2}\frac{df}{f} \tag{3.1}$$

In 3.1 KF_F is a parameter, nearly independent of the technology. W is the gate width and L represents the gate length. C_{OX} is the specific gate oxide capacitance. It is notable, that almost all technology effects are included in C_{OX}^2.

Matching Matching is an important criterion in analog circuits, especially in differential structures. The matching of V_{TH}, g_m , saturation current (I_{dsat}), and the device matching is mainly dependent on the precision of the manufacturing process. In deep submicron technologies additional factors become significant. Voltage matching, which is usually described by the difference of V_{TH} of two identical transistors, becomes less sensitive to the device dimensions, when technology scales [LYWM09]. Matching can be improved by increasing the device dimensions.

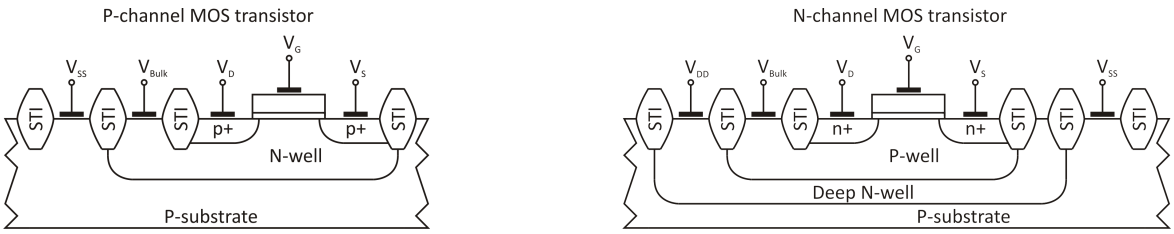

(a) P-channel MOSFET transistor

(b) N-channel MOSFET transistor

Figure 3.1: Cross-sections of MOSFET transistors in 65 nm triple-well process

Gate Leakage Current The gate leakage current is mainly limited by digital considerations, such as static power consumption. In nanometer CMOS technology gate leakage currents have to be considered in analog circuit design. The gate leakage current depends on the oxide thickness, the gate-source voltage U_{GS}, the gate-drain voltage (U_{GD}), and the gate area [LYWM09]. The gate leakage current affects the input bias currents, the gate leakage mismatch and the shot noise due to the gate current. In order to minimize the gate leakage high-K dielectrics for the gate insulator are developed [MJR+04].

Linearity Distortion in analog circuits in nanometer CMOS technology are mainly caused by the increased influence of the series resistance and velocity saturation. By scaling the CMOS technology, i.e. due to reduced supply voltage, the voltage headroom decreases and in analog bias conditions scaling worsens the linearity [vLTH+00].

3.2 65 nm CMOS Technology

65 nm bulk CMOS technology is developed for logic, SRAM, mixed-signal, and mixed-voltage I/O applications as well as for embedded DRAM applications. Besides the 65 nm CMOS base process, there exists a 65 nm low-power (LP) CMOS process. The 65 nm low-power process has an approximately 100 mV higher threshold voltage than the base process and hence a lower off-state leakage current. Both options have three different oxide thicknesses to support several supply voltages from 1.2 V to 3.3 V [LSE+04].

In the following circuits only the 65 nm CMOS low-power technology is used, thus only important characteristics of the low-power CMOS are highlighted. The 65 nm CMOS technology is a triple well process on a p-substrate. The PMOS transistor is located in an isolated N-well and the NMOS transistor is placed in an insulated P-well, which is itself embedded in a deep N-well. Cross-sections of the transistors are depicted in figures 3.1(a) and 3.1(b). Active devices are separated by a shallow trench isolation (STI). Stress engineered devices are offered and the stress is caused by the location and

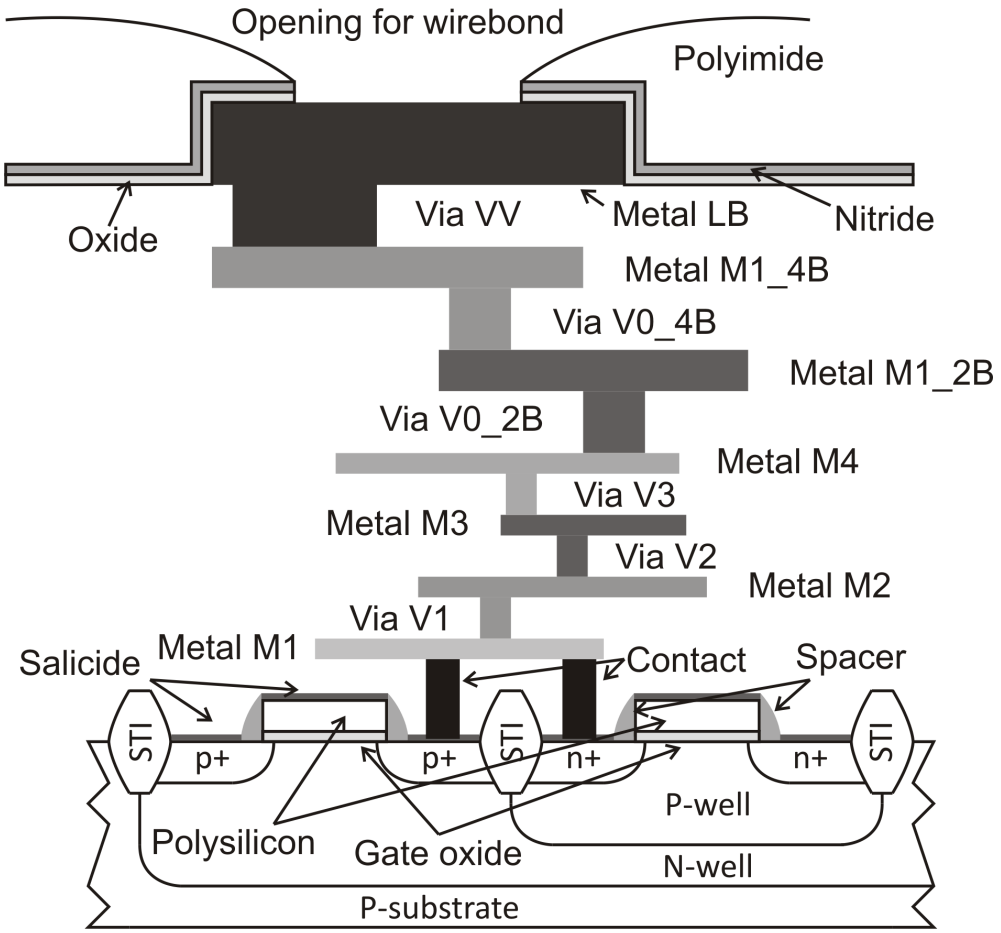

Figure 3.2: Cross section of the 65 nm low-power CMOS process

the dimension of the STI. Mechanical stress increases the carrier mobility in p-channel MOSFETs and deteriorates the carrier mobility in n-channel MOSFETs [MJC+04].

The nominal supply voltage in the 65 nm low-power CMOS process is 1.2 V and the maximum supply voltage is at 1.32 V. The cross-section of the 65 nm CMOS process technology is shown in figure 3.2. It should be noted that the aspect ratios are not displayed correctly. The process uses a P-substrate, wherein N-wells and triple P-wells are embedded. Inside the wells are the appropriate n+ and p+ diffusion regions [TBE+03]. The gate oxide isolates the polysilicon from the transistor channels, which is the gate conducting material. The spacers ensure the isolation between gate and source/drain areas. Self-aligned silicide, also called salicide, forms the interconnect between the semiconductor and metal layers. The contacts connect the salicide to the metal layer 1 (M1). Metal M1 to M4 are 1x thin metal layers, which are connected by the vias V1 to V3. Via V0_2B connects 1x thin metal M4 to thick metal (2x) M1_2B. And finally Via V0_4B contacts the last copper metal layer M1_4B, which is a 4x thick metal layer. In total there exist 6 copper metal layers. The last metal layer LB is used for wiring

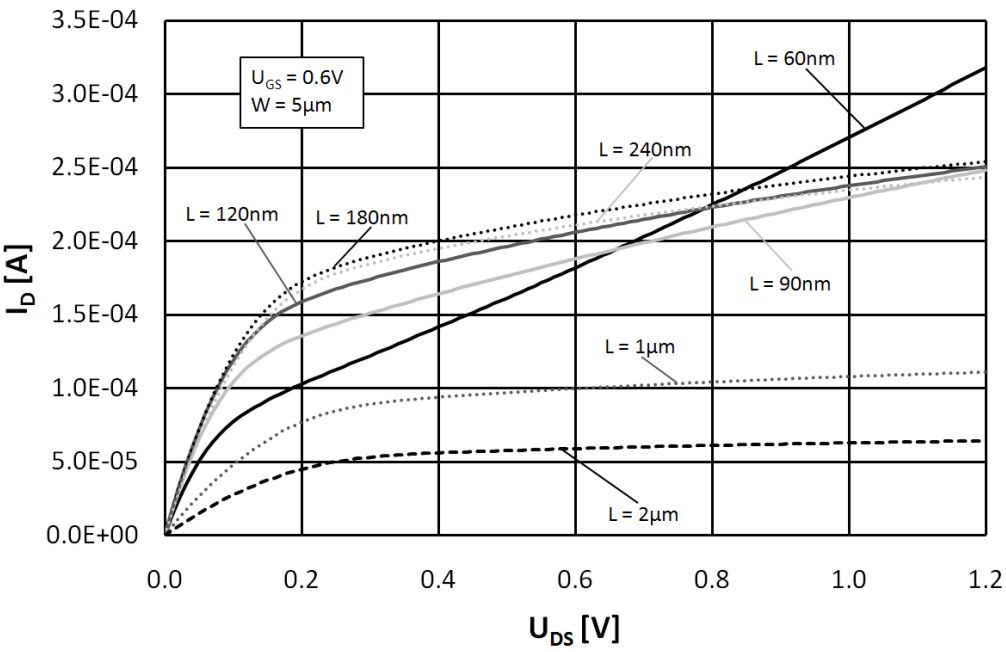

Figure 3.3: NMOS output characteristics at varied gate length L

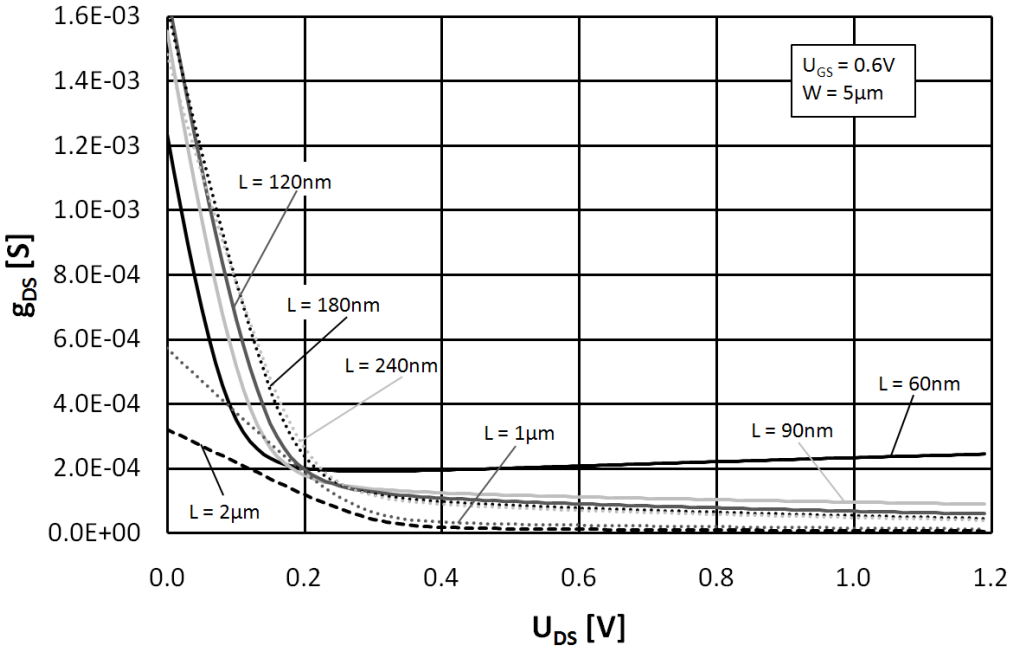

Figure 3.4: NMOS output conductance g_{DS} at varied gate length L

and wirebond. Metal LB is an aluminum wire level and is connected to M1_4B by the via VV. For wirebond the oxide and nitride film is opened as well as the polyimide passivation layer [BAB+04].

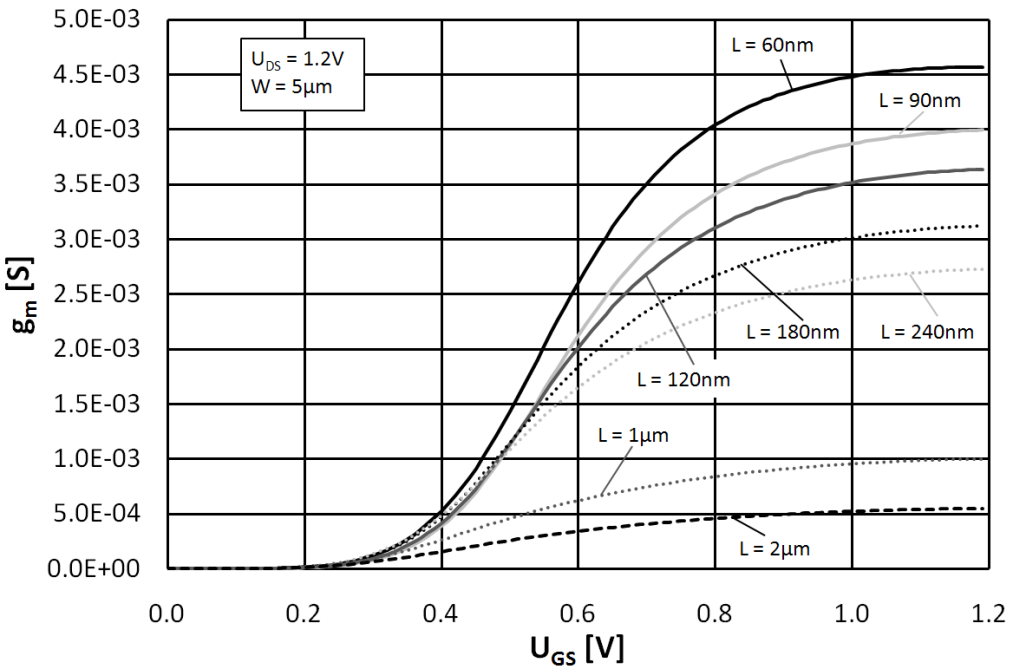

Figure 3.5: NMOS transconductance g_m at varied gate length L

Transistor characteristics The progress of scaling is noticeable in several transistor parameters and properties. Figure 3.3 shows the output characteristics of an NMOS transistor with varied gate length L in the 65 nm CMOS technology. The transistor width W is 5 μm and the gate source voltage U_{GS} of 600 mV is applied. The Early voltage declines with decreasing gate length L and is in a range of a few volts. At the gate length of 60 nm the Early voltage is only about 0.31 V. At a constant transistor width the drain current should increase at smaller gate lengths. In figure 3.3 it is different because of the threshold-voltage roll-off [JXC+09]. The threshold-voltage roll-off is caused by the short-channel effect and the fringing-field effect and results in a rising threshold-voltage at decreasing gate lengths. Figure 3.4 depicts the output conductance g_{DS} against the drain source voltage U_{DS} which is decreasing with increasing gate lengths.

The transconductance g_m of an NMOS transistor with the gate width of 5 μm is shown in figure 3.5. U_{DS} is 1.2 V. g_m is decreasing with larger lengths L as well as g_{DS}.

Figure 3.6 depicts the output characteristics of a PMOS transistor with various gate lengths and 5 μm gate width. The gate-source voltage is fixed at -600 mV. The threshold-voltage roll-off takes effect as well, but is not so obvious. The Early voltage of a PMOS minimum gate-length transistor is in the same range as of an NMOS transistor which is a few volts. The 60 nm PMOS transistor has an Early voltage of only about 0.26 V. Figure 3.7 shows the output conductance g_{DS}.

Figure 3.8 shows the transconductance of PMOS transistors while gate lengths L are

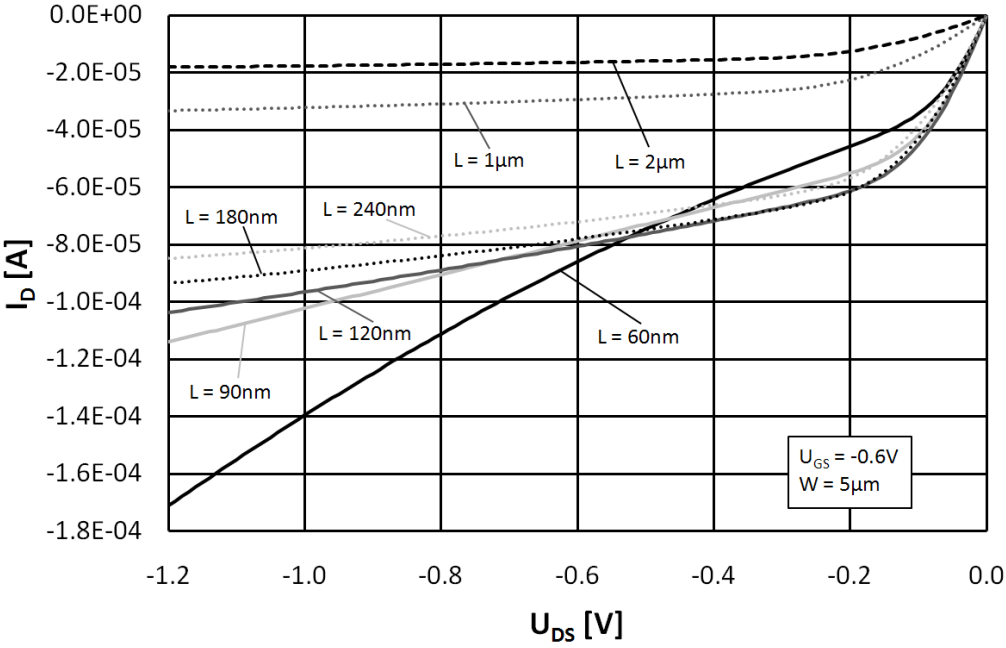

Figure 3.6: PMOS output characteristics at varied gate length L

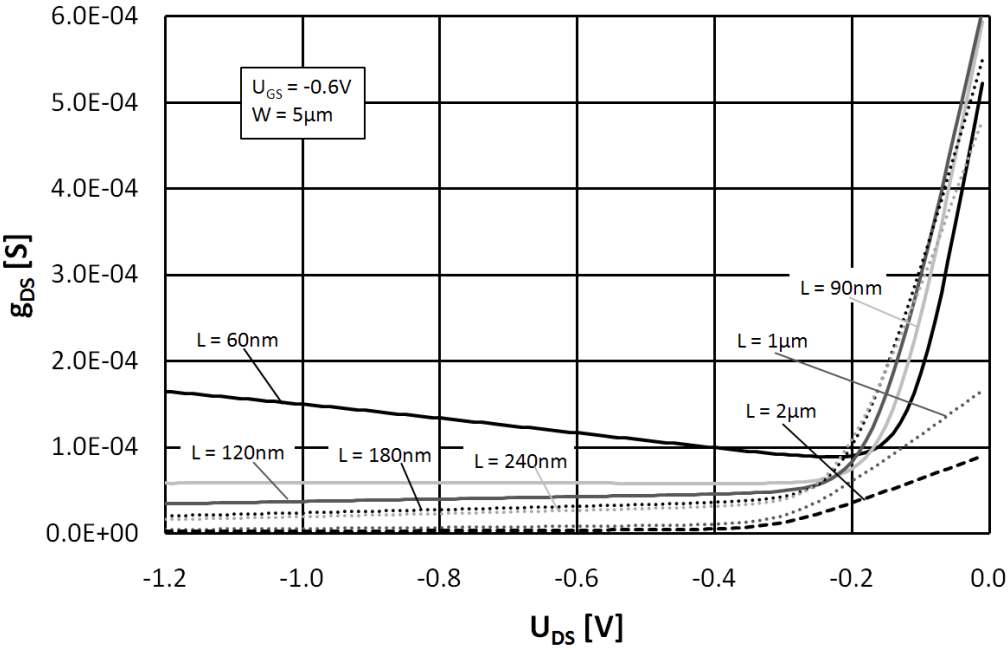

Figure 3.7: PMOS output conductance g_{DS} at varied gate length L

varied. The PMOS transistor has a gate width of 5 μm and is biased with a U_{DS} of 1.2 V. Again a larger L improves the transconductance g_m.

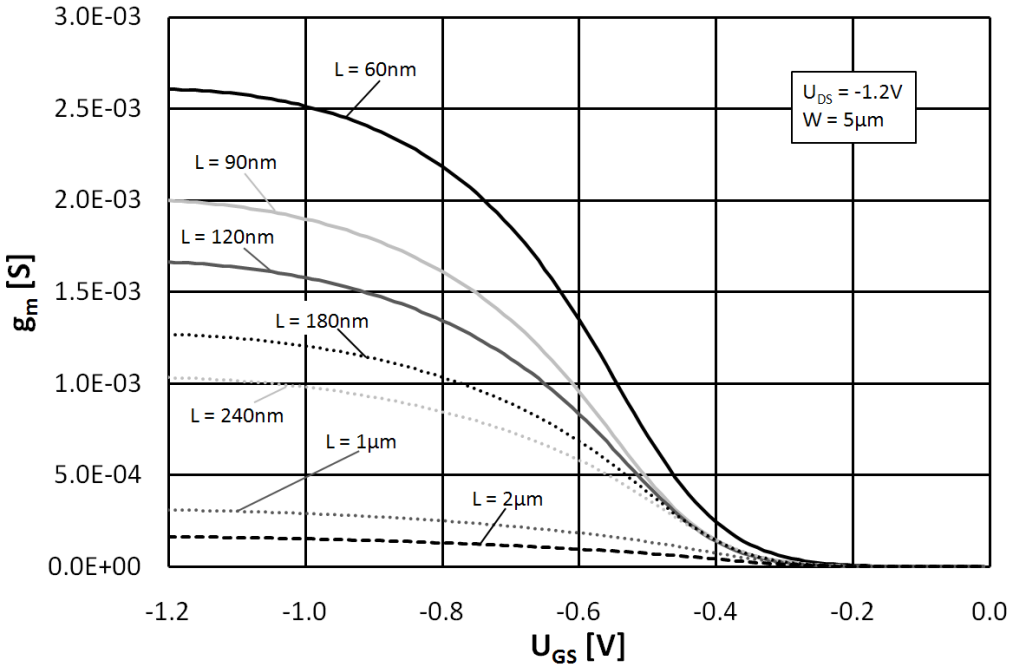

Figure 3.8: PMOS transconductance g_m at varied gate length L

Chapter 4

Current-Mode Filters

4.1 Current-Mode Technique

The application of current-mode signal processing has received remarkable attention and is investigated thoroughly. A strict separation of voltage-mode and current-mode circuits is not possible due to the inherent interrelation of voltage and current. A common classification of voltage-mode circuits is that system relevant signal quantities are represented by voltages. This is in contrast to current-mode circuits, where the important signal quantities are represented by currents [Gil68].

Mixed-signal design in digital low-power nanometer CMOS technology implicates a reduction of the supply voltage and the threshold voltage. In order to keep the static power consumption of digital circuits within limits, the threshold voltage is not scaled by the same factor as the supply voltage (cf. chapter 3). Concerning these limits there are some challenges in voltage-mode circuits. The low supply voltage makes it difficult to design voltage-mode circuits having high linearity and wide dynamic range [All91]. As a consequence of the small supply voltage, voltage-mode circuits suffer increasingly of a small signal headroom and a small effective gate-source voltage (V_{GS}-V_T) [Yua06b]. It is more difficult to achieve high linearity and wide dynamic range circuits. In addition voltage-mode circuits limit signal bandwidth at the existence of high impedance nodes and have low output impedances.

Current-mode circuits gain in importance and offer some advantages over voltage-mode counterparts. Signal quantities are represented by currents, which are not limited by the supply voltage. A wide dynamic range and a good linearity are achievable due to the supply voltage independent signal processing. They have potentially a higher bandwidth due to low impedance nodes [TLC89] and stray-inductance effects show less impact on circuit performance. Low input impedances are important for high bandwidth applications. Current-mode circuits have potentially a high slew-rate and are less sensitive to

power and ground fluctuations [Yua06b].

Signal processing in current-mode circuits is easy as well. Basic mathematical operations, like addition, subtraction, and multiplication by a constant are straight-forward realized [RS89].

The profound investigations in current-mode circuits deliver a huge amount of current-mode applications [Yua06a]. Important developments are optical communications, magnetic recording systems, high-speed bus transceivers, analog-to-digital converters, high-frequency filters, and signal processing. These applications use basic building blocks like current conveyors, current feedback operational amplifiers, sampled data current circuits, or dynamic current mirrors.

4.2 Filter Characterization

Several parameters exist to evaluate the quality and performance of filters. In the following important and applied indicators are presented.

Power consumption P: The power consumption reflects the consumed energy of the filter.

Filter order N: The filter order is related to the width of the transition band. The higher the filter order, the smaller is the transition band, and the greater the effort in filter design is.

-3 dB cut-off frequency f_c: The -3 dB cut-off frequency resides where the signal power at the filter output is the half of the signal power in the pass-band.

Noise: The minimum signal level, that a filter can handle, is dependent on the noise of the filter. The integrated in-band noise is denoted by $\overline{v_{\text{noise}}}$ for voltage noise and $\overline{i_{\text{noise}}}$ for current noise.

1 dB compression point: The 1dB compression point is the power level, at which the output power level is 1 dB below the ideal output power level (cp. fig. 4.1).

Total harmonic distortions (THD): The total harmonic distortions are given at a single frequency excitation as the sum of the powers of the harmonic power components (P_2 to P_k, k=2 ... ∞) to the power of the signal at the fundamental frequency (4.1). The harmonics occur at an integer multiple of the fundamental frequency.

$$THD = \frac{\sum_{k=2}^{\infty} P_k}{P_1} \tag{4.1}$$

At a dominant harmonic x the xth-order harmonics are specified and denoted as HD$_x$. HD$_x$ is defined by the ratio of the power of the xth harmonic to the power of the fundamental frequency [HS03b]. The THD can also be calculated by

$$THD = \sqrt{\sum_{x=2}^{\infty} HD_x^2}. \tag{4.2}$$

Intermodulation distortion: The excitation of a nonlinear system with two signals with the frequencies f_1 and f_2 cause intermodulation products. The frequencies of the modulation products can be derived by

$$Af_1 \pm Bf_2, \tag{4.3}$$

where the sum of A and B is the order of the intermodulation. The 3rd-order intermodulations (IM3) are commonly used and are defined by the output power at the frequencies $2f_1 \pm f_2$ and $2f_2 \pm f_1$.

Third-order intercept point (IP3): The third-order intercept point is a theoretical point, where the signal amplitudes of the fundamental frequencies f_1 and f_2 are equal to the intermodulation products of these signals at the frequencies $2f_1$-f_2 and $2f_2$-f_1. A graphical illustration of the IP3 is given in figure 4.1 [RP03]. The input power at the third-order intercept point is called input third-order intercept point (IIP3), the output power is called output third-order intercept point (OIP3).

Dynamic range (DR): The dynamic range is defined by the minimum signal level caused by noise and the maximum signal level that introduces a certain amount of THD. Typically the signal amplitude is used which causes a THD of 1 % (equal to -40 dB THD) and is called $\hat{a}_{1\%THD}$. The dynamic range is defined as

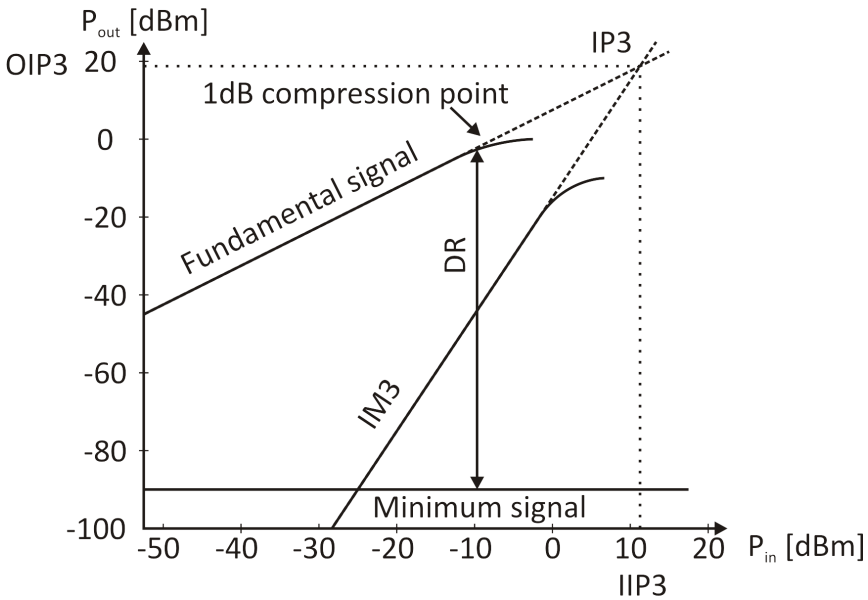

Figure 4.1: Output power versus input power: IP3 and DR

$$DR = \frac{\hat{a}^2_{1\%THD}}{2 \cdot \overline{noise}^2}. \tag{4.4}$$

$\overline{noise}^2$ denotes the integrated in-band noise. A graphical illustration of the DR is also given in figure 4.1. The DR is the difference (in logarithmic scale) of the fundamental signal at 1%THD and the minimal detectable signal of a system.

Figure of merit (FOM): The minimal power P_{min} per pole, that is needed to achieve a sufficient signal-to-noise ratio S/N, is dependent on the thermal noise power and the bandwidth f of a passive filter and is denoted as

$$P_{min} = 8k_BT \cdot f_c \cdot S/N. \tag{4.5}$$

k_B is the Boltzmann's constant and T is the temperature. The figure of merit (FOM_{Filter}) is used as a benchmark for analog filters and is defined by the ratio of the power consumption of the examined filter to the minimum power P_{min}:

$$FOM_{Filter} = \frac{P}{P_{min}} = \frac{P}{8k_BT \cdot f_c \cdot N \cdot DR}. \tag{4.6}$$

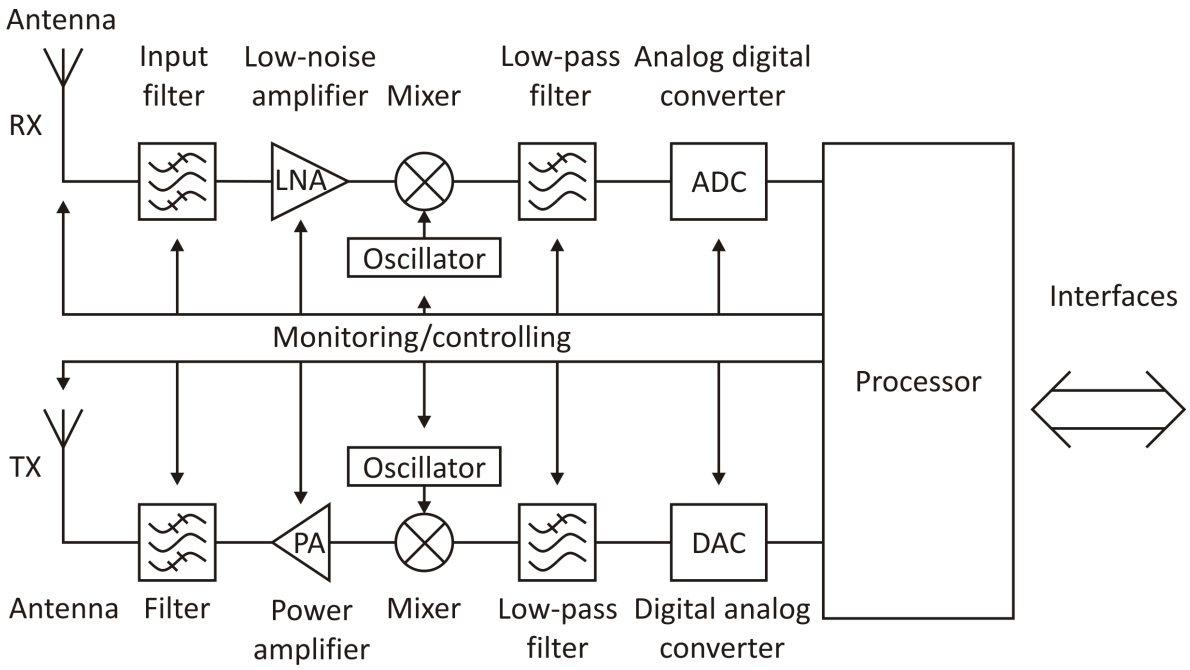

Figure 4.2: Software defined radio - receive and transmit path

In eqn. (4.6) P is the power consumption of the observed filter, k_B denotes Boltzmann's constant, T is the temperature, f_c is the -3 dB cut-off frequency, N is the number of poles, and DR is the dynamic range [TMG02].

4.3 Motivation

Radio communication is an important and fast growing domain in information and communication technologies and electronic industries. Nowadays, an electronic device, such as a mobile phone or a portable computer, combines several wireless communication standards. The idea to concentrate all communication standards on one chip is called Software Defined Radio (SDR). A software defined radio is able to reconfigure the radio interface by downloading any new wireless standard. Another definition is that a SDR is reconfigurable at any level in the radio protocol stack by software [Tut99]. A SDR system is able to change an existing standard or even new standards can be downloaded. A possible SDR solution is depicted in figure 4.2 [SDR10]. The signal is received by an antenna, filtered by an input filter and amplified by a low-noise amplifier. The mixer converts the signal directly into the base-band and the filter selects the desired bandwidth before the analog-digital converter samples the signal and hands it over to the processor.

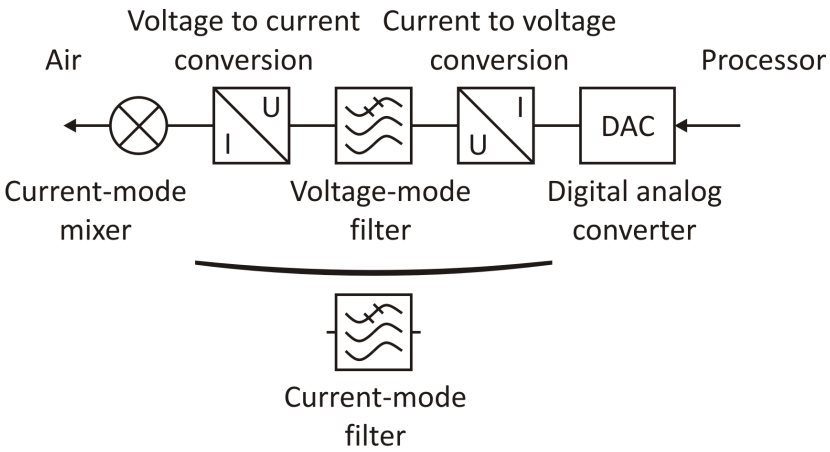

Figure 4.3: Detailed transmit path of the SDR system

The transmission of a signal starts at the digital-analog converter, fed with data by the processor. A filter shapes the analog signal from the DAC and the mixer does the up-conversion into the rf-band. A power amplifier drives the antenna, again filtering is necessary. The reconfiguration and adaption to different standards is done by the processor unit via monitoring and controlling networks. Filter bandwidths or corner frequencies, oscillator frequencies and LNA or PA gain are programmable and set by the processor. These monitoring and controlling networks are the core of a SDR system [RDB+09].

The proposed current-mode filter is an element of the transmit path of a SDR system. The areas of application in wireless systems are Bluetooth and Wideband Code Division Multiple Access (WCDMA) applications. The details of the transmit path are depicted in fig. 4.3. The target design uses a current-steering DAC and a current-mode mixer. The use of a conventional voltage-mode filter necessitates two signal transformations. Before the filter the voltage-mode signal has to be transferred into a current-mode signal and after the filter the voltage-mode signal has to be transferred into the current-mode domain again. The major targets of the current-mode filter design are saving of silicon area and power consumption. This is accomplished by the savings of the two transformation blocks and the low-voltage operation that is applicable for deep sub-micron and nanometer CMOS technology.

The supply voltage of nanometer CMOS technology is low, which results in a limited dynamic range in voltage-mode filters. It will be investigated, to what extent current-mode techniques impact the dynamic range of filters at low supply voltages. The power consumption of the filter impacts the dynamic range as well. Due to the fact that in a current-mode filter the signal quantities are represented by currents, the current consumption is proportional to the signal swings and the necessary bias conditions to avoid distortions. However, a tradeoff between dynamic range and power consumption is required.

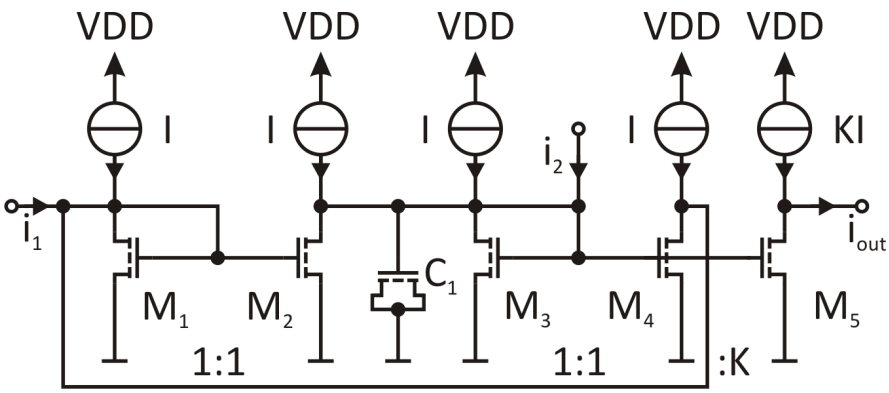

Figure 4.4: Continuous-time current-mode differential integrator [ZLA93]

4.4 State-of-the-Art

Analog filters are essential blocks in analog circuit design, hence there exist many filter publications. In the following the state-of-the-art is given with the focus on current-mode low-pass filters. The publications are sorted chronologically.

A continuous-time current-mode integrator is described in [LZAL91] for high-frequency low-power filters, which are used in video signal processing applications and magnetic disk-drive read channels. The current-mode integrator is designed in 2 μm standard digital CMOS technology and is applied in a fifth-order leapfrog all-pole low-pass filter. The filter cut-off frequency is tunable over a wide range from 25 MHz to 50 MHz by changing the bias currents and thus changing the transconductances of the applied integrators. At a -3 dB cut-off frequency of 30 MHz the filter dissipates 24 mW at a 5 V supply voltage. The total harmonic distortions are given at a cut-off frequency of 30 MHz and an input signal of 1 MHz. A THD of -55 dB is caused by an input signal amplitude of 50 mA_p.

A fifth-order continuous-time current-mode low-pass filter based on current-mode g_m-C integrators, which are suitable for the design of low-voltage high-frequency filters, is presented in [LZAL93]. The low-pass filter has a tunable -3 dB cut-off frequency from 24 to 42 MHz. At a -3 dB cut-off frequency of 40 MHz an input signal amplitude of 30 μA causes 1 % total intermodulation distortion. Together with a total integrated rms (root mean square) noise of 7.4 nA_{rms} over 40 MHz a DR of 69 dB is obtained. The filter is designed in 2 μm standard digital CMOS technology and has a power dissipation of 25.5 mW at a supply voltage of 5 V. The active chip area of the low-pass filter is 0.28 mm^2.

A third-order Chebyshev low-pass filter for video signal processing and magnetic disk-drive read-channel systems is described in [ZLA93]. In the filter continuous-time current-mode integrators as depicted in fig 4.4 are applied. The low-pass filter is designed in

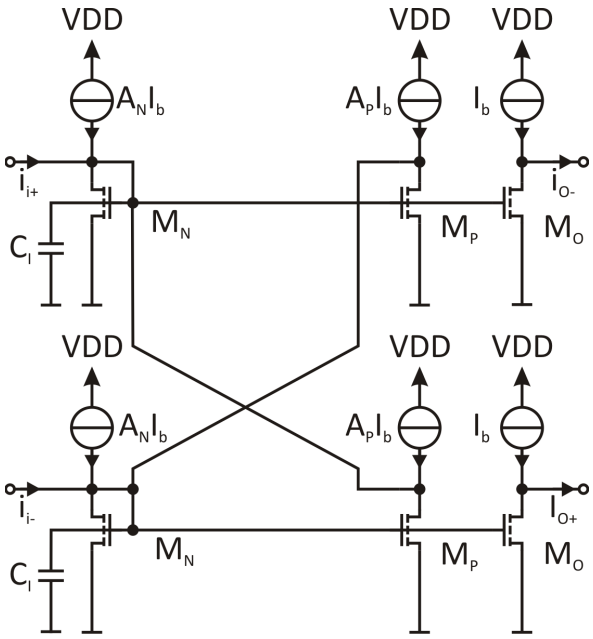

Figure 4.5: Fully differential current-mode integrator [SS96]

1.2 μm CMOS technology and requires 3000 μm^2 active area per pole. It has a supply voltage of 3 V while consuming 6 mW power per pole. The -3 dB cut-off frequency is 125 MHz. The filter produces 1 % THD at an input signal current of 300 μA_p and a total rms input referred noise over a bandwidth of 100 MHz of 182 nA_{rms}. This results in an DR of 62 dB.

A sixth-order Bessel low-pass filter in standard 2 μm CMOS technology, which occupies 0.77 mm^2 active area is demonstrated in [SS96]. The tunable -3 dB cut-off frequency ranges from 7.5 to 13.5 MHz. The filter consumes 4 mW at a supply voltage of 3.3 V. The over 12 MHz integrated output noise results in 714 nA_{rms}. 1 % THD is reached at an output signal amplitude of 440 μA_p and the DR calculates to 52 dB. The power supply rejection ratio PSRR at VSS and VDD is 24 dB. The sixth-order Bessel low-pass filter is based on the basic integrator shown in figure 4.5.

A fifth-order Chebyshev low-pass filter is introduced in [ZA96]. The filter has a power consumption of 75 μW/pole at a supply voltage of 1.5 V. The -3 dB cut-off frequency is tunable from 300 kHz to 1 MHz. The DR is 67 dB and the total integrated in-band noise is 3.53 nA_{rms} at a -3 dB cut-off frequency of 525 kHz. The PSRR is at minimum 40 dB and the common mode rejection ratio (CMRR) is 70 dB within the pass-band. The Chebyshev filter is designed and fabricated in 1.2 μm n-well CMOS process and requires 0.1 mm^2 chip area per pole.

A low-voltage current-mode integrator using voltage companding is applied in a fourth-order Chebyshev low-pass filter [PFE96]. The integrator is only composed of MOSFET

transistors and lacks of any functional capacitors, and hence fits for integration in digital CMOS technology very well. The cut-off frequency can be tuned from 20 Hz to 20 kHz. The filter consumes 1.16 μW per pole at a -3 dB cut-off frequency of 5 kHz. The dynamic range is 55 dB. Unfortunately the used detailed CMOS process is not mentioned.

A 3 V analog CMOS current-mode continuous-time filter with a negative resistance load is proposed in [HY96]. The designed third-order Butterworth low-pass filter has a -3 dB cut-off frequency of 50 MHz, a power consumption of 2.4 mW per pole at a 3 V supply voltage. The filter occupies 1 mm^2 in a 1.5 μm n-well standard CMOS technology.

A 5th-order elliptic current-mode low-pass filter with a g_m-C topology is presented in [KKH98]. The filter has a cut-off frequency of 50 MHz and it has a power consumption of 91 mW at a 3.3 V supply voltage. A low distortion level is achieved by scaling for minimum distortion and dynamic biasing for linearization. The current-mode filter is designed in 0.5 μm CMOS and has a core size of 0.56 mm^2. A 15 MHz input current signal of 500 μA_{pp} causes 55 dBc THD and the DR results in 60 dB.

An eighth-order continuous-time current-mode Butterworth low-pass filter is introduced in [DL01]. The filter is realized with simple current amplifiers and cascade connection of current-mode Sallen-Key biquads. The tuning range covers 237 to 326 MHz with programmable capacitor arrays for frequency tuning, the nominal -3 dB cut-off frequency is 250 MHz. The power consumption of the filter is 24 mW and the supply voltage is 1 V. The THD is -53.5 dB at an input signal of 300 mV_{pp}, however the voltage to current conversion is done by a not specified resistance. The Butterworth filter is designed and simulated in 0.25 μm CMOS technology, the estimated active chip area is 2.46 mm^2.

A low-voltage digitally programmable second-order current-mode low-pass filter which applies a digitally programmable current-mode integrator is presented in [Ham03]. The filter with a -3 dB cut-off frequency of about 80 MHz is integrated in 0.8 μm CMOS technology and needs a supply voltage of 3 V.

A fifth-order Butterworth low-pass filter by applying a current-mode integrator for low-frequency continuous-time filters is demonstrated in [YHCH03]. The -3 dB cut-off frequency is tunable from 160 Hz to 5.6 kHz. The filter consumes approximately 20 mW at a supply voltage of 5 V. The filter is designed and fabricated in an AMI 1.2 μm n-well CMOS process and occupies an active area of 0.08 mm^2 per pole.

A current-mode square-root domain filter with a novel current-mode geometric-mean and current squarer circuit is presented in [KR03]. The filter is used in current controlled oscillators and low-power low-voltage current-mode video frequency filters. The circuit is designed in 0.35 μm AMS CMOS technology, has a supply voltage of 3 V and a -3 dB cut-off frequency range from 1 MHz to 5 MHz. The THD is in the worst case -43 dB for an input amplitude equal to the dc bias current.

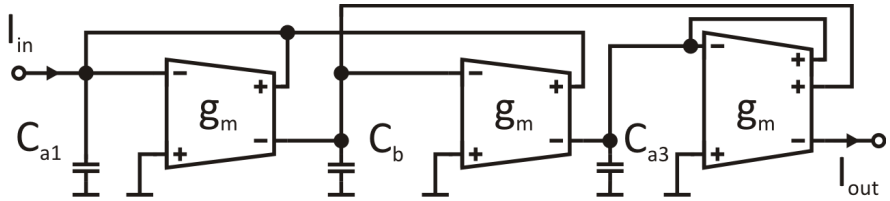

Figure 4.6: Current-mode third-order single-ended Butterworth low-pass g_m-C filter [HCLS06]

A digitally programmable analog current-mode filter for VHF/UHF applications is introduced in [OCA06]. The third-order current-mode Butterworth low-pass filter is tunable from 42 to 215 MHz and has a supply voltage of 2 V at a power consumption of 3.73 mW per pole. A differential input signal of 120 μA causes 1 % THD and the total rms input referred noise is 197 nA_{rms}. A DR of 53 dB is achieved. The filter is designed and fabricated in 0.35 μm n-well CMOS technology and occupies 0.025 mm^2 active area.

A current-mode third-order LC Butterworth low-pass filter using g_m-C techniques is realized in [HCLS06]. An outline of the filter structure is depicted in figure 4.6. The low-pass filter has a -3 dB cut-off frequency of 200 MHz and dissipates 16.77 mW power at a supply voltage of 1.8 V. A 200 MHz input signal of 0.4 mA causes total harmonic distortions of -46.5 dB. The filter is implemented in the TSMC 0.18 μm 1P6M process and the core area occupies 0.0303 mm^2.

A third-order current-input/output Butterworth low-pass filter for software-radio applications is presented in [KZ07]. The filter is fabricated in 65 nm CMOS technology and occupies an active chip area of 0.092 mm^2. The supply voltage is 1.2 V and the power consumption is 6.8 mA. The filter has two -3 dB cut-off frequencies which are 0.98 MHz and 4.06 MHz. The filter attenuates the signal slightly by 3.5 dB. The total integrated output noise is 29 nA_{rms} and 54 nA_{rms} for 0.98 MHz and 4.06 MHz, respectively. The dynamic range at a bandwidth of 0.98 MHz is 72.5 dB and at a bandwidth of 4.06 MHz it is 66.6 dB.

Another current-mode filter for software-radio applications is presented in [KYZ08]. The 3rd-order Butterworth filter consumes 6.3 mW at a supply voltage of 1.2 V. The filter is switchable between the -3 dB cut-off frequencies of 0.95 MHz and 3.75 MHz and reaches a dynamic range of 56.7 dB and 52.6 dB, respectively. An IIP3 of 2.13 mA is achieved in both frequency domains. The switchable filter is designed in 65 nm CMOS technology and needs 0.54 mm^2 active chip area.

A fifth-order low-pass continuous-time filter for low-voltage applications is introduced in [DBD08]. The filter has a cut-off frequency of 10 MHz and a power consumption of 5 mW at a supply voltage of 3 V. A DR greater than 50 dB is reached at an input signal of 20 μA and the PSRR is slightly larger than 50 dB. The filter is simulated in 1 μm

CMOS technology.

A fifth-order low-voltage CMOS current-mode low-pass filter is presented in [LP08]. The filter is designed in 0.35 μm BiCMOS process and has a power consumption of 21.1 μW at a supply voltage of 1.5 V. The -3 dB cut-off frequency is 482 kHz and the input referred noise at 10 kHz is 4 pA/$\sqrt{\text{Hz}}$. The dynamic range is 40.6 dB.

4.5 Realization of Current-Mode Filters

4.5.1 A 3rd-Order Current-Mode Continuous-Time Low-Pass Filter Using a Chip Area Saving Strategy

A 3rd-order current-mode continuous-time Butterworth low-pass filter is realized [UZ09a]. The aimed -3 dB cut-off frequencies are 1.1 MHz and 4.4 MHz observing the target specifications. Due to the relatively low cut-off frequencies big capacitors for the filter poles are needed. In order to save expensive chip area a capacitor saving strategy is developed. A test chip of the current-mode filter is designed and fabricated in 65 nm CMOS technology and its behavior is characterized.

The block diagram of the low-pass filter is depicted in figure 4.7. The filter has a differential topology. It has 3 basic building blocks, whereas the first two blocks, a 1st-order current-mode low-pass filter and a current-mode integrator represent a 2nd-order low-pass filter. The last block is another 1st-order current-mode low-pass filter to obtain an overall 3rd-order current-mode low-pass filter.

Current-mode integrator Integrators are essential parts in active filter design and their characteristics contribute to the filter performance and quality directly. In current-mode circuits current-mode integrators are of importance. Figure 4.8 shows the implemented fully differential current-mode integrator, which is an innovative modification of [SS96]. Figure 4.8(a) represents the detailed schematics of the current-mode integrator, the equivalent circuit is depicted in figure 4.8(b).

The integrator is assembled of two cross coupled current mirrors. The cross coupling is done between the transistors M_{1a} and M_{2b} as well as M_{1b} and M_{2a}. The cross coupling effects a high differential gain and a low common-mode gain. The unity-gain frequency is switchable between two frequencies, hence switchable capacitors (C_{1a}, C_{1b}, C_{2a}, C_{2b}) are implemented. The overall filter has relatively low -3 dB cut-off frequencies of 1.1 MHz and 4.4 MHz which need large integrating capacitors. Hence, the capacitors are an

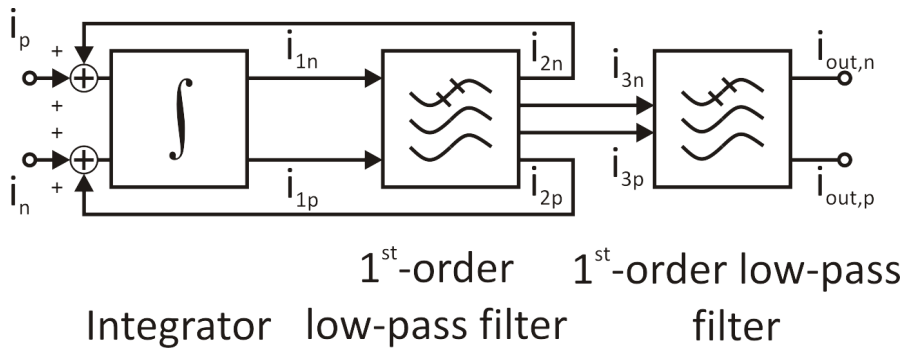

Figure 4.7: Block diagram of the 3rd-order current-mode Butterworth low-pass filter using a chip area saving strategy

important factor of integrated filters and need large chip area. The innovation is the adding of the resistors R_{1a} and R_{1b} to save chip area by keeping the characteristics of the integrator circuit. The transfer function of the modified integrator is derived in the following.

For the formation of the mathematical model figure 4.8(b) is used. The connections of I_{2n} and I_{2p} are used for feedback purposes (compare to figure 4.7) and are not important for the integrator functionality. Hence, the input currents I_{2n} and I_{2p} are supposed to be 0. For the calculations the switches for the frequency selection are open and only the capacitances C_{2a} and C_{2b} are active. The input currents i_p and i_n are given by

$$i_p = u_{GS1b} g_{m1b} + \frac{u_{GS1a} g_{m2a}}{1 + sR_{1a}C_{2a}} + g_{DS2a} u_{GS1b} + \frac{u_{GS1b}}{R_{1b} + \frac{1}{sC_{2b}}} \tag{4.7}$$

and

$$i_n = u_{GS1a} g_{m1a} + \frac{u_{GS1b} g_{m2b}}{1 + sR_{1b}C_{2b}} + g_{DS2b} u_{GS1a} + \frac{u_{GS1a}}{R_{1a} + \frac{1}{sC_{2a}}}. \tag{4.8}$$

An integrator behavior is realizable due to equal circuit elements: $M_{1a} = M_{1b} = M_{2a} = M_{2b}$; $M_{3a} = M_{3b}$; $R_{1a} = R_{1b} = R_1$; $C_{1a} = C_{1b} = C_1$; $C_{2a} = C_{2b} = C_2$. The bias currents I_{B1a}, I_{B1b}, I_{B2a}, and I_{B2b} are equal as well as I_{B3a} and I_{B3b}. By using these element parameters, solutions for u_{GS1a} and u_{GS1b} can be found which are inserted in the equations for the output currents

$$i_{1n} = -\frac{g_{m3} u_{GS1b}}{1 + R_1 C_2 s} - u_{DS3} g_{DS3} \tag{4.9}$$

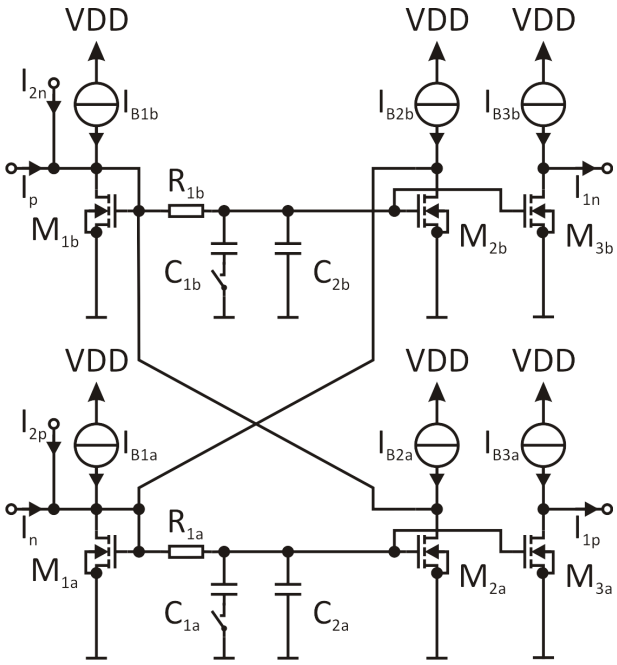

(a) Current-mode integrator - schematics

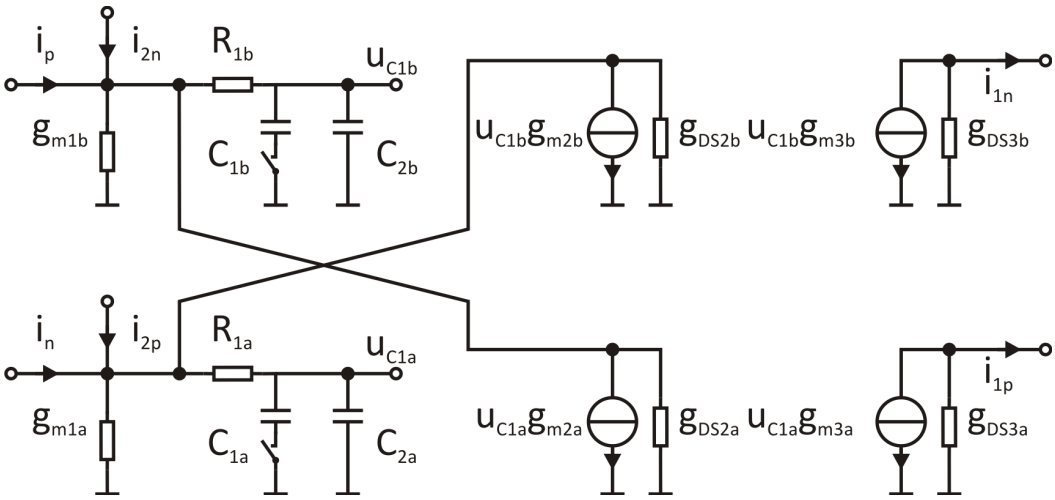

(b) Current-mode integrator - equivalent circuit

Figure 4.8: Current-mode integrator with capacitance saving strategy

and

$$i_{1p} = -\frac{g_{m3} u_{GS1a}}{1 + R_1 C_2 s} - u_{DS3} g_{DS3}. \tag{4.10}$$

Finally the transfer function of the current-mode integrator by using (4.10) and (4.9)

results in

$$H_I(s) = \frac{i_{1p} - i_{1n}}{i_p - i_n} = \frac{g_{m3}}{g_{DS2} + (R_1(g_{m1} + g_{DS2}) + 1)C_2 s}. \tag{4.11}$$

The innovation of the modification is clearly visible in (4.11). In the denominator a supplementary element R_1 appears in addition to C_2 and the transconductance of M_1 and M_3, which manage the unity-gain frequency of the integrator. By increasing the resistor R_1, a huge amount of chip area can be saved. Naturally the resistor increases the noise level of the integrator, hence a trade-off between noise and chip area has to be made. Low unity-gain frequencies can be realized by increasing the transconductance of M_1 as well. A high transconductance is realized by raising the transistor bias current, which deteriorates the power consumption of the integrator. Summarized the resistor R_1 in the current-mode integrator enables to save chip area and power dissipation at the expense of a higher noise level.

First-order current-mode low-pass filter The first-order low-pass filter is shown in figure 4.9(a), which consists of two current mirrors due to the differential structure of the overall low-pass filter. The dominant pole is defined by the combination of R_{2a}, C_{3a}, and C_{4a} as well as R_{2b}, C_{3b}, and C_{4b}. The split and switchable capacitors C_{3a}, C_{4a}, C_{3b}, and C_{4b} are implemented to obtain two different -3 dB cut-off frequencies of the 1st-order low-pass filter. A differential design of the entire 3rd-order low-pass filter needs the equality of upper and the lower half: $M_{4a} = M_{4b}$, $M_{5a} = M_{5b}$, $M_{6a} = M_{6b}$, $C_{3a} = C_{3b} = C_3$, $C_{4a} = C_{4b} = C_4$, $R_{2a} = R_{2b} = R_2$, $\mathrm{I}_{B4a} = \mathrm{I}_{B4b}$, $\mathrm{I}_{B5a} = \mathrm{I}_{B5b}$, and $\mathrm{I}_{B6a} = \mathrm{I}_{B6b}$. The transfer function of the 1st-order current-mode low-pass filter is

$$H_{LP}(s) = \frac{i_{2p} - i_{2n}}{i_{1p} - i_{1n}} = \frac{1}{C_4(R_2 + \frac{1}{g_{m4}}) + 1}. \tag{4.12}$$

It is assumed, that only the capacitor C_4 is active.

Two outputs are needed for the connections to the following block and the feedback ($\mathrm{i}_{2n/p}$ and $\mathrm{i}_{3n/p}$). Since a single current output cannot be used for both purposes due to the Kirchhoff's circuit laws, two output transistors of the current mirror are used. Therefore additional bias currents are necessary and increase the overall current consumption.

3rd-order current-mode Butterworth low-pass filter The current-mode integrator and the current-mode 1st-order low-pass filter in negative feedback generates a 2nd-order low-pass filter. The 2nd-order low-pass filter has two outputs (compare to figure 4.7):

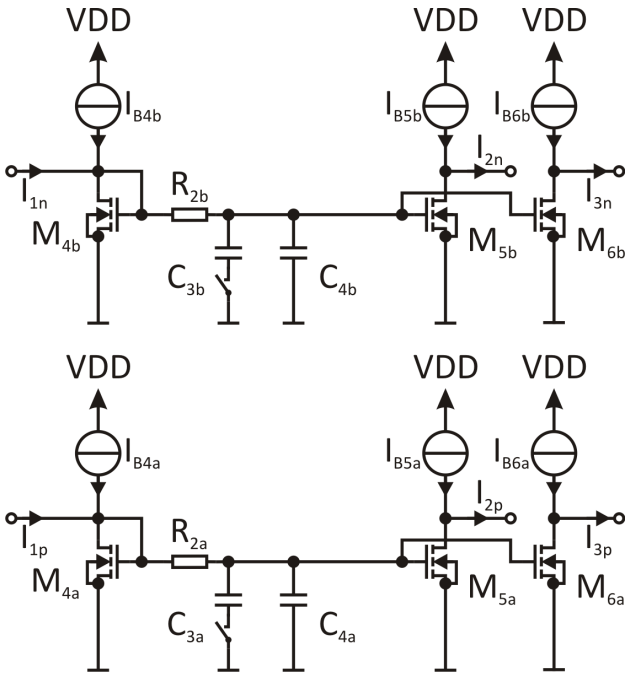

(a) First-order current-mode low-pass filter - schematics

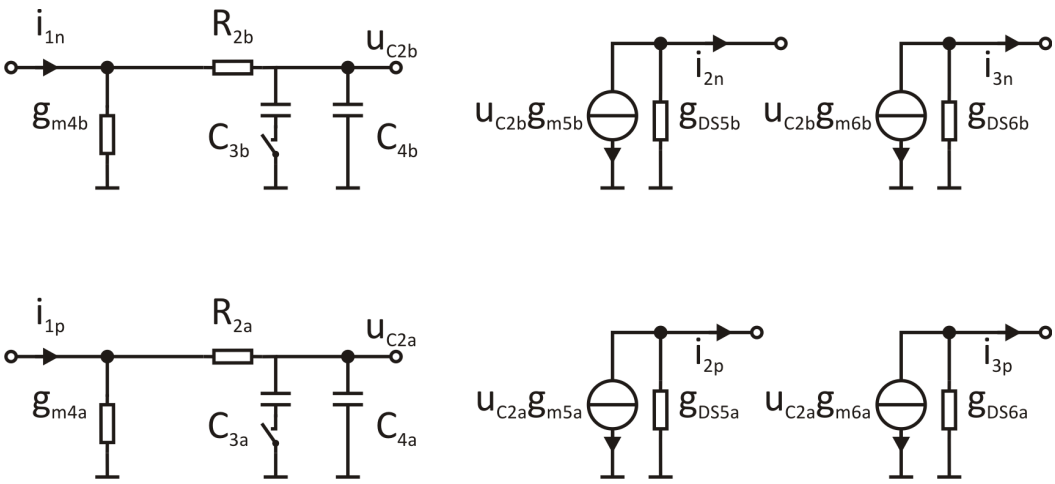

(b) First-order current-mode low-pass filter - equivalent circuit

Figure 4.9: First-order current-mode low-pass filter

I_{2n} and I_{2p} for feedback purposes and I_{3n} and I_{3p} is connected to the following 1st-order low-pass filter. The transfer function results in

$$H_{LP2} = \frac{1}{\alpha s^2 + \beta s + \gamma}. \tag{4.13}$$

The coefficients α, β, and γ are denoted as

$$\alpha = \frac{C_2 C_4}{g_{m3} g_{m4}} (R_2 g_{m4} + 1)(R_1(g_{m1} + g_{DS2}) + 1), \tag{4.14}$$

$$\beta = \frac{C_2}{g_{m3}} (R_1(g_{m1} + g_{DS2}) + 1) + \frac{C_4 g_{DS2}}{g_{m3} g_{m4}} (R_2 g_{m4} + 1), \tag{4.15}$$

and

$$\gamma = 1 + \frac{g_{DS2}}{g_{m3}}. \tag{4.16}$$

Due to the non-ideal manner of the current-mode integrator and the open-loop gain, is finite (lossy integrator). A limited open-loop gain may deteriorate the entire filter performance severely. To estimate the impact of the non-ideal integrator on the filter performance the quality factors (Q) of the 2nd-order low-pass filter using a lossy integrator is compared to the ideal 2nd-order low-pass filter

$$H_{ideal}(s) = \frac{1}{1 + s\tau + s^2 \tau \tau_2}. \tag{4.17}$$

τ denotes the time constant of the ideal integrator and τ_2 the time constant of the ideal 1st-order low-pass filter. The transfer function of a 2nd-order low-pass filter is calculated by using the lossy integrator transfer function

$$H_{lossy}(s) = \frac{A_0}{1 + A_0 \tau' s}. \tag{4.18}$$

τ' is the time constant of the lossy integrator. The transfer function of the 2nd-order low-pass filter by using (4.18) and a 1st-order low-pass filter with the time constant τ_2' results in

$$H(s) = \frac{A_0}{1 + A_0 + s(\tau_2' + A_0 \tau') + A_0 \tau' \tau_2' s^2}. \tag{4.19}$$

The quality factor of the ideal 2nd-order low-pass filter in (4.17) results in

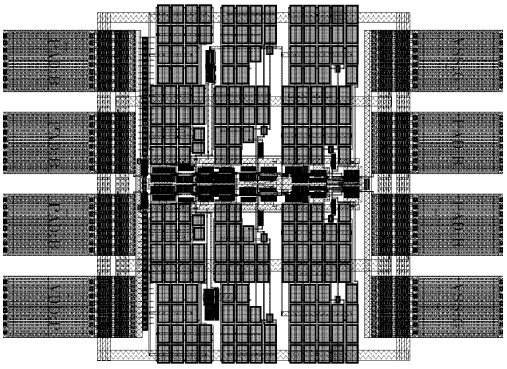

(a) Layout plot

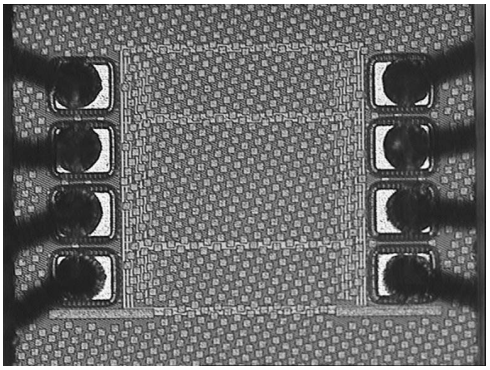

(b) Chip photograph

Figure 4.10: 65 nm CMOS 3rd-order Butterworth low-pass filter [UZ09a]

$$Q = \sqrt{\frac{\tau_2}{\tau}}. \tag{4.20}$$

In the 3rd-order Butterworth low-pass filter the embedded 2nd-order low-pass filter has a Q of 1 and induces

$$\tau = \tau_2. \tag{4.21}$$

The application of the lossy integrator in the 2nd-order low-pass filter (eqn. (4.19)) under the assumption of (4.21) leads to a quality factor Q_{lossy} of

$$Q_{lossy} = \sqrt{\frac{A_0}{1 + A_0}}. \tag{4.22}$$

The open-loop gain A_0 of the lossy integrator is

$$A_0 = \frac{g_{m3}}{g_{DS2}} \tag{4.23}$$

as given in (4.11). Observing (4.23), an open-loop gain of at least 10 is reasonable. The resulting Q is then at least 0.953 instead of 1 which means the relative deviation of Q is at most of -4.7 %. The lossy integrator does not deteriorate the filter performance significantly.

The required 3rd-order low-pass Butterworth filter is realized by connecting another 1st-order low-pass filter as presented in figure 4.9. The resulting transfer function is

$$H_{Filter}(s) = H_{LP2}(s) \cdot H_{LP}(s) \tag{4.24}$$

by inserting (4.13) and (4.12).

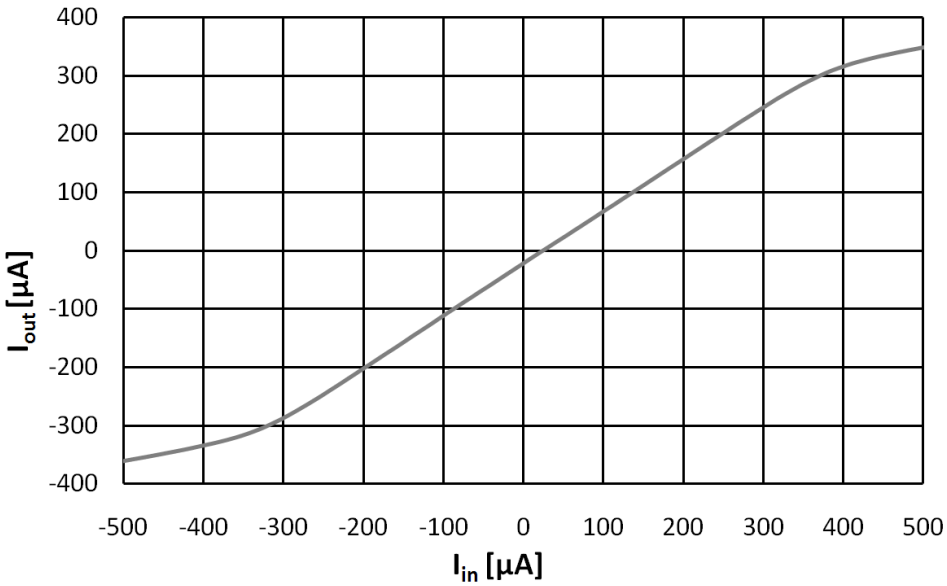

Figure 4.11: Chip area saving 3rd-order low-pass filter - differential DC characteristics

Experimental results The described 3rd-order Butterworth low-pass filter is designed and fabricated in 65 nm low-power CMOS technology [UZ09a, UZ07a] as described in chapter 3. Figure 4.10(a) shows the layout of the filter and figure 4.10(b) depicts the chip photograph, which is not illustrative due to the planarization and passivation layers. The filter has two pins for VSS, one for VDD, two for the differential input, two for the differential output, and one pin is used to switch between the two cut-off frequencies. The filter occupies 350 μm $\times$ 220 μm active area and including the pads 500 μm $\times$ 360 μm. The filter is powered with 1.2 V supply voltage and consumes 10.3 mA, which refers to 12.36 mW, at either cut-off frequency. The frequency dominating elements are C_1 = 7.4 pF, C_2 = 20.6 pF, R_1 = 13.5 kΩ, C_3 = 4 pF, C_4 = 11 pF, R_2 = 11 kΩ, C_5 = 4 pF, C_6 = 22 pF, and R_3 = 7 kΩ. For the resulting cut-off frequencies the parasitic gate-source capacitances and the capacitances from the switches have to be considered.

The differential DC measurement is depicted in figure 4.11. The low-pass filter shows a good linearity between an input current of -360 μA and +360 μA and an offset of about -20 μA.

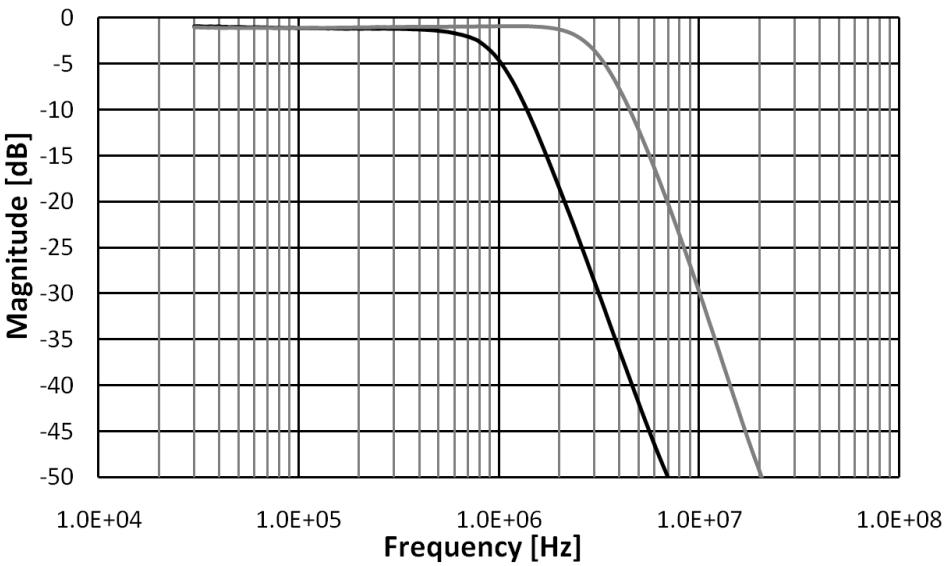

(a) Amplitude response

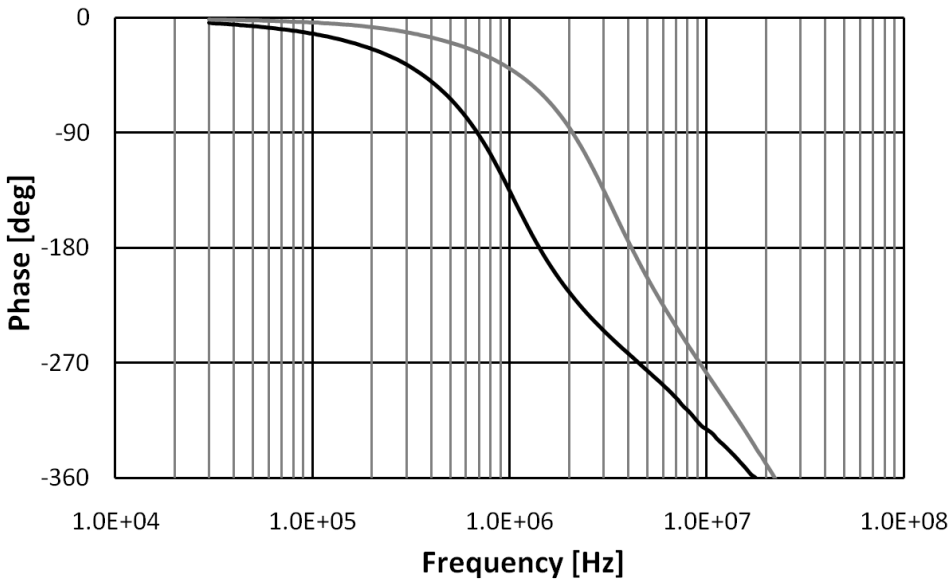

(b) Phase response

Figure 4.12: Chip area saving 3rd-order low-pass filter - frequency response

The AC characteristics is shown in figure 4.12. The amplitude response as shown in figure 4.12(a) exhibits the two cut-off frequencies (f_c) of 1.12 MHz and 4.46 MHz. The DC gain is -0.93 dB. The phase response is shown in figure 4.12(b).

The distortions are determined by single-tone and two-tone measurements. In the single-tone measurement the amplitude of the input current is varied at a frequency f_{tone} at 100 kHz at a filter bandwidth of 1.12 MHz. The applied frequency f_{tone} is 400 kHz at the

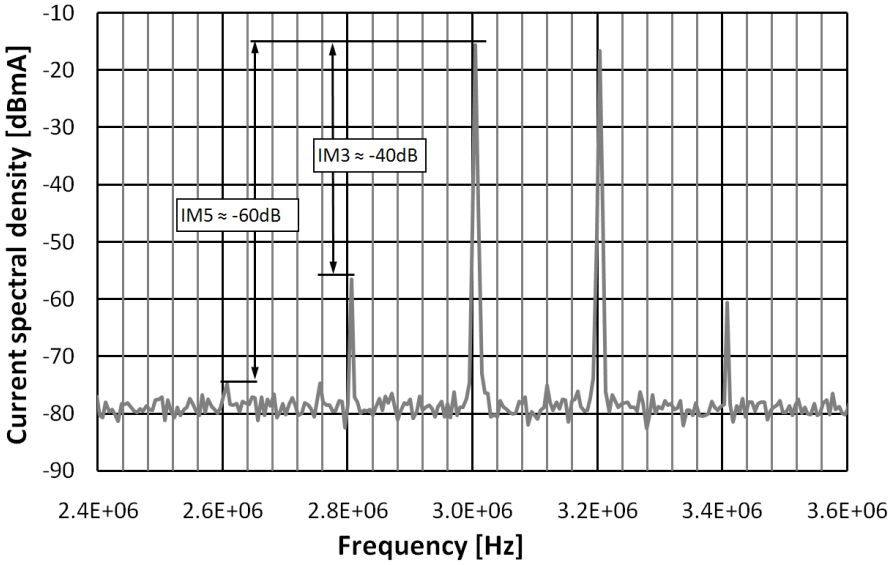

Figure 4.13: Chip area saving 3rd-order low-pass filter - two-tone measurement at f_c= 4.46 MHz

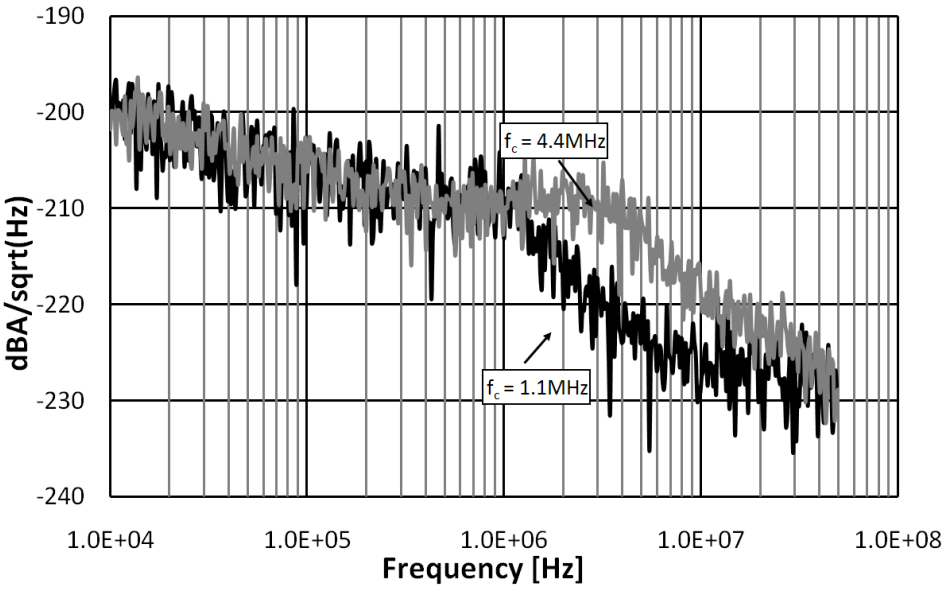

Figure 4.14: Chip area saving 3rd-order low-pass filter - spectral noise current density

filter bandwidth of 4.46 MHz. Table 4.1 shows the 3rd-order harmonic distortions (HD3) in dBc (decibels relative to the carrier) against the input amplitude current.

The total harmonic distortions are measured with a frequency of 100 kHz and 400 kHz at the -3 dB cut-off frequencies of 1.12 MHz and 4.46 MHz, respectively. The results are shown in table 4.2.

Table 4.1: Chip area saving 3rd-order low-pass filter - measured HD3

$\hat{I}_{in}$ Signal frequency	$\mathbf{f_c = 1.12\,MHz}$ $f_{tone} = 100\,kHz$	$\mathbf{f_c = 4.46\,MHz}$ $f_{tone} = 400\,kHz$
150 μA	-55.6 dBc	-61.4 dBc
200 μA	-58.1 dBc	-62.4 dBc
250 μA	-54.2 dBc	-51.1 dBc
300 μA	-44.1 dBc	-42.3 dBc

Table 4.2: Chip area saving 3rd-order low-pass filter - measured THD1%

f_c	$\hat{I}_{THD1\%}$
1.12 MHz	340 μA_p
4.46 MHz	330 μA_p

A two-tone measurement is used for a further distortion and intermodulation characterization. The filter is tested in both cut-off frequency settings. At f_c of 1.12 MHz two sinusoidal signals of 600 kHz and 700 kHz are applied and at f_c of 4.46 MHz two sinusoidal signals of 3.0 MHz and 3.2 MHz. In both -3dB cut-off frequency configurations an input amplitude of 180 μA_p of one input signal caused an IM3 of -40 dBc. Figure 4.13 depicts the two-tone measurement at a filter -3 dB cut-off frequency of 4.46 MHz. The input current of 180 μA_p at -40 dBc corresponds to a 3rd-order input intercept point (IIP3) of 1.8mA_p.

The noise measurement is shown in figure 4.14 for both -3 dB cut-off frequency settings. The current noise spectral density has a dominant contribution of the 1/f noise, which goes approximately up to 200 kHz. The spectral output-current noise density in the pass-band is about 31.16 pA/$\sqrt{\text{Hz}}$.

The analyses of the rating and performance is done by the criterions in chapter 4.2. At a -3 dB cut-off frequency of 1.12 MHz the DR is 77.2 dB and the FOM_{Filter} is 2115. At the other bandwidth of 4.46 MHz the DR is 70.9 dB and the FOM_{Filter} is 2304. A summary of the achieved filter performance is given in table 4.3 [UZ09a, UZ07a].

Table 4.3: Chip area saving 3rd-order low-pass filter - performance summary

Technology	65 nm CMOS	
Chip area	0.077mm^2	
Supply voltage	1.2 V	
Power consumption	12.36 mW	
DC gain	-0.93 dB	
-3 dB cut-off frequency	1.12 MHz	4.46 MHz
$\hat{I}$ @ THD1%	340 μA$_p$	330 μA$_p$
IIP3	1.8mA$_p$	
DR	77.2 dB	70.9 dB
FOM$_{Filter}$	2115	2304

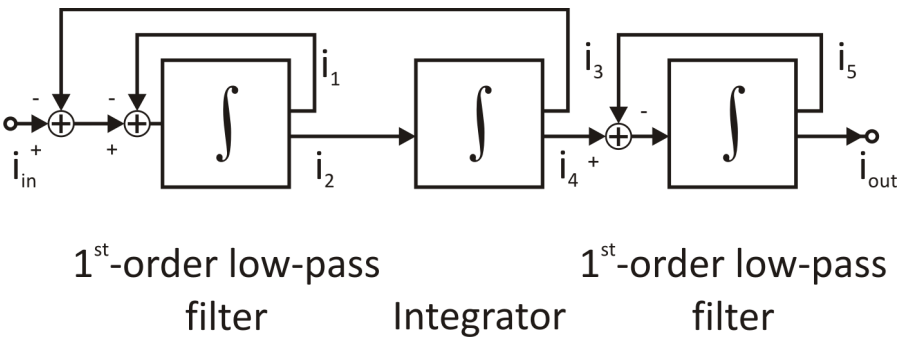

Figure 4.15: Block diagram of the chip area saving 3rd-order low-pass filter with virtual ground regulation

4.5.2 A Chip Area Saving 3rd-Order Current-Mode Continuous-Time Low-Pass Filter with Virtual Ground Regulation

A 3rd-order current-mode continuous-time Butterworth low-pass filter is realized by observing the same specifications as in section 4.5. The aimed -3 dB cut-off frequencies are again 1.1 MHz and 4.4 MHz. The benefit of the chip area saving strategy is exploited and additional cascode transistors of the active load transistors are used [UZ08c, UZ08b]. Furthermore a fully differential filter topology is designed and a virtual ground regulation on the filter input is realized. The virtual ground regulation is used for lowering the input impedance. The 3rd-order current-mode low-pass filter is made of three integrator stages, as depicted in the simplified block diagram in figure 4.15. The frequency behavior of the 3rd-order low-pass filter is realized by appropriate feedback of the integrators which is shown analytically in the following.

The basic functional block of the filter is the integrator which is defined by the transfer function

$$H_{I1}(s) = \frac{A_o}{s}, \tag{4.25}$$

where A_0 is the gain of the integrator. The integrator in negative feedback results in a first-order low-pass filter:

$$H_{LP1}(s) = \frac{1}{1 + \frac{1}{A_0}s}. \tag{4.26}$$

The second-order low-pass is realized by the first-order low-pass filter in series with another integrator and its gain of B_0. Both blocks are again in negative feedback and generate the transfer function

$$H_{LP2}(s) = \frac{1}{\frac{1}{A_0 B_0} s^2 + \frac{1}{B_0} s + 1}. \tag{4.27}$$

The 3rd-order low-pass filter is realized by a further integrator in feedback as in (4.26) (gain: C_0) connected to the outputs of the second-order low-pass filter. The transfer function is

$$H_{Filter}(s) = \frac{A_0 B_0 C_0}{(A_0 B_0 + A_0 s + s^2)(C_0 + s)}. \tag{4.28}$$

Cascoded current-mode integrator with virtual ground regulation The central component of this filter is the current-mode integrator. Current-mode integrators are presented in [ZA96, SS96]. They define the transit frequency of the integrators by the integrating capacitance and the transconductances of the transistors. The proposed cascoded current-mode integrator has an additional parameter to adjust the transit frequency. The schematics and the simplified equivalent circuit is depicted in figures 4.16(a) and 4.16(b), respectively [UZ08c]. The integrator consists of two cross-coupled cascoded current mirrors, which are made of the transistors M_{1a} to M_{6a} and M_{1b} to M_{6b}. The cascodes are used for a better integrator accuracy. The load transistors are not cascoded, due to the limited signal headroom. For a sufficient output impedance, load transistors with large gate lengths are implemented. The output is mirrored twice, one is used for feedback purposes and the other is fed into the subsequent block. Due to the need of two outputs of the current mirror the current-consumption of the filter is increased.

The fully differential integrator functionality is realized considering some requirements. M_{1a}, M_{1b}, M_{4a}, and M_{4b} are equal in their dimensions and tagged with M_1. The cascode transistors M_{2a}, M_{2b}, M_{5a}, M_{5b}, M_{8a}, M_{8b}, M_{11a}, and M_{11b} are equal. The load transistors M_{3a}, M_{3b}, M_{6a}, M_{6b}, M_{9a}, M_{9b}, M_{12a}, and M_{12b} are equal as well. The output current mirroring transistors M_{7a} and M_{7b} as well as M_{10a} and M_{10b} are equal. Due to the symmetric integrator structure the resistors R_{1a} and R_{1b} are equal and denoted as R. The capacitors C_{1a} and C_{1b} and accordingly C_{2a} and C_{2b} are equal. For the following calculations they are subsumed as C. The dominant pole of the first integrator in 1st-order low-pass filter configuration is given by $R_1 = 20\,\mathrm{k\Omega}$ $C_1 = 4.4\,\mathrm{pF}$, and $C_2 = 1.2\,\mathrm{pF}$. The transit frequency of the second integrator is defined by $R_1 = 20\,\mathrm{k\Omega}$, $C_1 = 4.8\,\mathrm{pF}$,

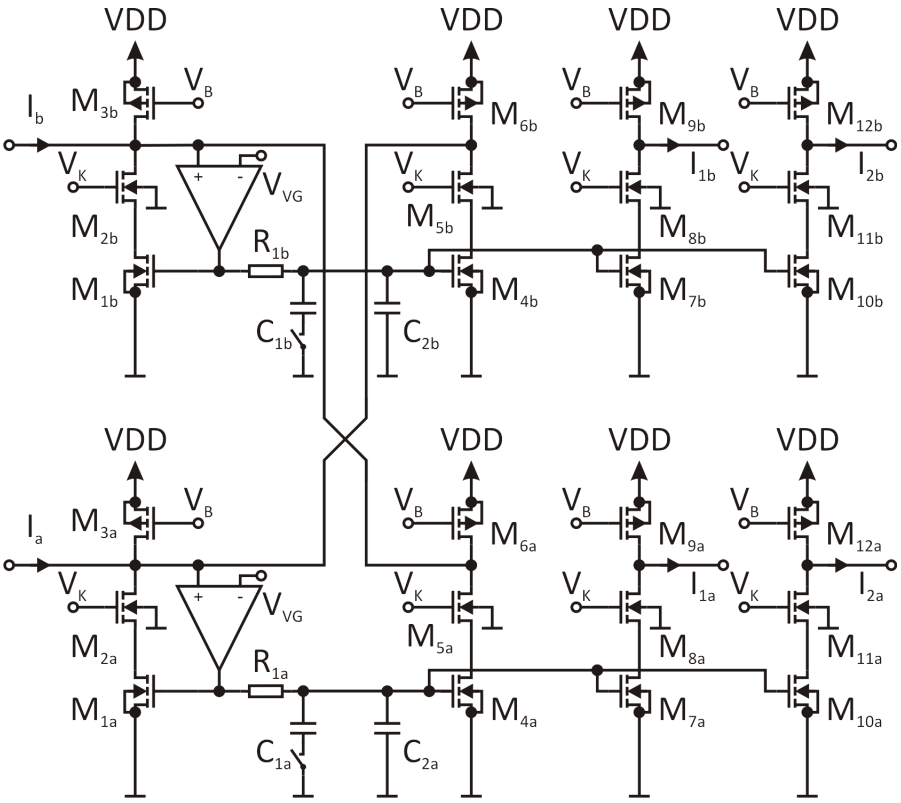

(a) Schematics

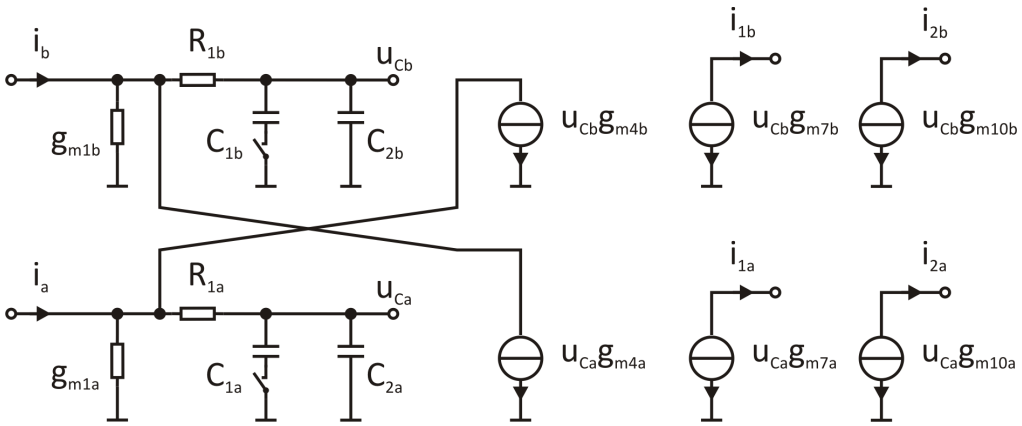

(b) Equivalent circuit

Figure 4.16: Cascoded chip area saving current-mode integrator with virtual ground

and $C_2 = 1.3\,\mathrm{pF}$. The last 1st-order low-pass filter is defined by $R_1 = 20\,\mathrm{k\Omega}$, $C_1 = 4.4\,\mathrm{pF}$, and $C_2 = 1.2\,\mathrm{pF}$.

The transfer function of the integrator is calculated with respect to figure 4.16(b) and evaluates to

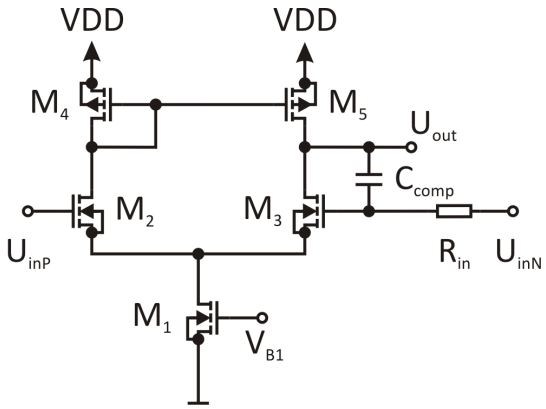

Figure 4.17: Virtual ground regulator - schematics

$$H_I(s) = \frac{i_{1a} - i_{1b}}{i_a - i_b} = -\frac{g_{m7}}{(1 + g_{m1}R)Cs}. \tag{4.29}$$

Equation (4.25) clarifies the influence of the additional resistor R. Usually the capacitance C and the transconductance g_{m1} are adjusted to set the transit frequency of the integrator. The extra resistor provides an additional parameter for the transit frequency. Low transit frequencies can be accomplished by big capacitors, at the cost of large chip area, or by the increase of the transconductance g_{m1}, which is not power efficient. Increasing the resistor R is an easy way to realize low transit frequencies. Adverse is the noise of the additional resistor, thus a trade-off has to be found to meet the target specifications.

A high output impedance is realized by a large L of the load transistors. The cascode transistors are used for integrator accuracy enhancement. For the system balance the cascode transistors are also inserted in the branches of the current mirrors.

The transit frequency is switchable. Two frequency ranges are achieved by switched capacitors (C_{1a}, C_{1b}, C_{2a}, C_{2b}). The switches are realized as NMOS transistors.

The first integrator of the 3rd-order low-pass filter has a virtual ground regulation. The schematics of the virtual ground regulator is depicted in figure 4.17. It contains an NMOS differential pair (M_2 and M_3) with active PMOS (M_4 and M_5) load. Biasing is done by transistor M_1 and the bias voltage V_{B1}. R_{in} decouples the set point of the virtual ground voltage from the regulation and C_{comp} is the compensation capacitor for the differential pair. The virtual ground regulation stabilizes the input voltage and reduces the input resistance. Only the first block at the input is equipped with a virtual ground regulation. The others have the input nodes directly connected to the gates of M_{1a} and M_{1b}. Apart from that the other blocks are identical to the first block.

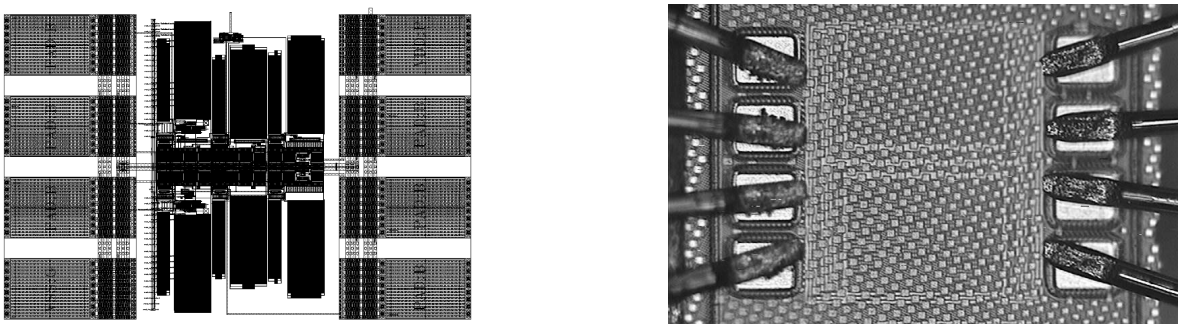

(a) Layout plot (b) Chip photograph

Figure 4.18: Cascoded chip area saving 3rd-order current-mode Butterworth low-pass filter with virtual ground regulation [UZ08c]

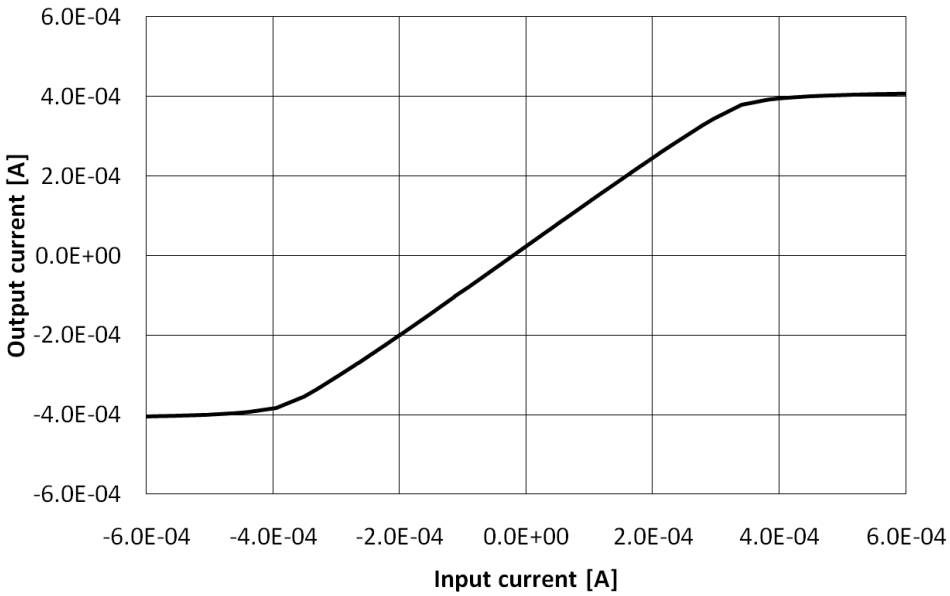

Figure 4.19: Cascoded chip area saving current-mode 3rd-order low-pass filter with virtual ground regulation - differential DC characteristics

Experimental results The 3rd-order Butterworth low-pass filter is designed and fabricated in 65nm LP CMOS technology. The layout plot and the chip photograph is depicted in figure 4.18(a) and 4.18(b), respectively. The active area of the filter is $215\,\mu$m $\times$ 221 μm and the chip area including the pads is $470\,\mu$m $\times$ $340\,\mu$m. The eight pads are assigned as VSS, VDD, cut-off frequency selection, virtual ground voltage V_{VG}, two differential inputs, and two differential outputs.

The current consumption of the entire filter is 10 mA at a supply voltage of 1.2 V, which corresponds to a power consumption of 12 mW. The virtual ground regulation sets the voltage on the input nodes to 700 mV. The differential DC measurement is shown in

Table 4.4: Cascoded chip area saving current-mode 3rd-order low-pass filter with virtual ground regulation - measured HD3

$\hat{I}_{in}$ Signal frequency	$\mathbf{f_c = 1\,MHz}$ $f_{tone} = 100\,kHz$	$\mathbf{f_c = 4\,MHz}$ $f_{tone} = 400\,kHz$
100 μA	-56 dBc	-55 dBc
200 μA	-49.5 dBc	-50 dBc
300 μA	-41.8 dBc	-40.5 dBc
400 μA	-35 dBc	-33.5 dBc

figure 4.19 and shows good linearity from -360 μA to 340 μA input current. The filter shows an offset of 20 μA.

The measured frequency response of the cascoded chip area saving 3rd-order current-mode Butterworth low-pass filter is shown in figure 4.20. Figure 4.20(a) depicts two -3 dB cut-off frequencies of 1 MHz and 4 MHz, depending on the settings of the switches. The gain in the pass band is about 0.9 dB. The phase response is depicted in figure 4.20(b)

Harmonic distortions are measured in a single tone measurement. The input current is varied at a frequency f_{tone} of 100 kHz at a filter bandwidth of 1 MHz and at a frequency f_{tone} of 400 kHz at the filter bandwidth of 4 MHz. Measured 3rd-order harmonic distortions (HD3) are presented in table 4.4.

THD1% is measured at the same input signal frequencies. Results are given in table 4.5.

Table 4.5: Cascoded chip area saving current-mode 3rd-order low-pass filter with virtual ground regulation - measured THD1%

f_c	$\hat{I}_{THD1\%}$
1 MHz	322 μA_p
4 MHz	322 μA_p

In the two-tone measurement two sinusoidal input signals are applied and the amplitude is increased until an IM3 of -40 dB is reached. At the -3 dB cut-off frequency of 1 MHz the test signals are at 600 kHz and 700 kHz. An input amplitude of 154.5 μA of both

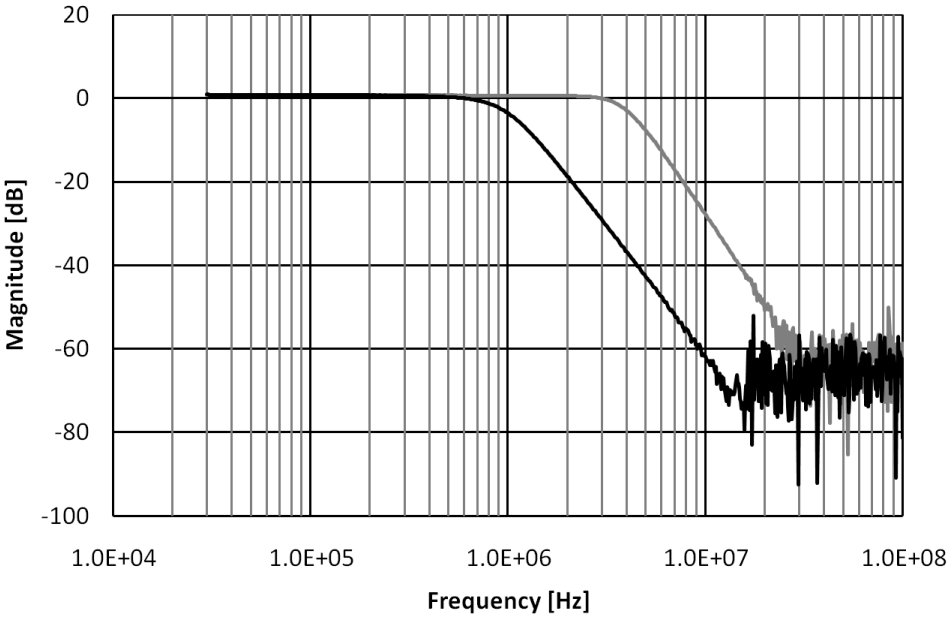

(a) Amplitude response

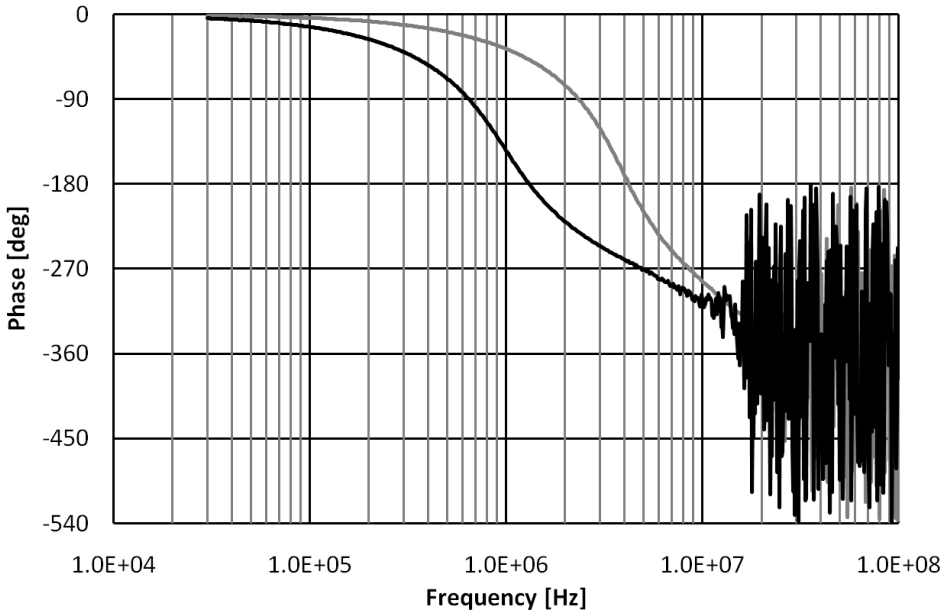

(b) Phase response

Figure 4.20: Cascoded chip area saving current-mode 3rd-order low-pass filter with virtual ground regulation - frequency response

input signals causes an IM3 of -40 dB, which corresponds to an IIP3 of 1.54 mA_p. At the -3 dB cut-off frequency of 4 MHz the test signals are at 2.4 MHz and 2.5 MHz. An input amplitude of 154.5 μA of both input signals causes an IM3 of -40 dB, which corresponds to an IIP3 of 1.54 mA_p, as well. The two-tone measurement at the 4 MHz -3 dB cut-off

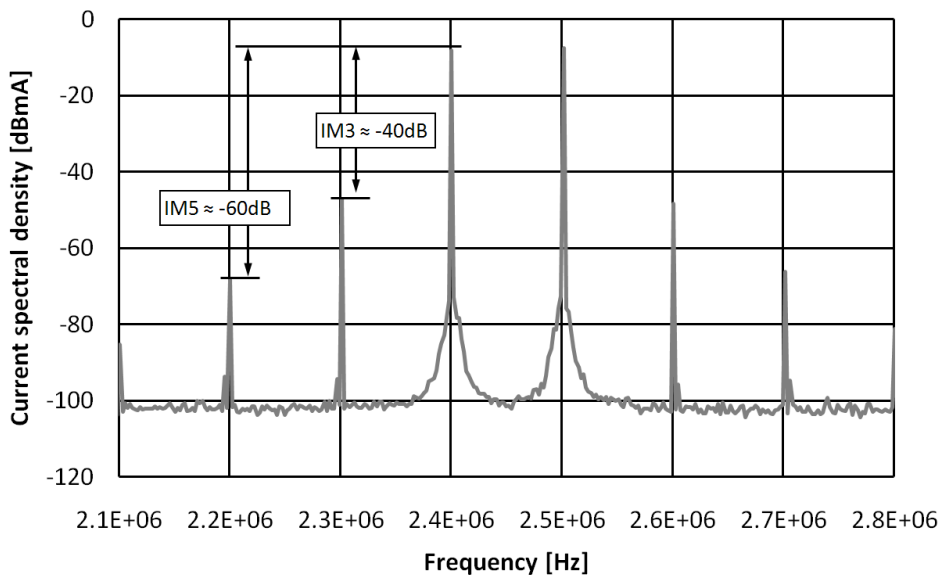

Figure 4.21: Cascoded chip area saving current-mode 3rd-order low-pass filter with virtual ground regulation - two-tone measurement

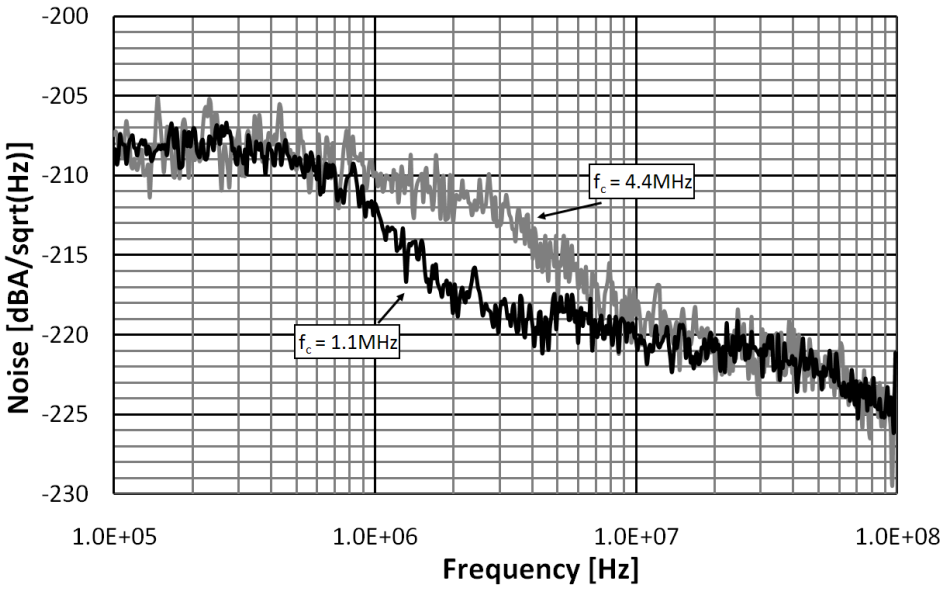

Figure 4.22: Cascoded chip area saving current-mode 3rd-order low-pass filter with virtual ground regulation - noise measurement

frequency setting is given in figure 4.21.

The noise measurement is depicted in figure 4.22. The spectral output noise density in the pass-band is $31.6\,\mathrm{pA}/\sqrt{\mathrm{Hz}}$.

The 3rd-order Butterworth low-pass filter reaches at a -3 dB cut-off frequency of 1 MHz a DR of 77.3 dB and a FOM_{Filter} of 2258.9. At the -3 dB cut-off frequency of 4 MHz the DR is 71.3 dB and the FOM_{Filter} is 2238.3. A summarized overview of the filter performance is given in table 4.6 [UZ08c, UZ08b].

Table 4.6: Cascoded chip area saving current-mode 3rd-order low-pass filter with virtual ground regulation - performance summary

Technology	65 nm CMOS	
Chip area	0.0475mm^2	
Supply voltage	1.2 V	
Power consumption	12 mW	
DC gain	0.9 dB	
-3 dB cut-off frequency	1 MHz	4 MHz
$\hat{I}$ @ THD1%	$322\,\mu\text{A}_p$	
IIP3	$1.54\,\text{mA}_p$	
DR	77.3 dB	71.3 dB
FOM_{Filter}	2258.9	2238.3

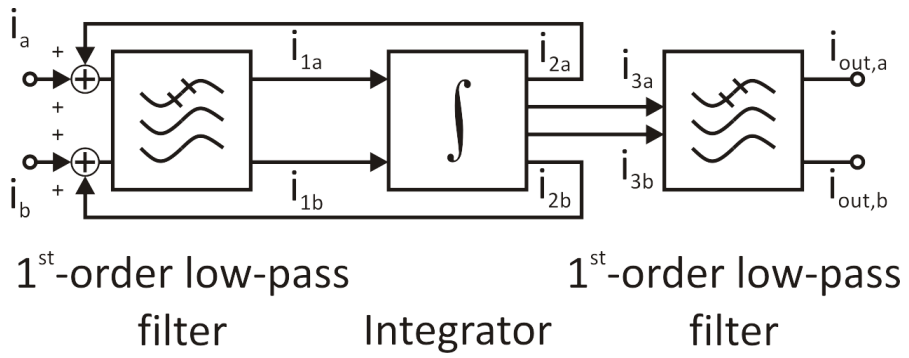

Figure 4.23: Block diagram of the 3rd-Order Current-Mode Low-Pass Filter Using Capacitance Multiplication

4.5.3 A 3rd-Order Low-Voltage Current-Mode Continuous-Time Low-Pass Filter Using Capacitance Multiplication and Virtual Ground Regulation

A 3rd-order current-mode Butterworth low-pass filter using capacitance multiplication and a virtual ground regulation on the input is realized. The block diagram is depicted in figure 4.23. The first block is a first-order current-mode low-pass filter including a virtual ground regulation and using a capacitance multiplication technique. The second block is a cascoded current-mode integrator. The third block is a first-order current-mode low-pass filter using again the capacitance multiplication technique, but without virtual ground regulation.

1st-order current-mode low-pass filter using capacitance multiplication and virtual ground regulation The capacitance multiplication technique is important and effective to save expensive chip area [UZ08a]. The schematics and the equivalent circuit is shown in figure 4.24(a) and 4.24(b), respectively.

For a 1st-order low-pass filter functionality the transistors have to be designed as following. $M_{1a} = M_{1b}$ and is denoted as M_1. $M_{3a} = M_{3b}$ and is denoted as M_3. $M_{4a} = M_{4b} = M_4$; $M_{6a} = M_{6b} = M_6$; $M_{7a} = M_{7b} = M_7$; $M_{9a} = M_{9b} = M_9$. The cascode transistors M_{2a}, M_{2b}, M_{5a}, M_{5b}, M_{8a}, and M_{8b} are equal. Long gate lengths of the load transistors are inserted due to a larger output resistance. The symmetry requires the equality of $R_{1a} = R_{1b} = R_1$, $C_{1a} = C_{1b} = C_1$, and $C_{2a} = C_{2b} = C_2$. The switches to change the cut-off frequencies are assumed to be open and only C_2 is active. By using this denomination the transfer function of the 1st-order low-pass filter results in

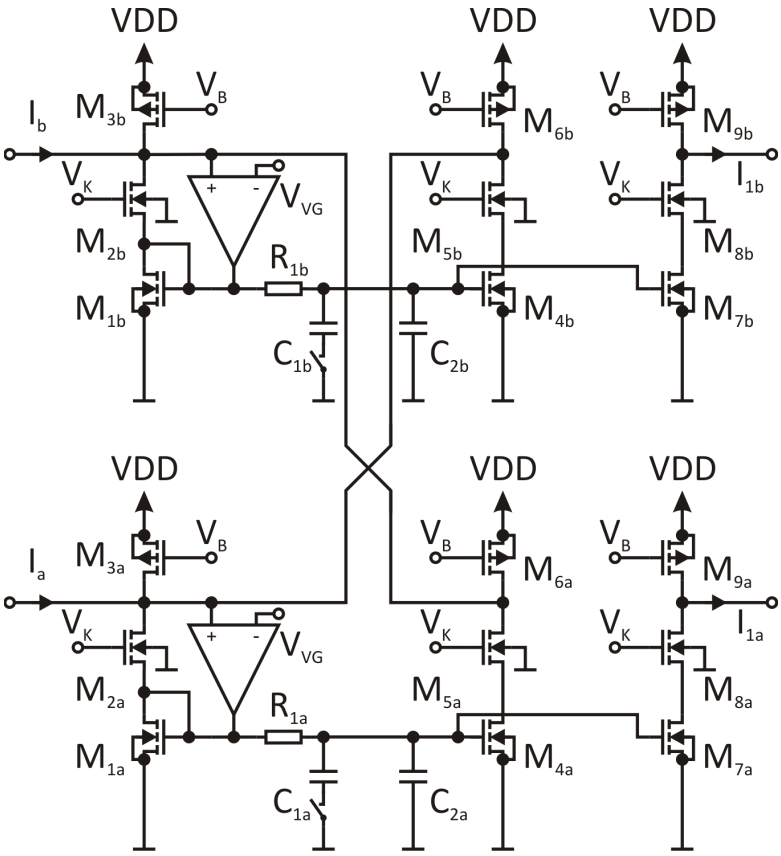

(a) Schematics

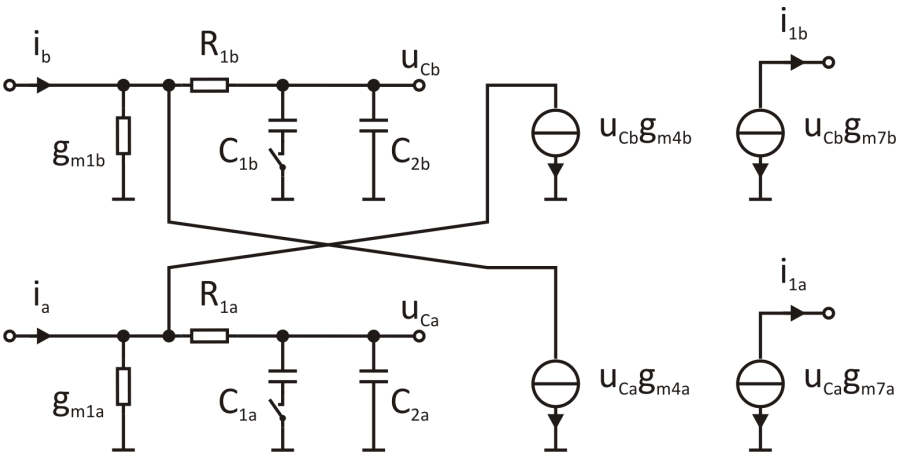

(b) Equivalent circuit

Figure 4.24: Cascoded current-mode 1st-order low-pass filter using capacitance multiplication

$$H_{LP}(s) = \frac{i_{1b} - i_{1a}}{i_a - i_b} = \frac{\zeta_1 \frac{g_{m7}}{g_{m1}}}{\zeta_1 C_2 (R_1 + \frac{1}{g_{m1}})s + 1}. \tag{4.30}$$

In equation (4.30) the factor ζ_1 is called the capacitance multiplication factor and is defined as

$$\zeta_1 = \frac{g_{m1}}{g_{m1} - g_{m4}}. \tag{4.31}$$

A 1st-order low-pass filter behavior needs the condition of the transconductances $g_{m4} < g_{m1}$. (4.30) points out that an increase of the capacitance multiplication factor ζ_1 shifts the cut-off frequency to lower frequencies. The capacitance multiplication factor can be raised by increasing the transconductance g_{m4}. The proposed 1st-order low-pass filter has a ζ_1 of 3. The new development results in an enlargement of the effective capacitance of 30%. However, the saving of chip area is at the cost of the dynamic range. Due to the current-transmission ratio the current in M_4, M_5, and M_6 is smaller than in M_1, M_2, and M_3. The gain of the 1st-order low-pass filter can be adjusted by the transconductance g_{m7}. The multiplication factor ζ_1 can be increased by approaching g_{m4} to g_{m1}. However, process tolerances have to be considered and $g_{m4} < g_{m1}$ has to be assured. Therefore a ζ_1 of 3 is used.

Cascoded current-mode integrator The second block of the 3rd-order current-mode low-pass filter, the integrator, is shown in figure 4.25. The transfer function is given by

$$H_I(s) = \frac{i_{2b} - i_{2a}}{i_{1a} - i_{1b}} = \frac{i_{3b} - i_{3a}}{i_{1a} - i_{1b}} = \frac{g_{m10}}{(1 + g_{m10}R_2)C_4 s} \tag{4.32}$$

under the following assumptions: The transistors $M_{10a} = M_{10b} = M_{13a} = M_{13b} = M_{16a} = M_{16b} = M_{19a} = M_{19b}$ are equal and denoted as M_{10}. The load transistors are equal: $M_{12a} = M_{12b} = M_{15a} = M_{15b} = M_{18a} = M_{18b} = M_{21a} = M_{21b}$. The cascode transistors are equal: $M_{11a} = M_{11b} = M_{14a} = M_{14b} = M_{17a} = M_{17b} = M_{20a} = M_{20b}$. The cascodes provide a better integrator accuracy. The resistors R_{2a} and R_{2b} are equal and denoted as R_2, the capacitors C_{3a} and C_{3b} are equal and denoted as C_3. The capacitors C_{4a} and C_{4b} are equal and denoted as C_4. The switch is assumed to be open and the effective capacitance is C_4. The output is mirrored twice because of the current-mode signal which increases the current consumption of the filter.

By combining (4.30) and (4.32) the 2nd-order low-pass filter results in

$$H_{LP2} = \frac{g_{m7} g_{m10} \zeta_1}{Ds^2 + Es + F}. \tag{4.33}$$

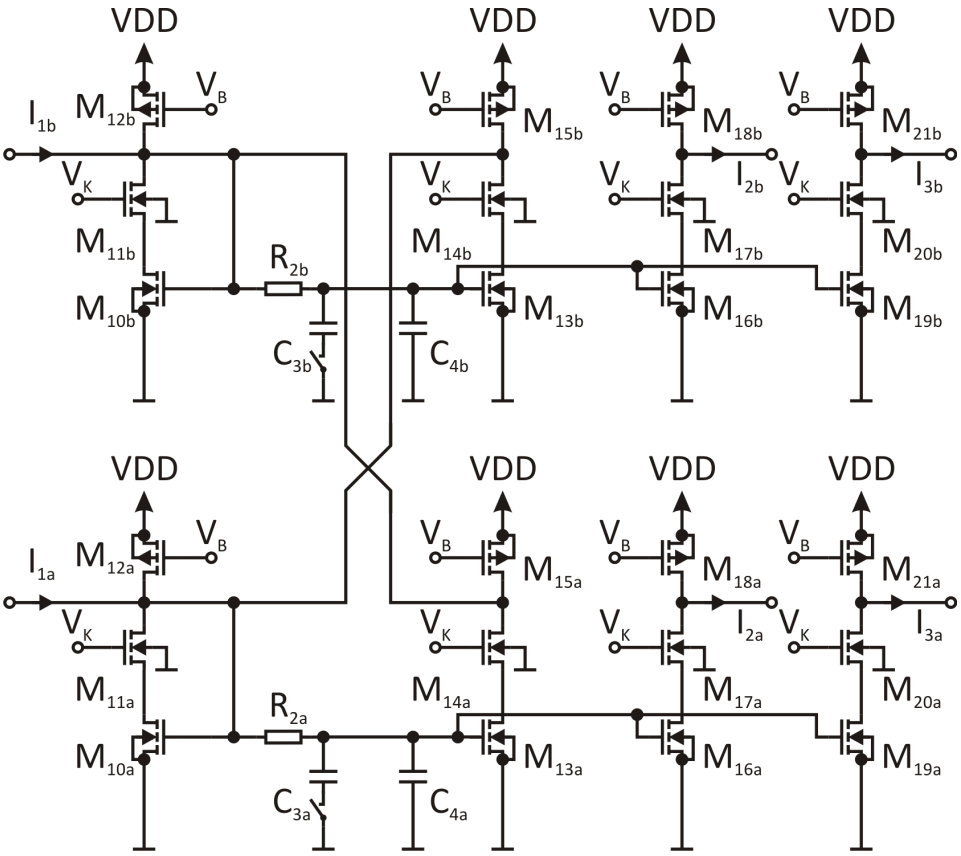

(a) Schematics

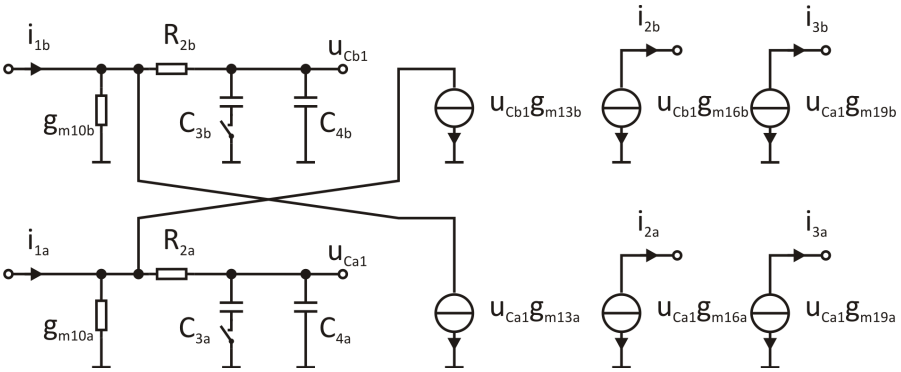

(b) Equivalent circuit

Figure 4.25: Cascoded current-mode integrator without virtual ground regulation

The coefficients D, E, and F represent:

$$D = C_2 C_4 \zeta_1 (R_1 g_{m1} + 1)(1 + g_{m10} R_2), \tag{4.34}$$

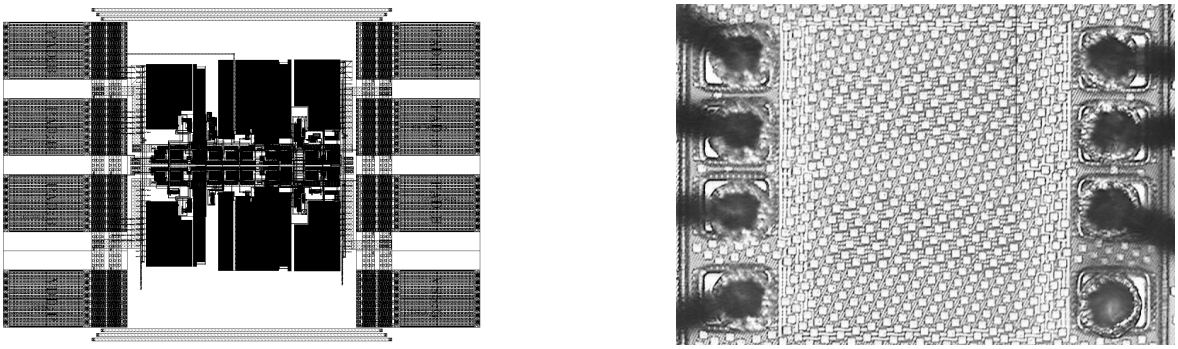

(a) Layout plot (b) Chip photograph

Figure 4.26: Low-voltage 3rd-order current-mode Butterworth low-pass filter using capacitance multiplication [UZ08a]

$$E = (1 + g_{m10}R_2)C_2 g_{m1}, \text{ and} \tag{4.35}$$

$$F = \zeta_1 g_{m7} g_{m10}. \tag{4.36}$$

The final 3rd-order current-mode Butterworth low-pass filter is realized with another 1st-order current-mode low-pass filter using capacitance multiplication as introduced in figure 4.24. The only difference is the omitted virtual ground regulation. With a consecutive numbering of the circuit devices the 3rd-order Butterworth low-pass filter results in

$$H_{Filter}(s) = \frac{g_{m7}g_{m10}\zeta_1}{Ds^2 + Es + F} \cdot \frac{\zeta_2 \frac{g_{m28}}{g_{m22}}}{\zeta_2 C_6 (R_3 + \frac{1}{g_{m22}})s + 1}. \tag{4.37}$$

Measurement results The 3rd-order Butterworth low-pass filter is designed and fabricated in 65nm LP CMOS technology. The active area of the filter is $215\,\mu$m $\times$ $215\,\mu$m and the chip size including the pads is $510\,\mu$m $\times$ $360\,\mu$m. The layout plot is shown in figure 4.26(a) and the chip photograph is depicted in 4.26(b). The chip pins are VSS, VDD, cut-off frequency select, virtual ground voltage V_{VG}, two differential inputs, and two differential outputs.

The supply voltage of the 3rd-order current-mode Butterworth low-pass filter is only 1 V for power saving reasons at a current consumption of 9.6 mA. This results in a power consumption of 9.6 mW. The differential DC characteristics at a virtual ground voltage

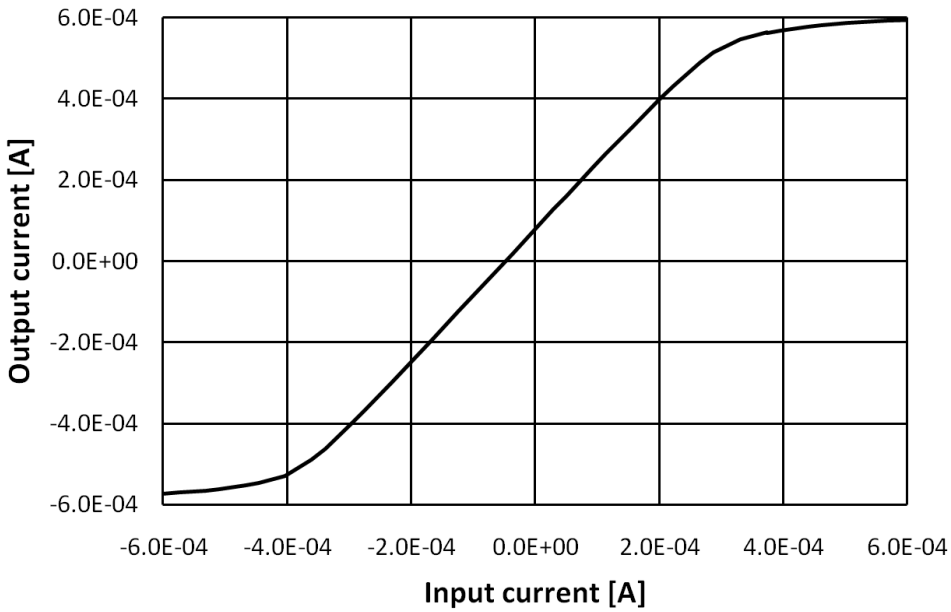

Figure 4.27: Current-mode 3rd-order low-pass filter using capacitance multiplication - differential DC characteristics

Table 4.7: Current-mode 3rd-order low-pass filter using capacitance multiplication - measured THD1%

f_c	$\hat{I}_{THD1\%}$@V_{VG} = 0.4 V	$\hat{I}_{THD1\%}$@V_{VG} = 0.5 V	$\hat{I}_{THD1\%}$@V_{VG} = 0.6 V
1 MHz	272 μA_p	277 μA_p	277 μA_p
4 MHz	272 μA_p	277 μA_p	268 μA_p

of 500 mV is shown in figure 4.27. The input-output current relation is linear at an input range from -480 μA to 480 μA. The offset at the output is about -50 μA at 0 V input voltage.

The frequency response in figure 4.28 shows the Butterworth low-pass filter characteristics at a virtual ground voltage of 500 mV. The -3 dB cut-off frequencies of 1 MHz and 4 MHz are digitally switchable. The -3 dB cut-off frequencies are determined at the input voltages of 400 mV, 500 mV, and 600 mV. In both frequency settings the deviation of the -3 dB cut-off frequencies was lower than 1%. The filter has a gain of 4 dB at all three virtual ground voltages at the input node.

Single-tone measurements were performed to show the in-band distortions. The results are given in table 4.8 for the two -3 dB cut-off frequencies of 1 MHz and 4 MHz and for the input node voltages of 400 mV, 500 mV, and 600 mV.

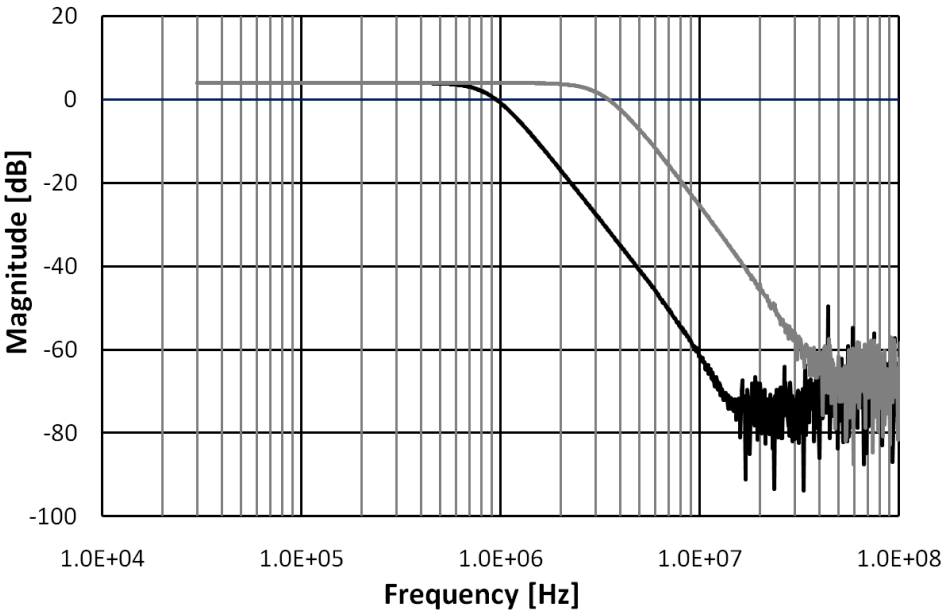

(a) Amplitude response

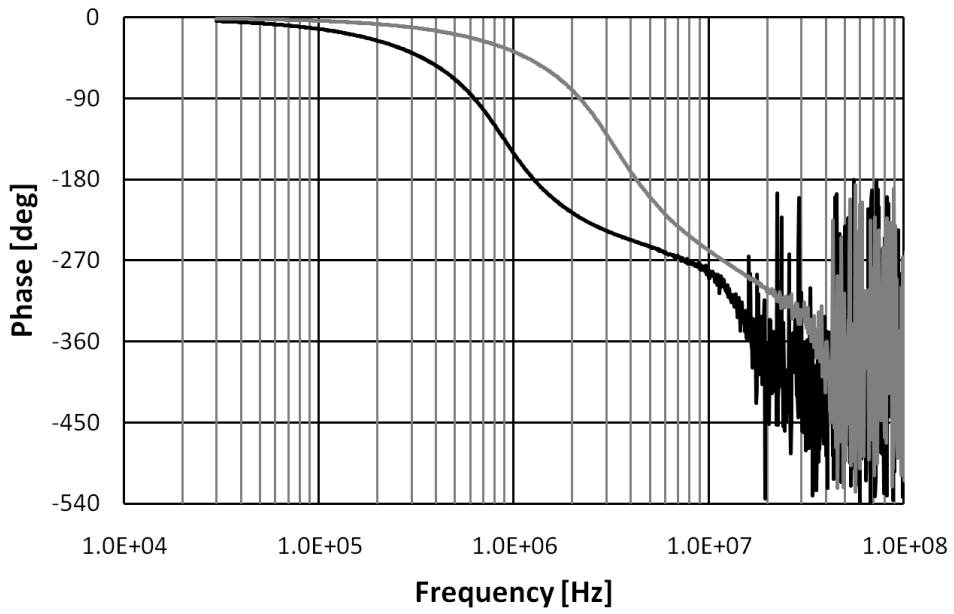

(b) Phase response

Figure 4.28: Current-mode 3rd-order low-pass filter using capacitance multiplication - frequency response

The THD1% is measured at all three virtual ground voltages. The test signal frequency at the -3 dB cut-off frequency of 1 MHz and 4 MHz was 100 kHz and 400 kHz, respectively. The input amplitudes which lead to 1% THD are listed in table 4.7.

Two-tone measurements were performed in order to identify the 3rd-order intermodulations. The frequencies of the two sinusoidal input signals at 1 MHz -3 dB cut-off frequency were 500 kHz and 600 kHz. The amplitude of both input signals are raised until a IM3 of -40 dB is reached. The resulting amplitudes of both input signals at different virtual ground voltages and the corresponding IIP3 are denoted in table 4.9. The frequencies of the input signals at f_c = 4 MHz were 2.4 MHz and 2.5 MHz. The results are given in table 4.9 as well.

The spectral output noise current density at a virtual ground voltage of V_{VG} = 500 mV is depicted in figure 4.29. The average spectral output noise density in the pass-

Table 4.8: Current-mode 3rd-order low-pass filter using capacitance multiplication - measured HD3 for different virtual ground voltages

$\hat{I}_{in}$ Signal frequency	$\mathbf{f_c = 1\,MHz}$ f_{tone} = 100 kHz	$\mathbf{f_c = 4\,MHz}$ f_{tone} = 400 kHz
V_{VG}	400 mV	
100 μA	-55.8 dBc	-57.5 dBc
150 μA	-54 dBc	-50.8 dBc
200 μA	-50 dBc	-48.1 dBc
250 μA	-44.8 dBc	-42.6 dBc
300 μA	-39 dBc	-36.8 dBc
V_{VG}	500 mV	
100 μA	-52.5 dBc	-52.4 dBc
150 μA	-54.5 dBc	-51.6 dBc
200 μA	-49.2 dBc	-49.2 dBc
250 μA	-45.5 dBc	-43.7 dBc
300 μA	-38.5 dBc	-37.8 dBc
V_{VG}	600 mV	
100 μA	-58 dBc	-52.6 dBc
150 μA	-54 dBc	-53.8 dBc
200 μA	-48.9 dBc	-50.9 dBc
250 μA	-45.4 dBc	-43.5 dBc
300 μA	-39.8 dBc	-38.8 dBc

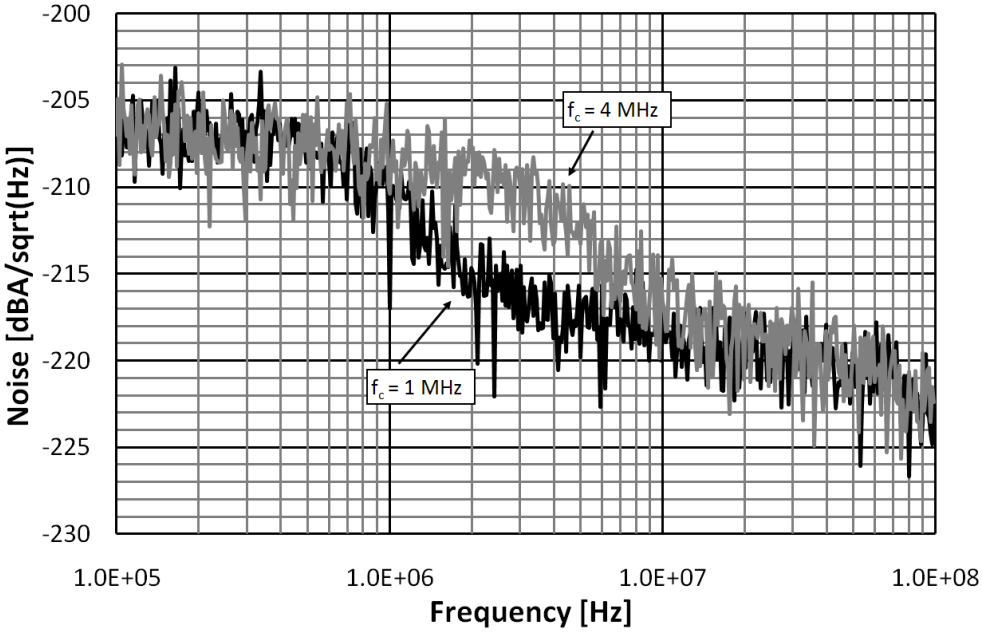

Figure 4.29: Current-mode 3rd-order low-pass filter using capacitance multiplication - noise measurement

Table 4.9: Current-mode 3rd-order low-pass filter using capacitance multiplication - intermodulation measurements

	$\mathbf{f_c = 1\,MHz}$	$\mathbf{f_c = 4\,MHz}$
Signal frequencies	$f_{tone1} = 500\,kHz$	$f_{tone2} = 2.4\,MHz$
	$f_{tone2} = 600\,kHz$	$f_{tone2} = 2.5\,MHz$
V_{VG}	400 mV	
$\hat{I}_{in}$	$164\,\mu A_p$	$154\,\mu A_p$
IIP3	$1.6\,mA_p$	$1.5\,mA_p$
V_{VG}	500 mV	
$\hat{I}_{in}$	$168\,\mu A_p$	$159\,\mu A_p$
IIP3	$1.7\,mA_p$	$1.6\,mA_p$
V_{VG}	600 mV	
$\hat{I}_{in}$	$168\,\mu A_p$	$145\,\mu A_p$
IIP3	$1.7\,mA_p$	$1.5\,mA_p$

band is $40\,\mathrm{pA}/\sqrt{\mathrm{Hz}}$ which corresponds to an input referred average noise density of $25\,\mathrm{pA}/\sqrt{\mathrm{Hz}}$.

The presented low-voltage current-mode 3rd-order Butterworth low-pass filter using capacitance multiplication has a DR of 73.8 dB and a FOM_{Filter} of 3873 at the -3 dB cut-off frequency of $\mathrm{f}_c = 1\,\mathrm{MHz}$. At $\mathrm{f}_c = 4\,\mathrm{MHz}$ the DR is 67.8 dB and the FOM_{Filter} results in 4034. A performance summary of the filter is printed in table 4.10 [UZ08a].

Table 4.10: Current-mode 3rd-order low-pass filter using capacitance multiplication - performance summary

Technology	65 nm CMOS	
Chip area	$0.0462\mathrm{mm}^2$	
Supply voltage	1.0 V	
Power consumption	9.6 mW	
DC gain	4 dB	
-3 dB cut-off frequency	1.0 MHz	4.0 MHz
$\hat{I}$ @ THD1%	$377\,\mu\mathrm{A}_p$	
IIP3	$1.7\,\mathrm{mA}_p$	$1.6\,\mathrm{mA}_p$
DR	73.8 dB	67.8 dB
FOM_{Filter}	3873	4034

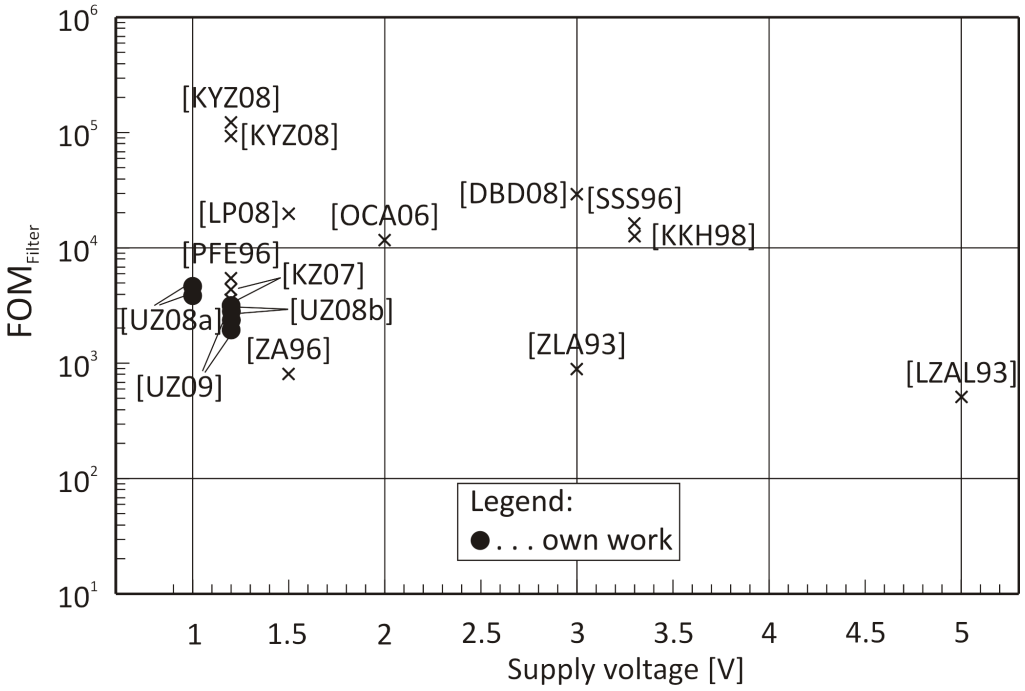

Figure 4.30: Figure of merit of current-mode filters - state-of-the-art

4.6 Comparison to the State-of-the-Art

For the comparison to the state-of-the-art table 4.11 lists the most important key data of various current-mode filters which are mentioned in the state-of-the-art (chapter 4.4). Unfortunately only a small number of publications of current-mode filters in deep-sub-micron and nanometer CMOS are available, hence older micrometer and sub-micrometer technologies are involved in the comparison as well. Voltage-mode counterparts are omitted in the comparison due to their inherently different structure and performance. For example, current-mode circuits need sufficient bias currents to guarantee a good distortion behavior. In general, circuits in deep-sub-micron and nanometer CMOS technologies have a higher power consumption at the same performance compared to circuits in micron and submicron technologies as explained in chapter 3. The effect of 1/f noise in deep-sub-micron and nanometer CMOS technology is considerable; especially in filters with low cut-off frequencies the noise has a significant impact on the filter performance. The figure of merit tries to combine significant filter characteristics to show the filter performance. Generally, a fair and comprehensive comparison by just one figure of merit is difficult. The figure of merit, as given in (4.6), is printed against the supply voltage in figure 4.30, if calculable. It should be kept in mind, lower values of FOM_{Filter} are better.

Simulation results of a 5th-order leapfrog all-pole low-pass filter are presented in [LZAL91].

The filter is designed in 2 μm CMOS and has a 5 V supply voltage. Not any numbers of noise or dynamic range are given, hence a FOM_{Filter} cannot be calculated. A good FOM_{Filter} is reached in [LZAL93] (2 μm CMOS) and [ZLA93] (1.2 μm CMOS) due to the extensive use of cascoding in the current amplifier of the filter at a high supply voltage (5 V and 3 V). A moderate FOM_{Filter} and DR is reached in [SS96] even in 2 μm CMOS at a 3.3 V supply voltage and a power consumption of 4 mW. An ultra low-power current-mode filter is presented in [ZA96], which reaches a good FOM_{Filter}. The supply voltage is 1.5 V and the power consumption is 375 μW at a -3 dB cut-off frequency of 525 kHz. Only simulations are presented in [PFE96] and reach a good FOM_{Filter}, although the used technology is not mentioned. The 4th-order Chebyshev low-pass filter consumes only 1.16 μW at a bandwidth of 5 kHz. Simulation results for a 3rd-order Butterworth filter at 3 V supply voltage and 7.2 mW power dissipation are presented in [HY96]. No FOM_{Filter} is available due to missing noise, distortion, and DR figures. The power consumption in [KKH98] is extremely high at a supply voltage of 3.3 V because of the high bias currents. These are needed for a low distortion filter design. However, the high power consumption (18.8 mW per pole) leads to a moderate FOM_{Filter} in 0.5 μm CMOS. Results in [DL01] and [Ham03] are achieved only by simulations in 0.25 μm CMOS and 0.8 μm CMOS, respectively. Distortions and noise performance are missing, hence a FOM_{Filter} cannot be calculated. Measurement results of a 5th-order Butterworth filter in 1.2 μm CMOS at 5 V supply voltage are presented in [YHCH03]. Anyhow no FOM_{Filter} is available due to missing THD1% and noise figures. A current-mode square-root domain filter in 0.35 μm CMOS is presented in [KR03]. Not even the power consumption is reported, hence no FOM_{Filter} is available. A more recent technology is used in [OCA06]. At a supply voltage of 2 V and power consumption of 3.73 mW per pole only a decent DR of 53 dB and a moderate FOM_{Filter} is reached. A filter in 0.18 μm technology is presented in [HCLS06]. The filter consumes 16.77 mW at 1.8 V supply voltage. Unfortunately THD1% or the DR is missing, a FOM_{Filter} is not available. 65 nm CMOS technology is used in [KZ07, KYZ08]. A good FOM_{Filter} is achieved in [KZ07] at a supply voltage of 1.2 V, which is well comparable to this work. Only a moderate FOM_{Filter} is reached in [KYZ08] due to the moderate dynamic range. A 5th-order low-pass filter is presented in [DBD08]. Simulations in 1 μm CMOS with a power consumption of 5 mW show a moderate FOM_{Filter} and DR with a high supply voltage. [LP08] is the only representative of a current-mode filter in a 0.35 μm BiCMOS technology at a supply voltage of 1.5 V. It is an ultra low-power design (21.1 μW) with a low -3 dB cut-off frequency at the cost of a high DR, hence the FOM_{Filter} is moderate.

[UZ09a, UZ08b, UZ08a] are own designs in low-power 65 nm CMOS technology and all presented results are measurements. The nanometer CMOS technology issues are solved and these designs reach good DR and FOM_{Filter} figures. Using capacitance saving techniques and capacitance multiplication for current-mode integrators up to 30% capacitor area could be saved. Despite the system specified low cut-off frequencies the 1/f noise does not deteriorate the integrated noise too much. [UZ08b, UZ08a] are realized with virtual ground regulations. This is at the cost of chip area and current consumption, which affects the FOM_{Filter} negatively as well.

Table 4.11: Comparison to the state-of-the-art

Citation	Technology	Supply voltage	Power consumption	Filter order	-3 dB cut-off frequency	Active area	DR	FOM_{Filter}
State-of-the-art								
[LZAL91]	2 μm CMOS	5 V	24 mW@30 MHz	5	25 - 50 MHz	n.a.†	n.a.†	n.a.†
[LZAL93]‡	2 μm CMOS	5 V	25.5 mW@40 MHz	5	24 - 42 MHz	0.28 mm^2	69 dB	484
[ZLA93]‡	1.2 μm CMOS	3 V	18 mW	3	125 MHz	0.009 mm^2	62 dB	914
[SS96]‡	2 μm CMOS	3.3 V	4 mW	6	7.5 - 13.5 MHz	0.774 mm^2	52 dB	12694
[ZA96]‡	1.2 μm CMOS	1.5 V	375 μW	5	300 kHz - 1 MHz	0.5 mm^2	67 dB	860
[PFE96]‡	digital CMOS†	1.2 V	1.16 μW@5 kHz	4	20 Hz - 20 kHz	n.a.†	55 dB	5535
[HY96]	1.5 μm CMOS	3 V	7.2 mW	3	50 MHz	n.a.†	n.a.†	n.a.†
[KKH98]‡	0.5 μm CMOS	3.3 V	91 mW	5	50 MHz	0.56 mm^2	60 dB	10985
[DL01]	0.25 μm CMOS	1 V	24 mW	8	277 - 326 MHz	n.a.†	n.a.†	n.a.†
[Ham03]	0.8 μm CMOS	3 V	n.a.†	2	80 MHz	n.a.†	n.a.†	n.a.†
[YHCH03]	1.2 μm CMOS	5 V	20 mW	5	160 Hz - 5.6 kHz	0.4 mm^2	n.a.†	n.a.†
[KR03]	0.35 μm CMOS	3 V	n.a.†	2	1 - 5 MHz	n.a.†	n.a.†	n.a.†
[OCA06]‡	0.35 μm CMOS	2 V	11.1 - 55.8 mW	3	42 - 215 MHz	0.075 mm^2	53 dB	13324
[HCLS06]	0.18 μm CMOS	1.8 V	16.77 mW	3	200 MHz	0.303 mm^2	n.a.†	n.a.†
[KZ07]‡	65 nm CMOS	1.2 V	8.16 mW	3	0.98 MHz	0.092 mm^2	72.5 dB	4710
[KZ07]‡	65 nm CMOS	1.2 V	8.16 mW	3	4.06 MHz	0.092 mm^2	66.6 dB	4432
[KYZ08]‡	65 nm CMOS	1.2 V	6.3 mW	3	0.95 MHz	0.054 mm^2	56.7 dB	142625
[KYZ08]‡	65 nm CMOS	1.2 V	6.3 mW	3	3.75 MHz	0.054 mm^2	52.6 dB	92873

† ... not available; ‡ ... plotted in figure 4.30

Table 4.11: Comparison to the state-of-the-art

Citation	Technology	Supply voltage	Power consumption	Filter order	-3 dB cut-off frequency	Active area	DR	FOM_{Filter}
[DBD08]‡	1 μm CMOS	3 V	5 mW	5	10 MHz,	n.a.†	50 dB	30179
[LP08]‡	0.35 μm BiCMOS	1.5 V	21.1 μW	5	482 kHz	n.a.†	40.6 dB	23013
Own publications								
[UZ09a]‡	65 nm CMOS	1.2 V	12.36 mW	3	1.12 MHz	0.077 mm^2	77.2 dB	2115
[UZ09a]‡	65 nm CMOS	1.2 V	12.36 mW	3	4.46 MHz	0.077 mm^2	70.9 dB	2304
[UZ08b]‡	65 nm CMOS	1.2 V	12 mW	3	1 MHz	0.0475 mm^2	77.3 dB	2259
[UZ08b]‡	65 nm CMOS	1.2 V	12 mW	3	4 MHz	0.0475 mm^2	71.3 dB	2238
[UZ08a]‡	65 nm CMOS	1 V	9.6 mW	3	1 MHz	0.0462 mm^2	73.8 dB	3873
[UZ08a]‡	65 nm CMOS	1 V	9.6 mW	3	4 MHz	0.0462 mm^2	67.8 dB	4034

† ... not available; ‡ ... plotted in figure 4.30

Chapter 5

Operational Amplifier RC Low-Pass Filter

5.1 Motivation

Handheld terminals, such as mobile phones, mobile computers, or personal digital assistants (PDA) increase their functionalities for marketing reasons. In order to boost the sales figures the scope of operation ranges from various sensors, like GPS and several interfaces, like Bluetooth and WLAN, to entertainment, like internet or gaming. Television (TV) is an important fraction in entertainment industries, hence television is offered for handheld mobile terminals. Nearly every device, like a mobile phone, a music player, or even a camera has a suitable display and can be used for the information transport. Entertainment and news are a constant companion all-around and at any time for a huge mass of customers.

Watching television on mobile phones, mobile television, is already available via the universal mobile telecommunication system (UMTS). UMTS was designed to join existing digital cellular systems together with future terrestrial and satellite communication services. UMTS covers voice services, messaging, fax, data communication, video streaming, local area networks, teleshopping, and information distribution. UMTS increases the density of mobile devices and allows a large amount of UMTS terminals in parallel use. For video streaming applications UMTS has some inherent structural weaknesses. These are poor data rates and its unicast oriented data transmission. Unicast data transmission is defined as a point-to-point connection with an exclusive information transfer between one transmitter and one receiver. However, unicast communication is pretty inefficient and expensive, if many receiving terminals demand the identical data stream like in television. Every video stream is transferred separately and stresses the service environment [Rap96].

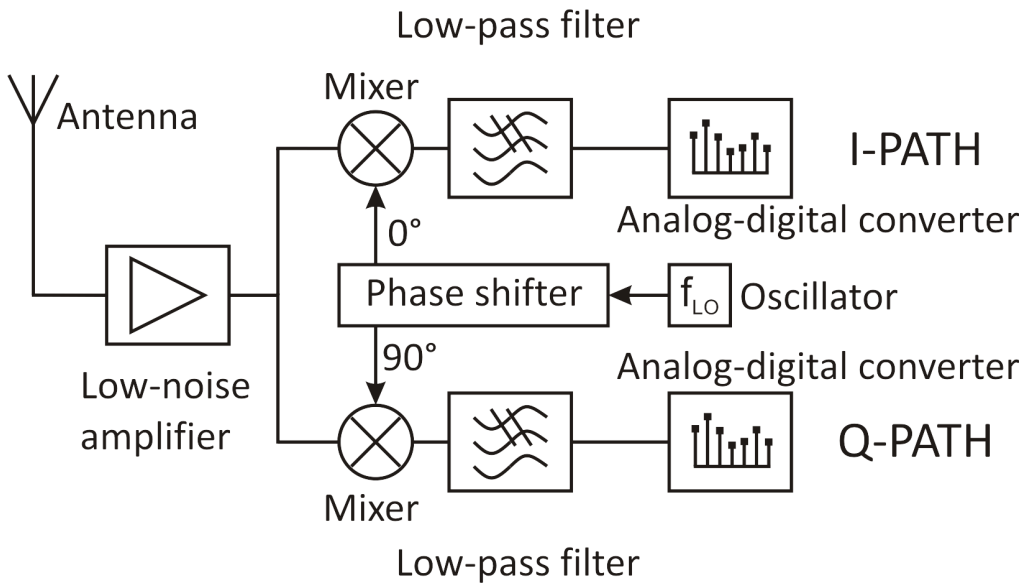

Figure 5.1: Direct conversion receiver - architectural overview

A broadcast network is more efficient for serving information to numerous customers compared to an unicast network. An existent and widely spread TV broadcast service is digital video broadcasting - terrestrial (DVB-T). The physical radio transmission of DVB-T is performed by orthogonal frequency division multiplex (OFDM) multi carrier modulation. It allows high-speed point-to-multipoint connections with the possibility to receive the broadcast service with portable devices. TV is available at a speed range that reaches from pedestrians to fast moving cars. DVB-T is used in many countries and hence, it has a huge geographical coverage.

The existent standard of DVB-T together with its suitability for fast moving television receivers caused the development of the standard for digital video broadcast - handheld (DVB-H). DVB-H is compatible to DVB-T to a large extent. Hence there is no need to establish a new and expensive broadcast network, the existing can be employed. DVB-H is optimized for mobile multimedia devices which result in some challenges:

- They have no external power supply and are battery supplied, are light weighted and pocket size. The limited power consumption is important for long operating time.
- The broadcast service provides audio and video streaming in adequate quality. Sufficient data rates are necessary.
- Mobility is a fundamental factor for handheld devices. Television reception should be possible indoor and outdoor at a speed from walking to driving. The antenna of the mobile system has limited dimensions and cannot be adjusted to the sender while moving. Multiple antennas are impossible due to space restrictions. Occur-

ring transmission errors have to be corrected and a time slicing technique for the transmission is used. Positive side effects of the time slicing are battery power saving and a soft handover between two adjacent transmission cells.

- Due to the re-use of the existing DVB-T broadcast network the DVB-H transmission should not interfere with DVB-T channels noticeable [KM07].

In near future the DVB-H will be substituted by Long Term Evolution (LTE). LTE is a new and simplified data centric (all IP) core network featuring collapsed architecture and improved redundancy [Mot07]. Important points of an LTE system are:

- high data rates up to 100 Mbps downlink and 50 Mbps uplink,
- scalable bandwidth from 1.25 MHz to 20 MHz,
- good throughput and spectrum efficiency,
- short package latency,
- operating at mobile speed up to 350 km/h in special cases,
- reduced costs, and
- interworking and handover with existing systems [Bes08].

The ambition of the work is the implementation of a first-order low-pass filter in the receiver chain of a DVB-H receiver. The overall receiver structure is a direct conversion receiver. The architectural overview is depicted in figure 5.1. An antenna receives the rf-signal and the low-noise amplifier boosts the signal before it is split into an in-phase (I) and a quadrature (Q) component. The mixers convert the signals directly into the base-band. The base-band signals are filtered by low-pass filters and the analog-to-digital converters convert the selected channel into the digital domain. Direct conversion receiver architectures are preferable to superheterodyne receiver architectures, especially for highly integrated and low-power systems [Abi95].

The industry partner wished to see the improvement of a new operational amplifier in the DVB-H receiver in comparison to their prior work. Target is the implementation of the low-pass filter as a first-order operational amplifier RC low-pass filter, which converts the current-mode output signal of the passive mixer into a voltage-mode signal. Furthermore the filter amplifies the signal with 40 dB and selects the channel bandwidth of 4 MHz. For the signal conversion and amplification a first-order operational amplifier RC low-pass filter is chosen. The use of a 2nd-order low-pass filter should be avoided because it would result in a lower in-band signal-to-noise ratio. Operational amplifiers are investigated that fulfill gain bandwidth product, open-loop gain, noise, and linearity specifications for a robust and cheap receiver, that do not deteriorate the in-band phase and group delay in the DVB-H receiver.

5.2 Operational Amplifiers - An Overview

The idea of the concept of operational amplifiers (opamp) was firstly mentioned by Tellegen and called "ideal amplifier" in 1954. In 1964, Widlar created the first integrated operational amplifier. They were often used in analog calculations for mathematical operations like addition or integration. Until today operational amplifiers are very important in analog circuits and often used in various applications [IF04].

Ideal operational amplifiers can be seen as voltage controlled voltage sources. The basic operational amplifier offers three pins: two differential inputs v_{in}^{+} and v_{in}^{-} and one single ended output v_{out}. The input impedance is infinity, thus no input current is flowing into the input nodes v_{in}^{+} and v_{in}^{-}. The output impedance is zero and the output voltage v_{out} is defined by the differential input voltage $(v_{in}^{+} - v_{in}^{-})$ and the open-loop gain A_0:

$$v_{out} = (v_{in}^{+} - v_{in}^{-})A_0. \tag{5.1}$$

The differential open-loop gain is infinite over a frequency range from DC to infinity. The common-mode rejection is infinite, i.e. the common-mode gain is zero. The use of operational amplifiers in open-loop configurations is not reasonable. Due to the high open-loop gain the output of the opamp is always in saturation. A feedback circuit enables a well defined circuit behavior. The output is mainly defined by the feedback. The ideal operational amplifier is often used for circuit analysis. The result is a good approximation for the practical operational amplifier, however, practical operational amplifiers have non idealities [TS02].

Real operational amplifiers do not exhibit an ideal behavior. Important non-idealities are summarized shortly [GHLM01]. Input bias currents flow into bipolar operational amplifier inputs and cause voltage drops in the feedback network. At MOS input stages the input bias currents are in general very small. In nanometer CMOS technologies tunneling currents result in increasing input bias currents. The input offset current is the difference between the input bias currents and is caused due to mismatch. The input offset voltage is the differential input voltage, which drives the output to zero and is also caused by mismatch. The common-mode input range is the range of the input DC voltage level at which all transistors in the input stage are in their active region. The common-mode rejection ratio describes the effect of a common-mode input signal to the output. The influence of variations in the power supply at the operational amplifier output is described by the power supply rejection ratio.

The input resistance can usually be neglected in feedback configuration due to the high voltage gain of the operational amplifier. In MOS input stages the input resistance is near infinity. Transistor properties of nanometer CMOS like tunneling currents, however, reduce the input resistance. The output resistance is caused by the output stage of the operational amplifier. The output resistance has a negligible influence on the closed-loop

performance, provided that the output resistance in combinations with the load keeps the operational amplifier stable.

The frequency response of a real operational amplifier declines towards high frequency due to the internal parasitic nodes. To ensure closed-loop stability compensation capacitances are implemented. A large gain is an elementary property of operational amplifiers, which is demanding in nanometer CMOS technologies. An intrinsic gain of a transistor close to 10 and an Early voltage of about 0.3 V lead to limitations of the operational amplifier gain.

5.3 Characterization of Operational Amplifiers

The used performance and quality parameters of operational amplifiers additional to section 4.2 are shortly described.

Load capacitance The load capacitance (C_L) is an important factor in operational amplifier circuits. C_L affects the power consumption and the bandwidth of an operational amplifier.

Gain-bandwidth product The gain-bandwidth product (GBW) is the product of the low-frequency gain and the bandwidth. The GBW is a very important criterion in amplifier design. In operational amplifier design the GBW is determined as the frequency at which the gain of the opamp is unity.

DC gain The DC gain or low-frequency gain is the open-loop gain of the operational amplifier. It should be high in order to sustain the approximation with an ideal opamp.

Phase margin A operational amplifier is usually operated in negative feedback. A phase lag of 180° turns the negative feedback into positive feedback and oscillations are the possible consequence. Oscillations occur at a positive feedback if the gain of the opamp is greater than 1. The phase margin (PM) is the difference of the phase lag at unity gain (GBW) and the critical 180°. A PM greater than 90° guarantees no peaking, a PM converging to 0° causes peaking, and a negative PM results in oscillation.

Power supply rejection ratio The power supply rejection ratio (PSRR) describes the influence of a power supply ripple on the output of the operational amplifier. The PSRR is defined as ratio of the noise in the supply rails to the resulting signal at the output. PSRR_{VDD} is the power supply rejection ratio for the positive power supply and PSRR_{VSS} is the power supply rejection ratio for the negative power supply:

$$PSRR_{VDD} = \frac{A_{dm}}{A_{VDD}} \text{ and } PSRR_{VSS} = \frac{A_{dm}}{A_{VSS}}. \tag{5.2}$$

A_{dm} denotes the differential gain, A_{VDD} is the small-signal gain from the positive power supply to the output and A_{VSS} is the small-signal gain from the negative supply to the output.

Common-mode rejection ratio The common-mode rejection ratio (CMRR) determines the influence of a common-mode input signal on the output. The CMRR is defined by the ratio of the differential gain to the common-mode gain:

$$CMRR = \frac{A_{dm}}{A_{cm}}. \tag{5.3}$$

A_{dm} is the differential gain and A_{cm} is the common-mode gain.

Figure of merit A simple but often used figure of merit of operational amplifiers is defined as

$$FOM_{Opamp} = \frac{GBW[MHz] \cdot C_L[pF]}{I[mA]}. \tag{5.4}$$

The GBW is inserted in MHz, the load capacitance C_L in pF and I is the current consumption of the operational amplifier in mA [San06].

5.4 Challenges for Operational Amplifier Design in Nanometer CMOS

Operational amplifier design in nanometer CMOS technology has notable constraints. The most important ones are shortly discussed.

Two-stage operational amplifiers are very common in micrometer and submicrometer technologies. In nanometer CMOS technologies it is difficult to achieve sufficient gain with a common two-stage design. The small channel length entails a low gain per transistor. Hence, the gain per stage is limited and more gain stages are needed to

provide sufficient gain. An often used gain enhancement technique is the use of cascode transistors. Cascoding needs sufficient supply voltage for a good performance. At a low supply voltage cascodes reduce the output swing and deteriorate the operational amplifier performance. Beside cascoding other gain enlargement techniques such as gain boosting or bootstrapping do not work properly at low supply voltages [SZ03].

Cascading is a technique that lines up the gain stages in series. The comparison of a cascoded and a cascaded amplifier results in equal gain under the assumption that the amount of cascode transistors and cascaded transistors are equal [San06]. However, the current consumption in the cascade is higher due to additional bias currents. A great advantage of cascaded amplifiers is the possibility of rail-to-rail output.

The GBW of a cascoded stage, which is a single-stage amplifier, is dependent on the driven load capacitance on the output. A cascaded stage is a two-stage amplifier and an additional capacitor for compensation is needed. The compensation capacitance is an additional load to C_L, hence more current is needed to drive the entire output capacitance and the overall power consumption is increased [San06].

5.5 State-of-the-Art of Operational Amplifiers

The publications of the state-of-the-art of operational amplifiers are sorted chronologically.

A low-voltage class AB operational amplifier for a sample and hold circuit is presented in [VGS01]. The opamp is supplied with 1.5 V and needs 4.5 μA which corresponds to a power consumption of 6.75 μW. The opamp has a gain of 106 dB, a GBW of 1 MHz, and a phase margin of 47° at a load of 5 pF. The power supply rejection ratio over VDD at DC $PSRR_{VDD}$ is 105 dB and the $PSRR_{VSS}$ is 115 dB. The operational amplifier is designed in AMS 0.8 μm CMOS technology and has an input referred noise spectral density of 95 nA/$\sqrt{\text{Hz}}$ at f = 1 kHz.

A fully differential operational amplifier in 0.13 μm CMOS is introduced in [MPHS02]. The current consumption is 3.1 mA at a supply voltage of 1.5 V. A GBW of 3.2 GHz at a PM of 44° and a gain of 50 dB is achieved. The CMRR is 118 dB.

A high-speed two-stage feed-forward operational amplifier for an opamp RC filter is published in [HW02]. The GBW is 2.6 GHz at a moderate phase margin of 35° and a load capacitance of 300 fF. The operational amplifier has a gain of 50 dB at a supply voltage of 1.8 V and a current consumption of 4 mA. The opamp is designed in 0.18 μm CMOS technology.

A three-stage fully differential operational amplifier in 0.12 μm digital CMOS is described in [SDZ03]. The supply voltage ranges from ± 0.3 V to ± 0.6 V. The opamp has a gain of 86 dB at a supply voltage of ± 0.6 V and a current consumption of 1.8 mA. The GBW is 46 MHz and the PM is 66° at a capacitive load of 10 pF. The fabricated chip has an active area of $155 \times 50\,\mu m^2$.

A medium-speed operational amplifier with a gain of 86 dB, a GBW of 392 MHz, and a phase margin of 73° at a C_L of 2 pF is presented in [SKF04]. The operational amplifier consumes 12 mW at 1.8 V single power supply. The opamp is designed in a TSMC P-well 0.18 μm standard digital CMOS technology.

A high-speed fully differential operational amplifier with a two-signal-path topology is published in [SZ04]. The opamp has a GBW at 1.5 GHz and a phase margin of 45° at a load of 3.2 pF twice. The gain is 40.4 dB and the slew-rate is 5000 V/μs. The opamp needs $100 \times 120\,\mu m^2$ active area in a 120 nm digital CMOS technology. It consumes 9.16 mA at 1.2 V supply voltage.

A fully differential six-stage opamp containing three signal paths in 0.12 μm digital CMOS technology is described in [SDZ04]. A differential gain of 120 dB at a supply voltage of 1.2 V and a power consumption of 27.5 mW is realized. At a C_L of 3.5 pF twice the opamp has a GBW of 866 MHz and a PM of 36°. The slew-rate is 890 V/μs and an active area of 0.0236 mm^2 is used.

A low-cost fully differential operational amplifier using a self-biased cascode output stage and a cross-coupled input stage is presented in [CC05]. The opamp is fabricated in 0.35 μm CMOS technology using $84\,\mu m \times 67\,\mu m$ silicon area. The opamp has 60 dB DC gain and at a load of 100 pF a slew-rate of 3 V/μs, a GBW of 7.8 MHz, and a PM of 67°. The opamp pulls 0.666 mA at a supply voltage of 3.3 V.

A low-noise operational amplifier with current driving bulk technology in 0.25 μm CMOS technology with an active area of 0.01053 mm^2 is introduced in [LMYY05]. The opamp needs 0.94 mA at a 2.5 V supply and has a DC gain of 76 dB. Driving a 5 pF load capacitance the opamp has a GBW of 280.5 MHz and a PM of 48°.

Single-, two-, and three-stage operational amplifiers in 0.18 μm CMOS technology at a supply voltage of 1.8V are compared in [HS05]. The single-stage opamp needs 35 mA to drive a 8.6 pF load capacitance twice at a GBW of 2.4 GHz and has a DC gain of 66 dB. The two-stage design has a DC gain of 27.1 dB and pulls 40 mA to drive a load of twice 7.4 pF at a GBW of 4.8 GHz. The three-stage opamp has a DC gain of 111 dB and a GBW of 1.27 GHz at a current consumption of 45 mA.

Two low-voltage class-AB operational amplifiers based on dynamic threshold voltage MOS transistors are published in [AFS06]. Both are designed in 0.18 μm CMOS, have a supply voltage of 1 V and are loaded with a 5 pF capacitor. The first operational

amplifier has a DC gain of 50.1 dB, a GBW of 26.2 MHz, and a CMRR of 78 dB at a power consumption of 550 μW. The second opamp is designed for biomedical applications with a power dissipation of 40 μW. It has a DC gain of 53 dB and a GBW of 1.3 MHz.

A CMOS Miller operational amplifier with a 1/f noise reduction technique is presented in [KLSK06]. It is implemented in 0.13 μm CMOS technology and occupies 0.09 mm^2 active area. The chip draws 1.2 mA at a 1.5 V supply and has a GBW of 10 MHz and a DC gain of 63.2 dB.

A fully differential three-stage operational amplifier with rail-to-rail input common-mode range in 120 nm CMOS is proposed in [YZ06]. The open-loop gain is 73 dB and the GBW is 4.4 MHz at a 5 pF load capacitance. The PM is 70° and the power consumption is 1.8 mW at 1.5 V supply. The PSRR$_{VDD}$ is 51.1 dB and the PSRR$_{VSS}$ is 54.8 dB and the CMRR is 57.3 dB. The chip area is 0.01 mm^2.

A 0.35 μm CMOS operational amplifier, which is suitable for low-voltage environments is introduced in [CTPD07]. It has rail-to-rail input and output voltage ranges. Driving a 17 pF capacitive load the opamp has a GBW of 8.1 MHz and a gain of 76.2 dB. The power dissipation is 385 μW, the CMRR is 70.5 dB at DC, the PSRR$_{VDD}$ is 45 dB, and the PSRR$_{VSS}$ is 40.5 dB. The active area is 0.0532 mm^2.

A cascoded operational amplifier with high gain in 0.35 μm CMOS technology is presented in [LK07]. An open-loop gain of 93 dB at a supply voltage of 3 V is achieved and the current consumption is 16.2 mA. The opamp has a phase margin of 61° at a GBW of 135 MHz and drives a load capacitor of 7 pF. The power supply rejection ratio for VSS is 58 dB and for VDD it is 68 dB. The CMRR is 40 dB.

A fully differential opamp with constant large- and small-signal behavior rail-to-rail input stage is introduced in [YZ07]. The operational amplifier has a GBW of 135 MHz at a 15 pF load capacitance and 51° PM. The open-loop gain is 76.3 dB and the slew-rate for the rising and the falling edge is about 105 V/μs. The chip has a power consumption of 17.25 mW at a voltage supply of $\pm$0.75 V and needs a chip area of 0.0097 mm^2 in 0.12 μm CMOS technology.

A fully differential folded cascode opamp and a fully telescopic opamp for a 40 MS/s 12-bit pipelined ADC are compared in [DNDR08]. Both are designed in 0.35 μm CMOS technology and are supplied with 3.3 V. The telescopic opamp has a DC gain of 86.4 dB and a slew-rate of 832 V/μs at a current consumption of 4.8 mA. A GBW of 570 MHz and a PM of 85.6° at a C_L of 1.4 pF are reached. The folded cascode opamp has a gain of 85.9 dB, a slew-rate of 472 V/μs and needs 4.8 mA. It is loaded with C_L = 1.4 pF and has a GBW of 350 MHz and a PM of 56°.

A low-voltage operational amplifier using a four-stage frequency compensation scheme is developed in [YKZ08b]. The opamp has a voltage supply of 1 V and has a power

dissipation of 1.4 mW. The open-loop gain is 108 dB and the GBW is 40.2 MHz at a PM of 62° driving a 500 pF load. The active area in 0.12 μm CMOS is 0.017 mm^2.

A fully differential rail-to-rail input/output with a current-mode common-mode feedback circuit for small-signal behavior control is presented in [YKZ08a]. The operational amplifier is designed in 65 nm CMOS technology and needs 0.014 mm^2. The open-loop gain is 100 dB, the GBW is 40 MHz, and the phase margin is 64° at a load of 15 pF. The supply voltage is $\pm$0.5 V and the power consumption is 0.72 mW. The operational amplifier has a PSRR at 10 Hz of 65 dB and a CMRR at 10 Hz of 74 dB. The input noise at 100 kHz is 186 nV/$\sqrt{Hz}$.

A rail-to-rail constant-g_m CMOS operational amplifier in 0.6 μm CMOS is described in [WRZW09]. An open-loop gain of 113.6 dB, a GBW of 11.9 MHz, and a PM of 53° is achieved at a supply voltage of 3 V.

A two-stage Miller operational amplifier is compared to a folded cascode opamp in 90 nm CMOS in [dCdRG$^+$09]. The two-stage Miller opamp has a DC gain of 52.4 dB, a GBW of 1014 MHz, a PM of 47.4°, and a slew-rate of 697.5 V/μs. The folded cascode opamp has a DC gain of 65.7 dB and a GBW of 539.4 MHz at a PM of 7.721°. The DC gain amounts to 103.2 dB.

A low-power, high-gain, fully differential ultra-wide bandwidth operational amplifier is presented in [GB10]. It is supplied with 1.8 V and has a current consumption of 13.9 mA to obtain a DC gain of 65 dB. The GBW is 2.3 GHz at a PM of 58° and 2 pF load. The CMRR, the PSRR$_{VDD}$, and the PSRR$_{VSS}$ are 96 dB, 62 dB, and 62.5 dB, respectively. The slew-rate is larger than 450 V/μs. The opamp is implemented in 0.18 μm CMOS technology and has an active area of 200 μm $\times$ 200 μm.

A pseudo differential two-stage operational transconductance amplifier in 0.18 μm CMOS technology is published in [SWKH10]. The amplifier has a DC gain of 72.8 dB and pulls a current of 0.154 mA at a supply voltage of 0.7 V. A GBW of 0.97 MHz at a PM of 70° is achieved.

5.6 State-of-the-Art of Voltage-Mode Filters

The publications of the state-of-the-art of voltage-mode filters are sorted chronologically.

A 350 MHz opamp RC filter using the operational amplifier as presented in section 5.5 is implemented in [HW02]. The 5th-order elliptic filter has a tuning range of the -3 dB cut-off frequency from 40 MHz to 350 MHz and a gain of 0 dB. The filter has a power

dissipation of 25.2 mW at a supply voltage of 1.8 V. The third-order in-band intercept point is -13 dBV_{rms} and the average noise in the pass-band is 24 nV/$\sqrt{\text{Hz}}$.

A 3rd-order Butterworth low-pass g_m-C filter is published in [YE03]. It is part of a transceiver designed for wireless sensor networks. The filter can handle a supply voltage range from 1.2 V to 1.8 V. The nominal -3 dB cut-off frequency is 50 kHz, however the tuning range of the cut-off frequency is between 13 kHz and 80 kHz, depending on the supply voltage. At the nominal bandwidth of 50 kHz at the supply voltage of 1.5 V the dynamic range at THD1% is 75 dB and the power consumption is 240 μW. The $PSRR_{VDD}$ is 30 dB and the CMRR is 47 dB. The filter is realized in 0.18 μm TSMC CMOS technology and has an active area of 0.113mm^2.

A complete base-band chain for WLAN using optimized g_m stages for linearity and low-voltage operation is presented in [ECBS05]. The 6th-order elliptic low-pass g_m-C filter is supplied with 1.4 V and has a power consumption of 13.5 mW. The variable gain amplifiers provide a gain range between 13.5 and 67.5 dB. The -3 dB cut-off frequency is switchable between 1, 10, and 100 MHz. The minimum input referred noise density is 19 nV/$\sqrt{Hz}$. The filter is designed in 90 nm CMOS technology and has 0.55 mm^2 active area.

A 4th-order continuous-time reconfigurable Bessel low-pass filter structure for UMTS/-WLAN is introduced in [DGB06]. The filter is implemented in 0.13 μm CMOS technology and occupies 0.9 mm^2. In the UMTS mode the filter has a cut-off frequency of 2.11 MHz and a DC gain of 4 dB. The input-referred integrated noise of 36 μV_{rms} results in a DR of 81 dB. The filter has a supply voltage of 1.2 V and a power consumption of 3.4 mW. In the WLAN mode the filter has a -3 dB cut-off frequency of 11 MHz and a DC gain of 4 dB. The DR at -40 dB THD is 81 dB and the input referred noise is 36 μV_{rms}. The filter in WLAN mode needs 11.8 mA at a supply voltage of 1.2 V.

Two baseband blocks consisting of a digital-to-analog converter and a low-pass filter for WLAN/UMTS and WLAN/Bluetooth are presented in [GVM+06]. Both are realized in 0.13 μm CMOS and have a supply voltage of 1.2 V. All filters are 4th-order Bessel low-pass filters. The WLAN mode filter of the first device has a -3 dB cut-off frequency of 11 MHz, a power consumption of 5.6 mW, and a DR of 55 dB. The UMTS mode of the first device has a bandwidth of 2.5 MHz, a power consumption of 3 mW, and a DR of 58 dB. The core area of the first device combining DAC and filter is 0.8 mm^2. The WLAN mode of the second device has a similar performance as the WLAN mode of the first device. The Bluetooth mode of the second device has a -3 dB cut-off frequency of 1 MHz, a power consumption of 3 mW, and a DR of 58.2 dB. The second device has a core area of 0.7 mm^2.

A 10 MHz 4th-order Bessel low-pass filter using composite source-followers is published in [DCB06]. The use of positive feedback enables complex poles with a single branch for a single-branch biquadratic cell. The filter consumes 2.28 mA at a supply voltage

of 1.8 V. The DC gain is -3.5 dB and the DR is 79 dB at a HD3 of -40 dB. The filter is implemented in 0.18 μm CMOS technology and has an active area of 0.26 mm^2.

A 4th-order active g_m-RC Butterworth filter for a WLAN receiver with high-linearity performance, operating at very low supply voltage, is presented in [MDGB07]. The filter has a gain of 0 dB and a -3 dB cut-off frequency of 11.3 MHz. It has a supply voltage of 550 mV and a power dissipation of 3.5 mW. The in-band IIP3 is 8 dBm and the DR is 60 dB at a THD of -40 dB. The filter is implemented in 0.13 μm CMOS technology and the core area is 0.45 mm^2.

A 4th-order wideband low-power band-pass filter for wireless receivers is published in [MDA+09]. It is a cascade of two active opamp RC cells. The pass-band of the filter ranges from 300 kHz to 8 MHz and the gain is 30.6 dB. The filter is supplied with 1.2 V and has a power dissipation of 1.3 mW. The IIP3 is -10 dBm and the DR is 52 dB. The filter is designed in 65 nm CMOS technology.

A wide tuning-range 3rd-order g_m-C Butterworth filter for Bluetooth, cdma2000, Wideband CDMA, and WLAN is introduced in [LHI09]. The filter has a tuning range from 500 kHz to 20 MHz to cover all specified cut-off frequencies. Depending on the tuned bandwidth the filter consumes 4.1 mW to 11.1 mW at a supply voltage of 1.2 V. The filter is implemented in TSMC 0.18 μm and occupies less than 0.23 mm^2.

A second-order Butterworth low-pass g_m-C filter for baseband communication in mobile radio receivers is introduced in [FM10]. The filter is designed in 0.18 μm CMOS technology and has a supply voltage of 1.8 V. The power consumption is 384 μW. The filter has a gain of 38 dB and a cut-off frequency of 24 MHz.

5.7 Realization of Operational Amplifiers and Operational Amplifier Filters

5.7.1 A Four-Stage Feed-Forward Operational Amplifier

A four-stage operational amplifier is realized and characterized [USSZ09]. Due to low intrinsic transistor gain and the limited supply voltage, four stages are necessary to obtain sufficient gain. For high-speed purposes a feed-forward path fastens the operational amplifier. A block diagram is depicted in figure 5.2 for a further clarification of the internal opamp structure.

The fully differential operational amplifier is organized in an input stage A_1, a high-gain

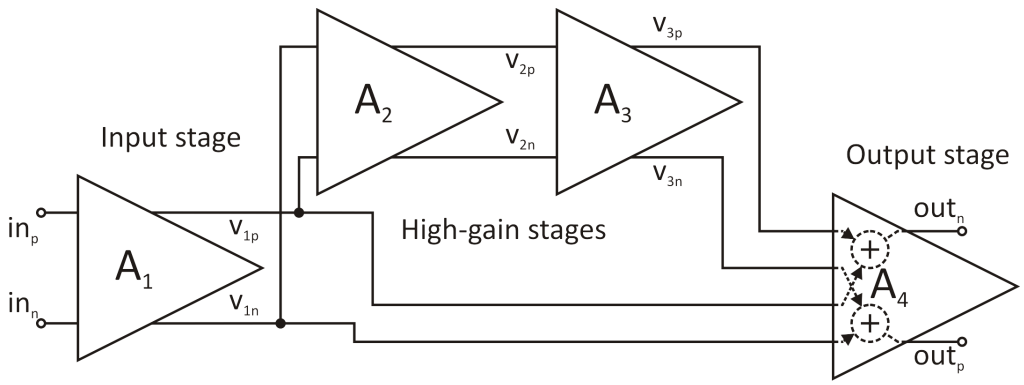

Figure 5.2: Four-stage feed-forward operational amplifier - block diagram

stage branch, consisting of the stages A_2 and A_3, and a summing and class AB output stage A_4. The feed-forward branch is realized from the input stage directly to the output stage. A detailed circuit schematic is depicted in 5.3. The biasing networks are omitted due to simplicity.

The input stage A_1 contains an NMOS differential pair biased by M_{3a}. For high-speed reasons the input transistors M_{1a} and M_{2a} have minimal gate length and thus cause a high level of 1/f noise. To reduce the noise contribution large W input transistors are used. The load of the differential pair are the PMOS transistors M_{4a}, M_{5a}, M_{6a}, and M_{7a}. These load transistors are split to ease a fast common mode regulation. 80% of the load (M_{6a} and M_{7a}) is biased constantly by V_{B2a}. The remaining part (M_{4a} and M_{5a}) is used for the common-mode regulation. The effect is a reduced gain in the common-mode feedback loop but the speed is increased due to the smaller parasitic load capacitance. The operational amplifier is realized with a separate common-mode feedback (CMFB) regulation for each gain stage. The common-mode level is detected by the resistors R_{1a} and R_{2a}. The common-mode regulator is another differential pair. The resistor R_{3a} is used for ac decoupling. The FET-diode M_{13a} keeps a fundamental current through M_{10a} if the load transistors shut off and bring a faster regulation. The capacitor C_{3a} adds a dominant pole to the regulation and is used for high-frequency compensation of the common-mode feedback loop. For high frequencies the CMFB level is set by the capacitors C_{1a} and C_{2a}.

The two cascaded differential amplifiers A_2 and A_3 form the high-gain amplifiers. A_2 contains an NMOS differential pair with similar structure to the input amplifier. M_{6b} and M_{7b} ensure a fundamental current even if the input transistors M_{1b} and M_{2b} shut off. In this way the delay at turn on of the load transistors M_{4b} and M_{5b} is reduced and ringing of the CFMB is minimized. The currents drawn from M_{6b} and M_{7b} are of the extent of approximately one tenth of the bias current through M_{3b}. A_3 contains a PMOS differential pair and a PMOS differential pair for the CMFB. The PMOS stage provides an output voltage range of v_{3p} and v_{3n} that is optimal for the output stage.

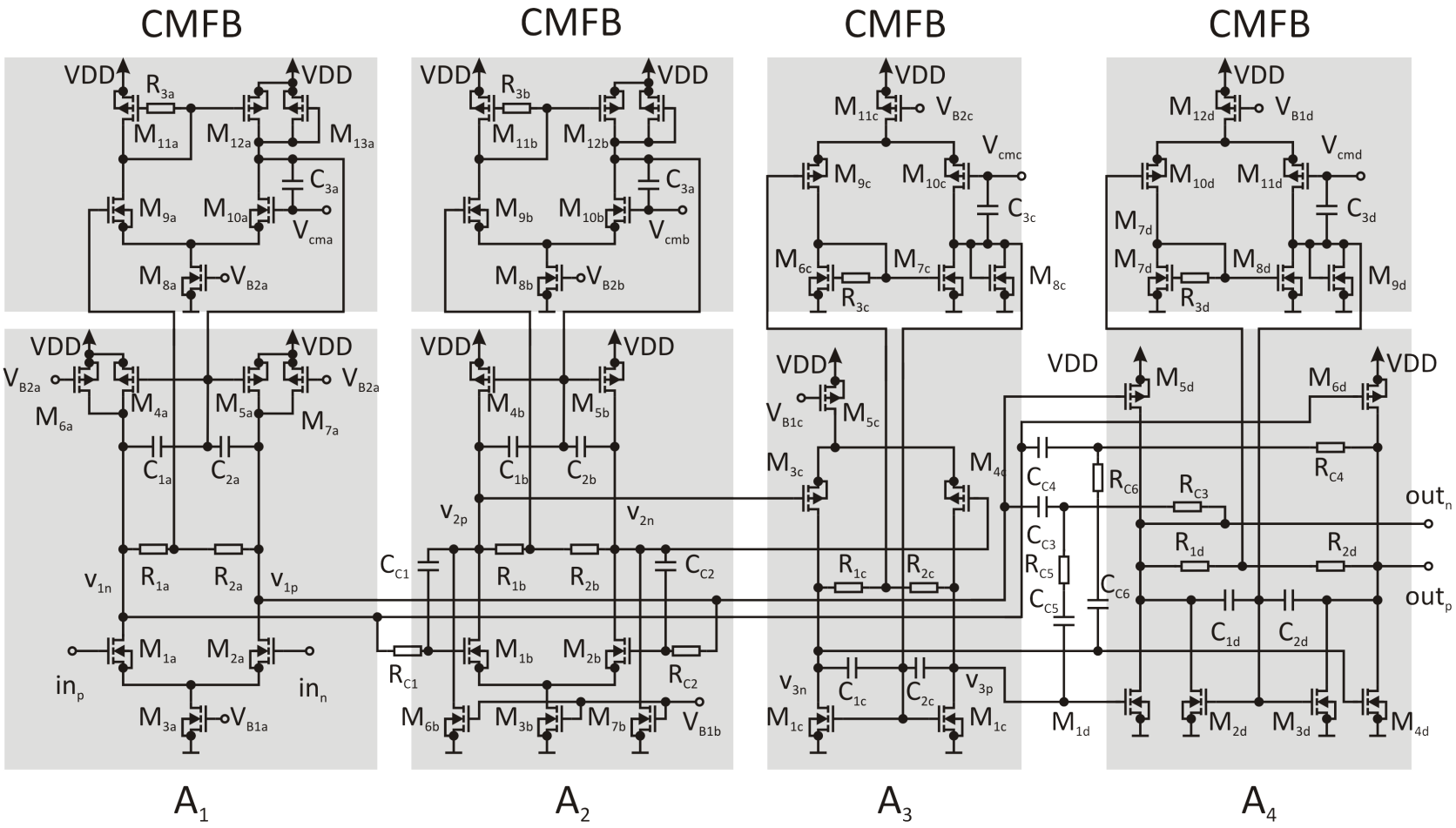

Figure 5.3: Four-stage feed-forward operational amplifier - schematic

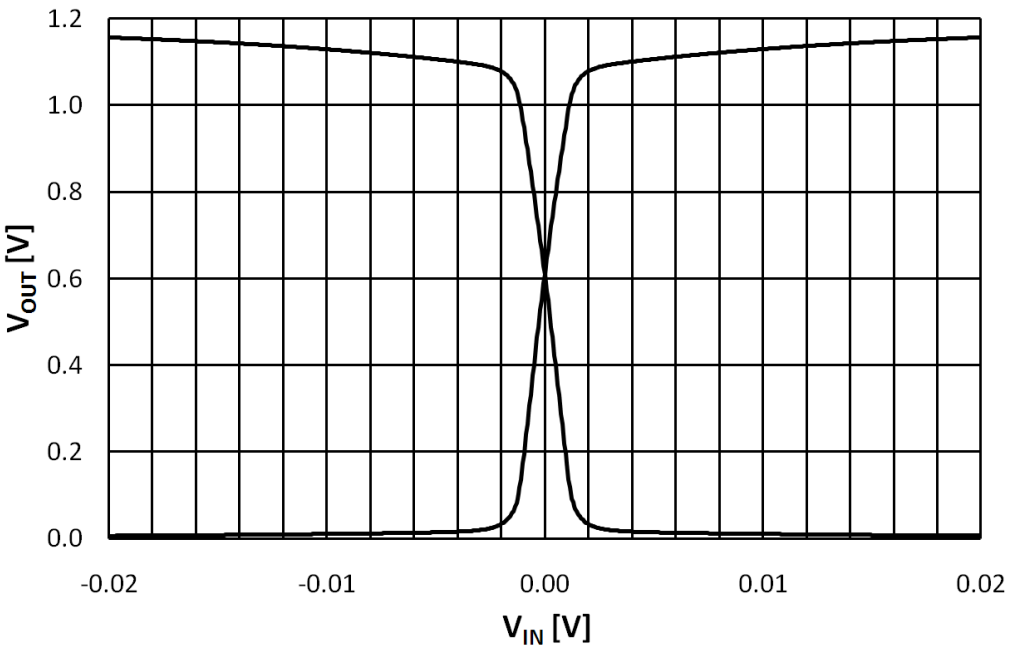

Figure 5.4: Four-stage feed-forward operational amplifier - DC characteristics

The output stage is a class AB amplifier with weak AB behavior. The common-mode output voltages of A_1 and A_3 are set to ensure the AB characteristics. Besides the amplification, the output stage merges the feed-forward signal directly from A_1 and the high-gain signal directly from A_3. The CMFB uses a PMOS differential pair and the output common-mode voltage is controlled by the transistors M_{2d} and M_{3d}.

The compensation is done by a modified nested Miller compensation. The Miller network consists of the resistors R_{C3} to R_{C6} and the capacitors C_{C3} to C_{C6} [PP02]. The modification is the separate compensation of the high-gain branch by the elements R_{C1}, R_{C2}, C_{C1}, and C_{C2}.

Simulation results The operational amplifier is designed in 65 nm CMOS technology and consumes 11.4 mW power at a supply voltage of 1.2 V. The driven load is 5 pF in parallel to 10 kΩ at each output.

The DC characteristics of the opamp is depicted in figure 5.4. The output common-mode level is set to 600 mV. A good linearity in an input voltage range of ± 1 mV is reached.

The frequency response is shown in figure 5.5. Figure 5.5(a) exhibits a GBW of 1 GHz and a gain of 58 dB. The phase response in figure 5.5(b) shows a phase margin of 62° at a load of 5 pF in parallel to 10 kΩ at each output pin.

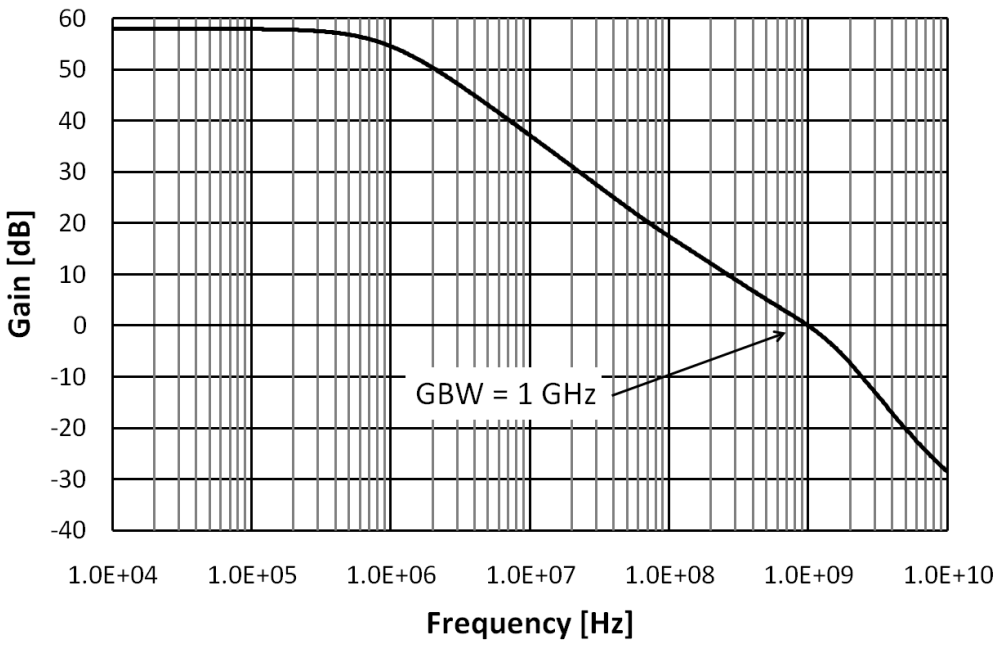

(a) Amplitude response

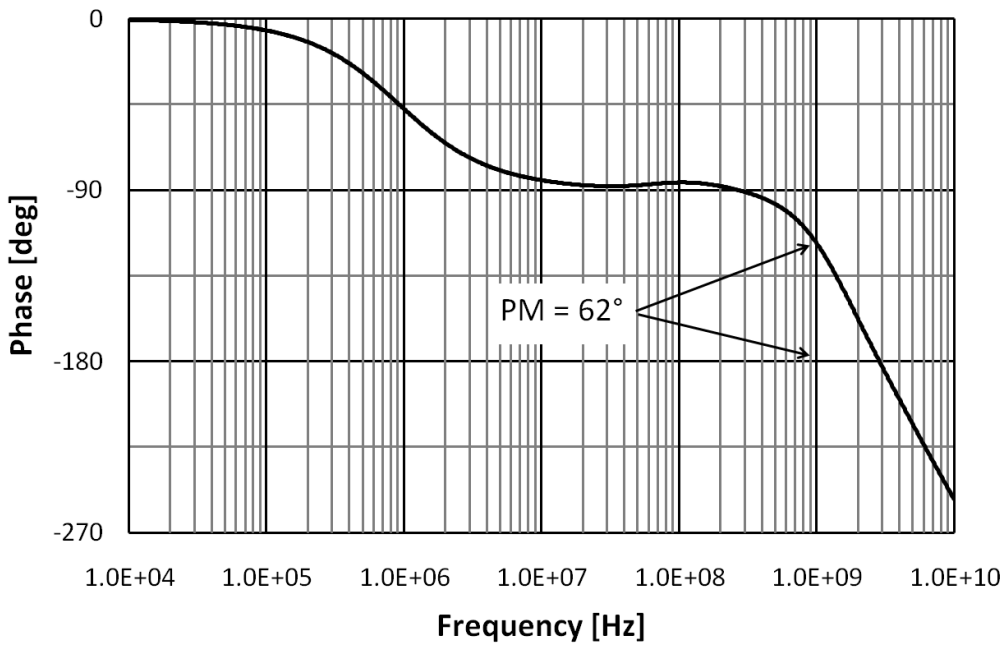

(b) Phase response

Figure 5.5: Four-stage feed-forward operational amplifier - frequency response

The input referred spectral noise density is depicted in figure 5.6. The very dominant 1/f noise goes up to about 100 kHz. The input referred spectral noise density at 10 kHz is about $15.4\,\mathrm{nV}/\sqrt{\mathrm{Hz}}$ and $5.7\,\mathrm{nV}/\sqrt{\mathrm{Hz}}$ at 1 MHz.

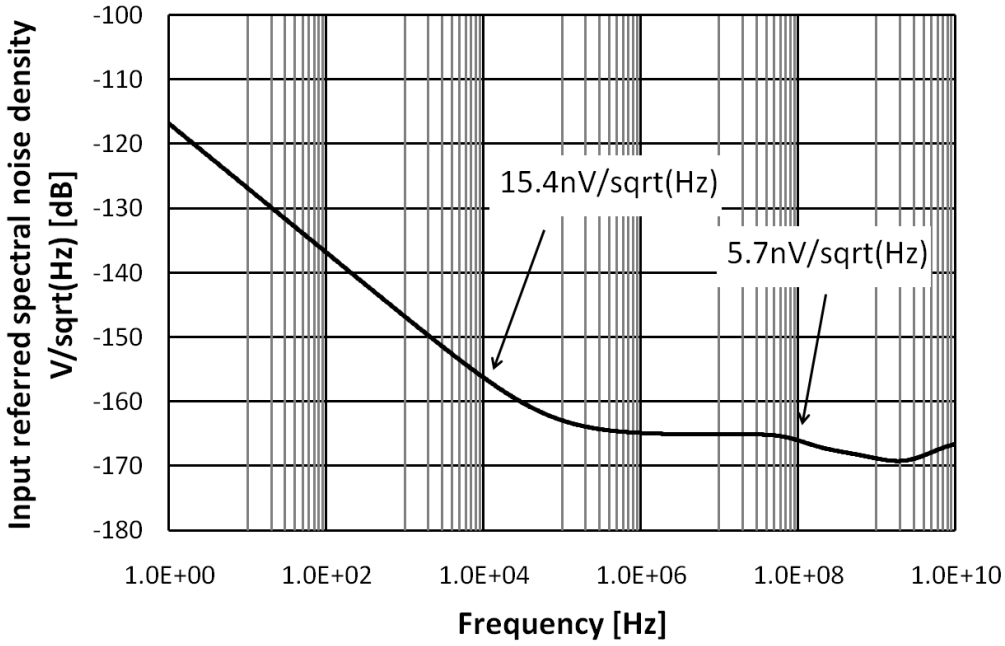

Figure 5.6: Four-stage feed-forward operational amplifier - spectral input referred noise density

The four-stage feed-forward operational amplifier reaches a FOM_{Opamp} of 1052 $\frac{MHz \cdot pF}{mA}$. A performance summary is given in table 5.1 [USSZ09].

Table 5.1: Four-stage feed-forward operational amplifier - performance summary

Technology	65 nm CMOS
Supply voltage	1.2 V
Power consumption	11.4 mW
DC gain	58 dB
GBW	1 GHz
Load	$2 \times 5\,\mathrm{pF}\|\|10\,\mathrm{k}\Omega$
PM	62°
FOM	1052 $\frac{MHz \cdot pF}{mA}$

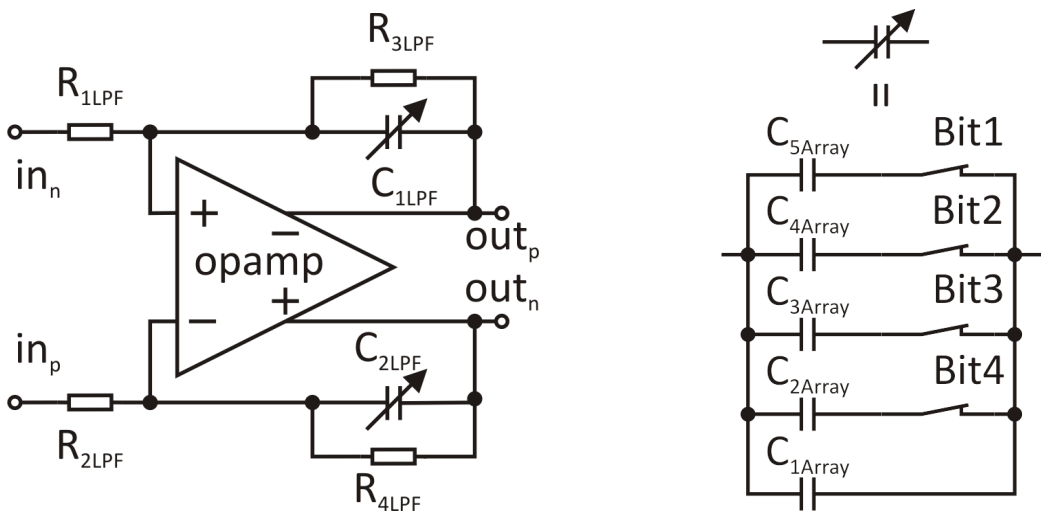

(a) Filter design

(b) Capacitor array

Figure 5.7: First-order opamp RC filter - schematics

5.7.2 A First-Order Operational Amplifier RC Low-Pass Filter Using the Four-Stage Feed-Forward Operational Amplifier

The introduced four-stage feed-forward operational amplifier was not fabricated separately but is used in a first-order opamp RC low-pass filter as depicted in figure 5.7. The gain of the filter is set by

$$-\frac{R_{3LPF}}{R_{1LPF}} \text{ and } -\frac{R_{4LPF}}{R_{2LPF}}. \tag{5.5}$$

The -3 dB cut-off frequency is given by

$$f_{-3dB} = \frac{1}{2\pi C_{1LPF} R_{3LPF}}, \tag{5.6}$$

or similar for C_{1LPF} and R_{3LPF}. The capacitors C_{1LPF} and C_{2LPF} are tunable in order to compensate for process variations. The capacitance tuning network is depicted in figure 5.7(b). The tuning network is a 4-bit controlled capacitor array, hence the cut-off frequency can be varied in $2^4 = 16$ steps. The capacitor values are 1.3 fF, 1.3 fF, 700 fF, 400 fF, and 200 fF for C_{1Array}, C_{2Array}, C_{3Array}, C_{4Array}, C_{5Array}, respectively. R_{1LPF} and R_{2LPF} are 100 Ω, which represents the equivalent mixer output resistance. R_{3LPF} and R_{4LPF} are 10 kΩ.

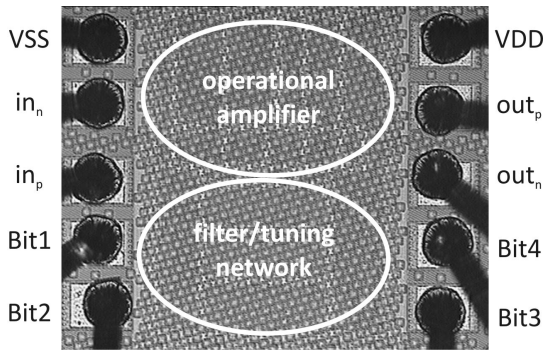

Figure 5.8: First-order opamp RC filter - chip photo

Table 5.2: First-order opamp RC Filter - 3rd-order harmonic distortions

Output amplitude V_{pp}	HD3
2.0 V_{pp}	-45.0 dBc
2.1 V_{pp}	-48.9 dBc
2.2 V_{pp}	-41.8 dBc

Measurement results The first-order operational amplifier RC filter is designed and fabricated in 65 nm CMOS technology. A chip photo is shown in figure 5.8. The circuit structures are hidden by the planarization and passivation layers as well as metal fill. The chip is supplied with 1.2 V via the pins VDD and VSS, the inputs and outputs are in_p, in_n and out_p, out_n, respectively. The pins Bit1 to Bit4 are used for tuning of the -3 dB cut-off frequency. The chip occupies 0.104 mm^2 active area and 0.254 mm^2 including the pads.

The DC filter characteristics are shown in figure 5.9. The low-pass filter has an almost linear output range of $\pm$ 1.1 V and a 10 mV offset. The filter is loaded with approximately 1.5 pF including the pads in parallel to 4.7 kΩ on each output pin. The load represents the expected load of the following ADC.

The AC characteristics are presented in figure 5.10. The filter gain is 38 dB which deviates from the adjusted 40 dB due to parasitic elements in the switches and the non-ideal operational amplifier. The tuning range spans from 3.5 MHz to 4.5 MHz.

For the distortion measurements the -3 dB cut-off frequency is set to 4 MHz. For single tone distortion measurements the input signal frequency is 100 kHz, hence HD3 and HD5 are in-band. The 3rd-order harmonic distortions at given input signals are given in table 5.2.

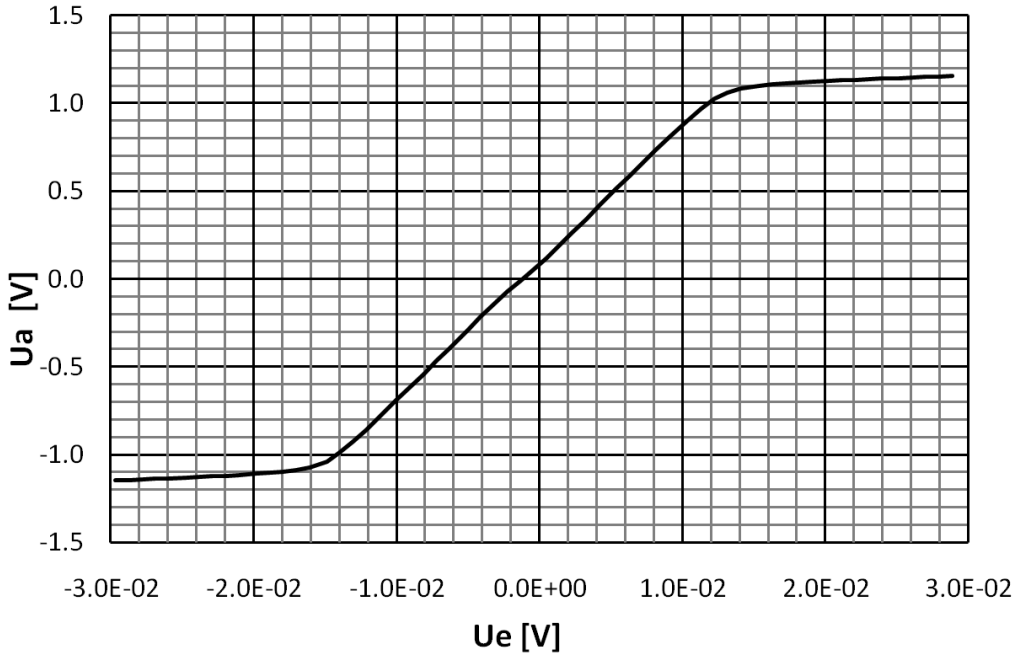

Figure 5.9: First-order opamp RC filter - DC characteristics

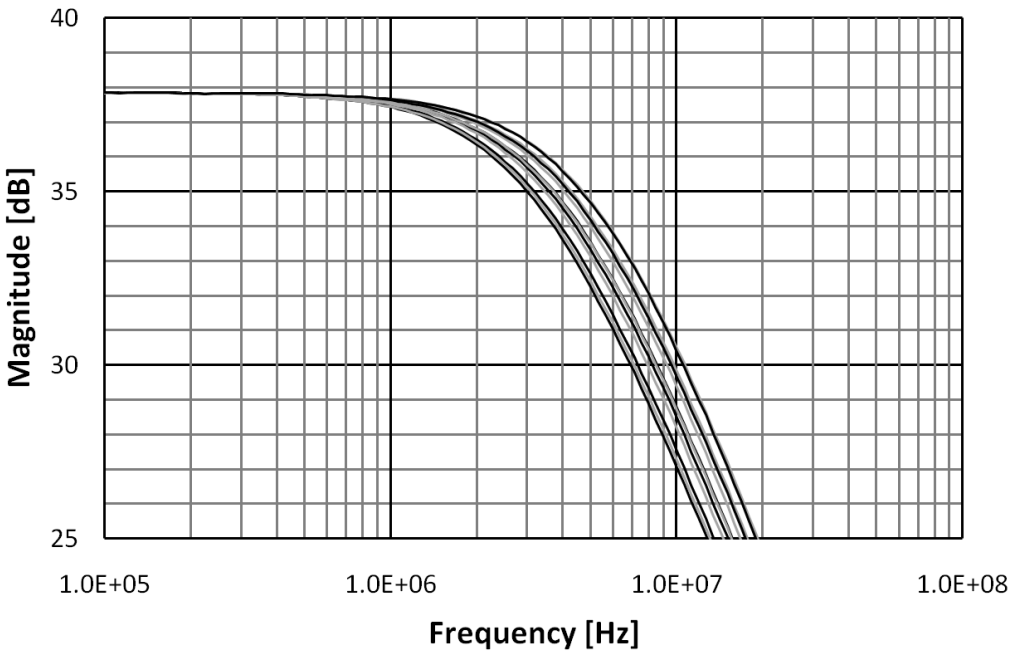

Figure 5.10: First-order opamp RC filter - AC characteristics, tuning range

The total harmonic distortions are estimated by using HD3 and HD5 (compare to (4.2)). An output signal swing of 2.15 V causes $THD_{1\%}$.

Table 5.3: First-order opamp RC low-pass filter - performance summary

Technology	65 nm CMOS
Supply voltage	1.2 V
Current consumption	8.34 mA
DC gain	38 dB
3 dB cut-off frequency	3.5 - 4.5 MHz
Load	$2 \times 1.5\,\text{pF}\|\|4.7\,\text{k}\Omega$
DR	57.2 dB
FOM_{Filter}	143945

The 3rd-order intermodulation products are measured in-band as well. The applied frequency of the input signals are 1 MHz and 1.1 MHz. The input amplitude of 15.5 mV of both input signals causes an IM3 of -40 dB.

The performance of the first-order opamp RC filter is rated with the dynamic range and the figure of merit. Using the simulated integrated noise from 0 to 4 MHz, a DR of 57.2 dB and a FOM_{Filter} of 143945 is reached. A summary of the filter performance is given in table 5.3 [UZ10].

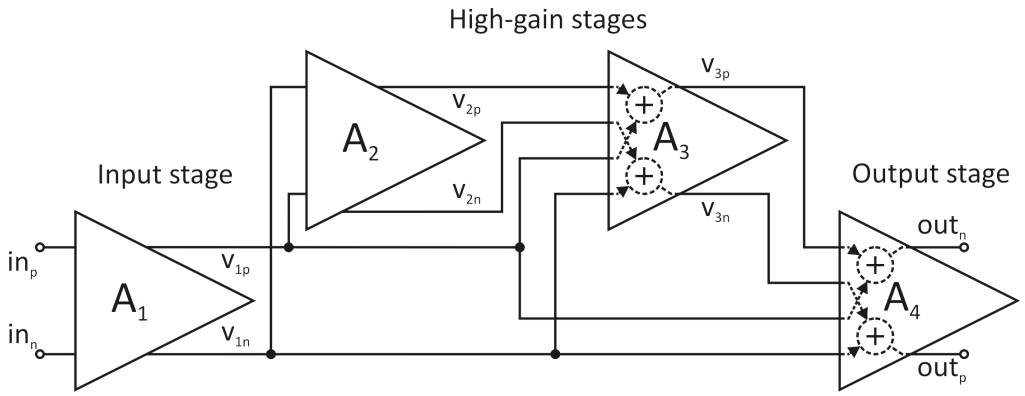

Figure 5.11: Four-stage multiple feed-forward operational amplifier - block diagram

5.7.3 A Four-Stage Multiple Feed-Forward Operational Amplifier

A fully differential four-stage operational amplifier with multiple feed-forward is designed in 65 nm CMOS [UZ09b]. Four stages are used to realize sufficient gain and two feed-forward branches enlarge the GBW of the operational amplifier. A block diagram is depicted in figure 5.11.

The four stages and two feed-forward branches are organized as following. After the input stage A_1 the amplified signal is split to all three remaining stages A_2, A_3, and A_4. The high-gain stages A_2 and A_3 are used for high DC gain, the feed-forward is used to keep the phase lag small. The output stage A_4 is a class AB amplifier and superposes the feed-forward signal from the input stage and the signal from the high-gain stage.

Figure 5.12 depicts a detailed schematic of the operational amplifier. The biasing networks are not shown. The input stage contains an NMOS differential pair. The input transistors M_{1a}, M_{2a}, M_{3a}, and M_{4a} are common centroid to improve matching in the input stage. The current source of the differential pair is split into two parts. The first, M_{5a} is constantly biased, the latter, M_{6a}, is used for the common-mode regulation. The loads of the input stage are the resistors R_{3a} and R_{4a}. The input referred noise is significantly reduced compared to active PMOS loads, however the gain of the input stage is reduced. The common-mode regulator contains a PMOS differential pair. The common-mode level is detected by the resistors R_{1a} and R_{2a}, the target common-mode level is set by V_{cma}. The loop-control is closed via M_{6a}, which is a part of the current-source, hence the common-mode control loop is faster.

The high-gain stages are two cascaded differential amplifiers (A_2 and A_3). The first high-gain stage A_2 uses an NMOS input pair (M_{1b} and M_{2b}) for signal amplification. The amplifier is constantly biased by the current source M_{3b}. The load transistors are split.

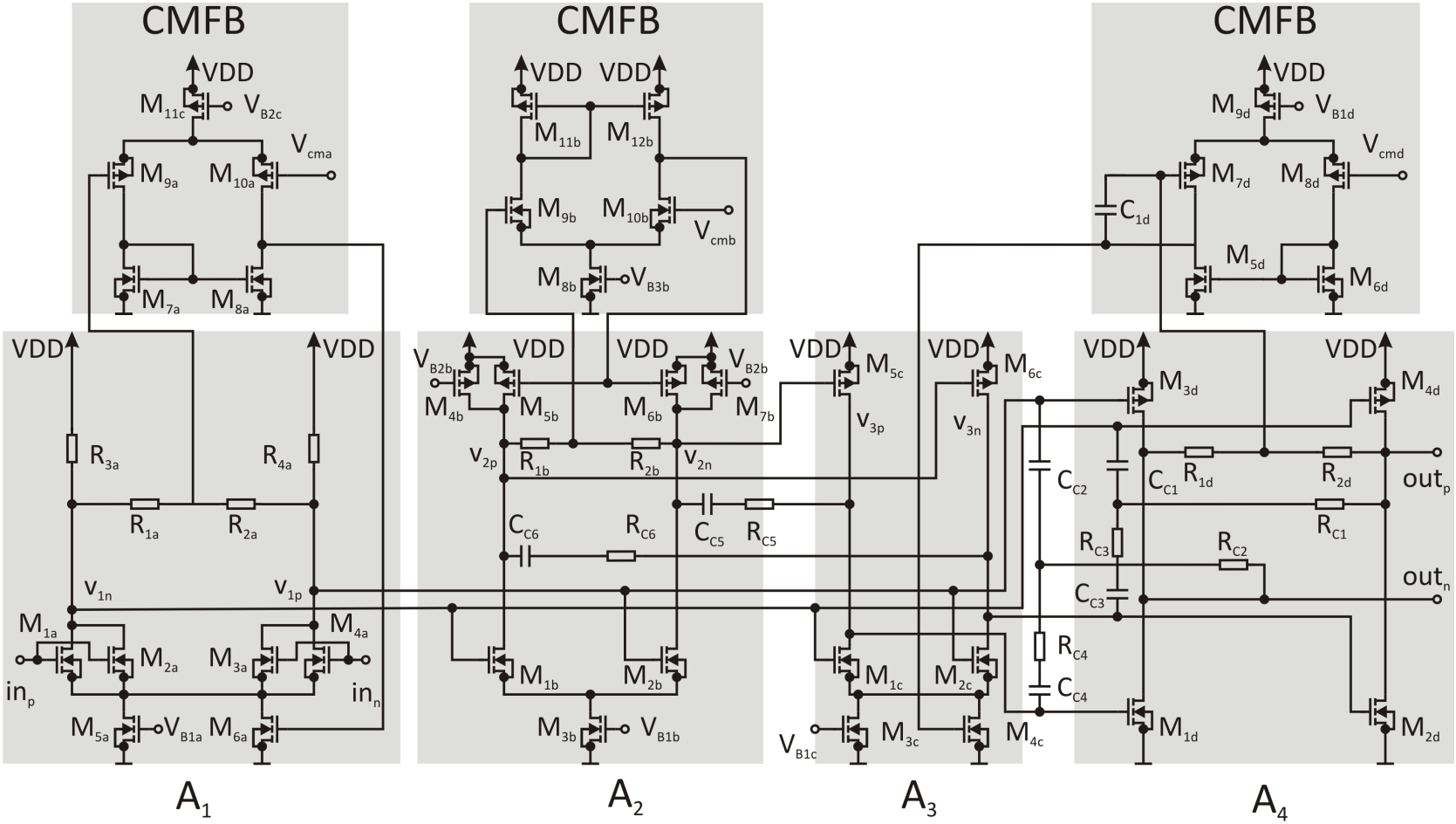

Figure 5.12: Four-stage multiple feed-forward operational amplifier - schematic

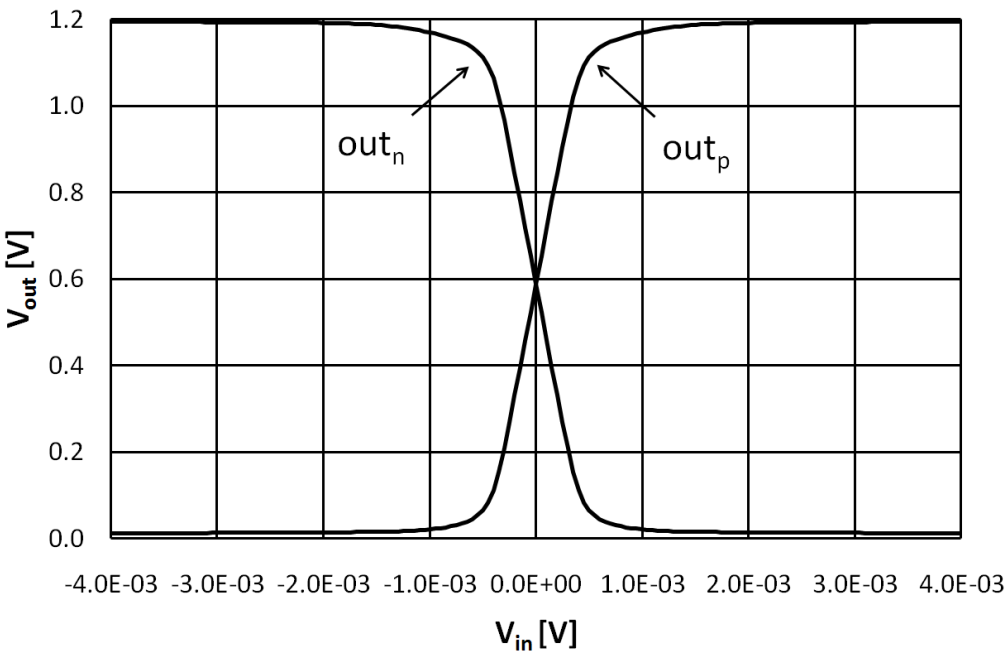

Figure 5.13: Four-stage multiple feed-forward operational amplifier - DC characteristics

M_{4b} and M_{7b} are constantly biased. M_{5b} and M_{6b} are for the common-mode regulation. The amplifier in the common-mode regulation contains an NMOS differential pair, the common-mode level is derived by R_{1b} and R_{2b}. The reference input is V_{cmb}. A_3, the second high-gain stage contains an NMOS differential pair as well and has two inputs. M_{1c} and M_{2c} are connected at the output of the input stage, hence they act as a feed-forward in the high-gain stages and has some speed benefits. M_{5c} and M_{6c} are driven by the output of the first high-gain stage A_2. The use of M_{5c} and M_{6c} brings an additional signal amplification in the high-gain branch. M_{3c} is the fixed part of the bias of A_3 and M_{4c} is used for the common-mode regulation.

The output stage A_4 is a class AB amplifier, realized by proper common-mode voltage setting of the previous stages A_1 and A_3. The output stage amplifies and adds up the feed-forward signal of A_1 and the high-gain signal of A_3. The common-mode regulation is done over the two stages A_3 and A_4. The common-mode level is tapped between R_{1d} and R_{2d} and is controlled by the part of the current source M_{4c} in A_3.

The overall operational amplifier is compensated with a nested Miller compensation [PP02]. The compensation network includes R_{C1} to R_{C4} and C_{C1} to C_{C4}. The high-gain stages are compensated by their own by R_{C5}, R_{C6}, C_{C5}, and C_{C6}.

Simulation results The operational amplifier is designed in 65 nm low-power CMOS technology and uses a supply voltage of 1.2 V. The current consumption is 9.6 mA and a

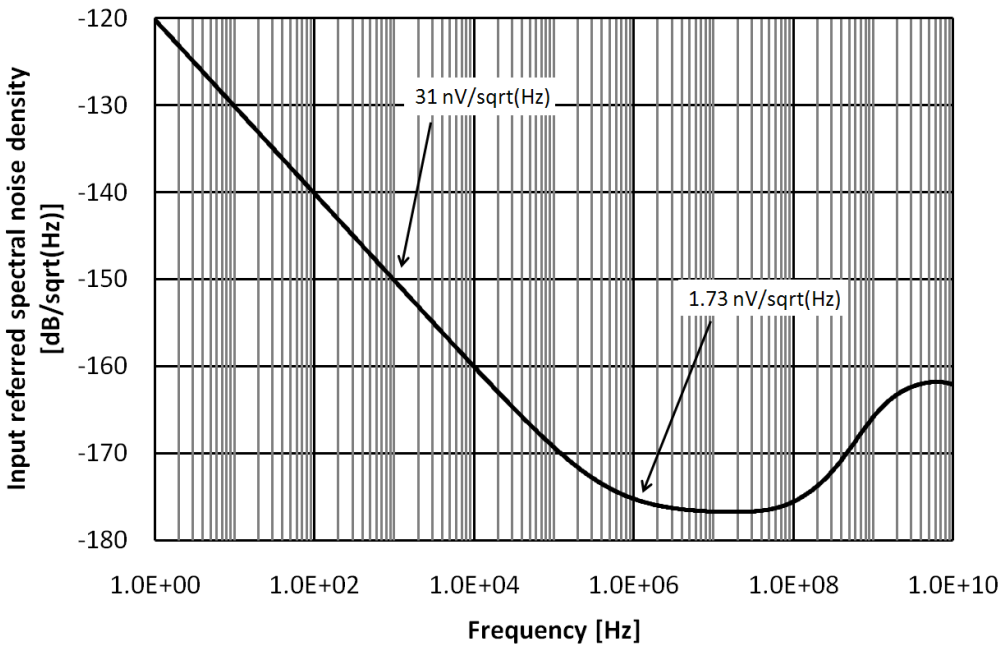

Figure 5.14: Four-stage multiple feed-forward operational amplifier - spectral input referred noise density

capacitive load of 4 pF in parallel to 10 kΩ on each of the differential outputs is driven.

The open-loop DC characteristics are depicted in figure 5.13. The common-mode level at the output is 600 mV and a good linearity is achieved at an input range of ± 0.5 mV.

The input referred spectral noise density is shown in figure 5.14. At 1 kHz the input-referred spectral noise density is $31\,\mathrm{nV}/\sqrt{\mathrm{Hz}}$ and at 1 MHz $1.73\,\mathrm{nV}/\sqrt{\mathrm{Hz}}$.

The frequency response is depicted in figure 5.15. The amplitude response in figure 5.15(a) exhibits a DC gain of 68 dB and a gain bandwidth product of 1 GHz. The phase response in figure 5.15(b) shows a phase margin of 60°, which is equivalent to a phase lag of 120°.

The power supply rejection ratio at DC is $\mathrm{PSRR_{VSS}} = 77.4\,\mathrm{dB}$ and $\mathrm{PSRR_{VDD}} = 77.7\,\mathrm{dB}$ at VSS and VDD, respectively. The operational amplifier has a figure of merit of 833 $\frac{MHz \cdot pF}{mA}$. A performance summary is given in table 5.4 [UZ09b].

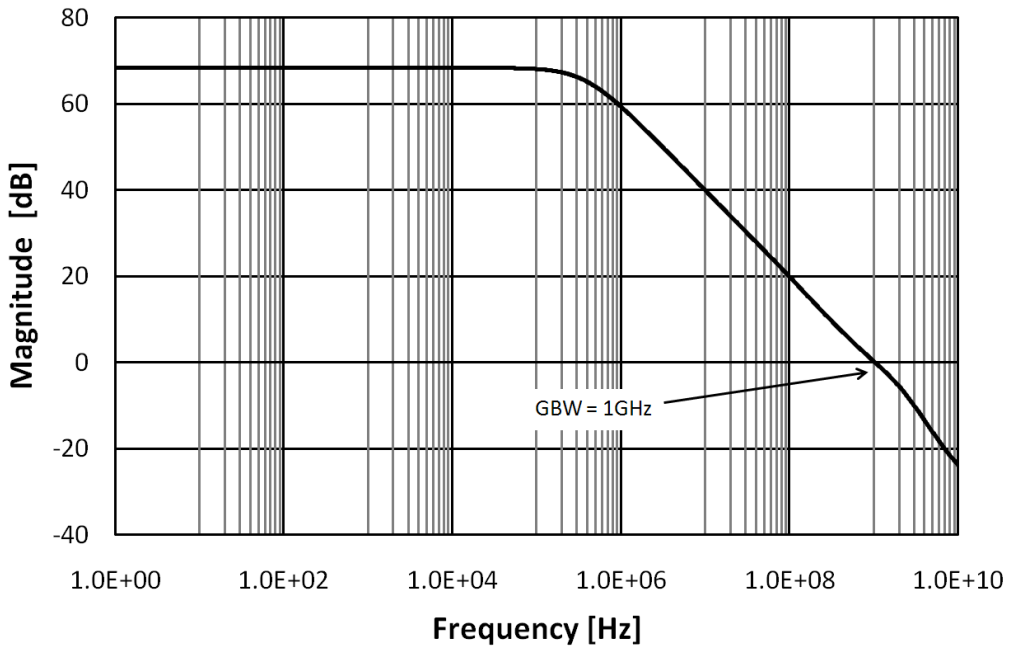

(a) Amplitude response

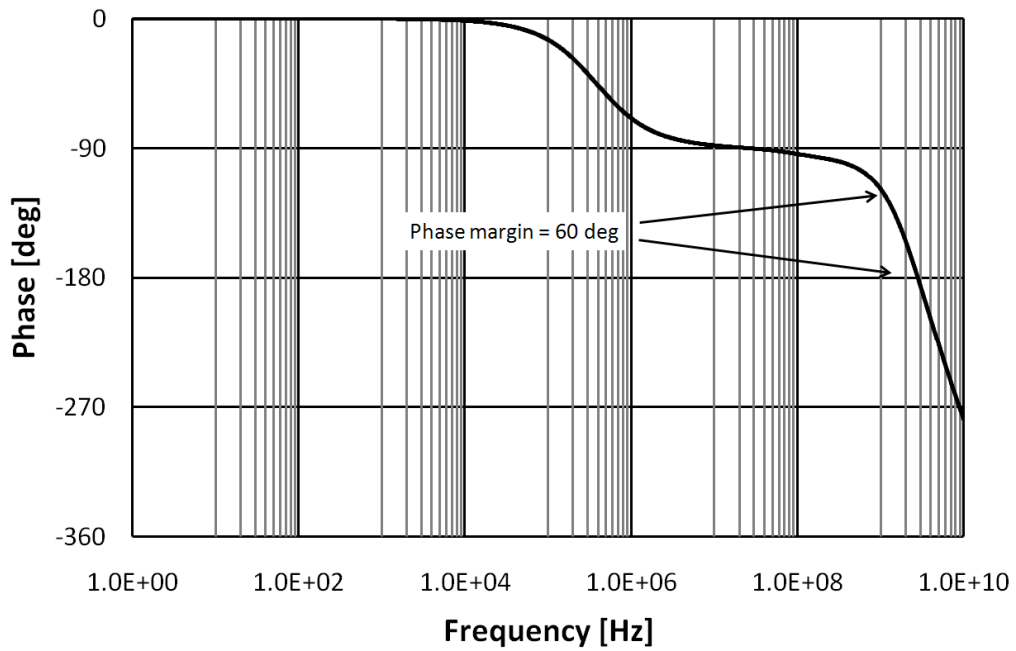

(b) Phase response

Figure 5.15: Four-stage multiple feed-forward operational amplifier - frequency response

Table 5.4: Four-stage multiple feed-forward operational amplifier - performance summary

Technology	65 nm CMOS
Supply voltage	1.2 V
Current consumption	9.6 mA
DC gain	68 dB
GBW	1 GHz
Load	$2 \times 4\,\text{pF}\|\|10\,\text{k}\Omega$
PM	60°
FOM_{Opamp}	$833\,\frac{MHz \cdot pF}{mA}$

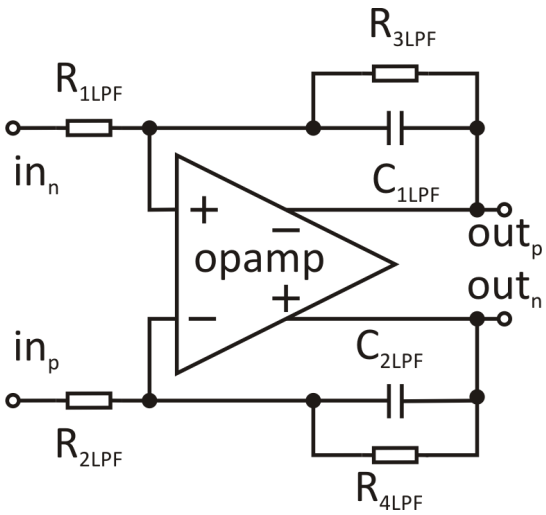

Figure 5.16: First-order opamp RC filter using the four-stage multiple feed-forward opamp - schematics

5.7.4 A First-Order Operational Amplifier RC Low-Pass Filter Using the Four-Stage Multiple Feed-Forward Operational Amplifier

The four-stage multiple feed-forward operational amplifier is used in an first-order opamp RC filter as depicted in figure 5.16. The gain and the -3 dB cut-off frequency is set like in (5.5) and (5.6). R_{1LPF} and R_{2LPF} correspond to the equivalent mixer output resistances and are 100 Ω. R_{3LPF} and R_{4LPF} define the gain of the filter and are 5 kΩ. The filter capacitances C_{1LPF} and C_{2LPF} are 8 pF.

Simulation results The filter was not fabricated because of a lack of chip area. The first-order opamp RC filter is supplied with 1.2 V and has a power consumption of 11.5 mW. The load of the filter is 4 pF in parallel of 10 kΩ. The differential DC characteristics are shown in figure 5.17. The common-mode level is 600 mV and the graph is linear in an input voltage range of ±11 mV.

The input referred spectral noise density is shown in figure 5.18. The input referred spectral noise density at 10 kHz is $10\,\mathrm{nV}/\sqrt{\mathrm{Hz}}$ and at 1 MHz $2.5\,\mathrm{nV}/\sqrt{\mathrm{Hz}}$. The average integrated noise density from 500 Hz to 4 MHz is $2.94\,\mathrm{nV}/\sqrt{\mathrm{Hz}}$.

The AC characteristics are shown in figure 5.19. The amplitude response in figure 5.19(a) shows a filter DC gain of 40 dB and a -3 dB cut-off frequency of 4 MHz. The phase response is depicted in figure 5.19(b). The distortion measurement is performed with

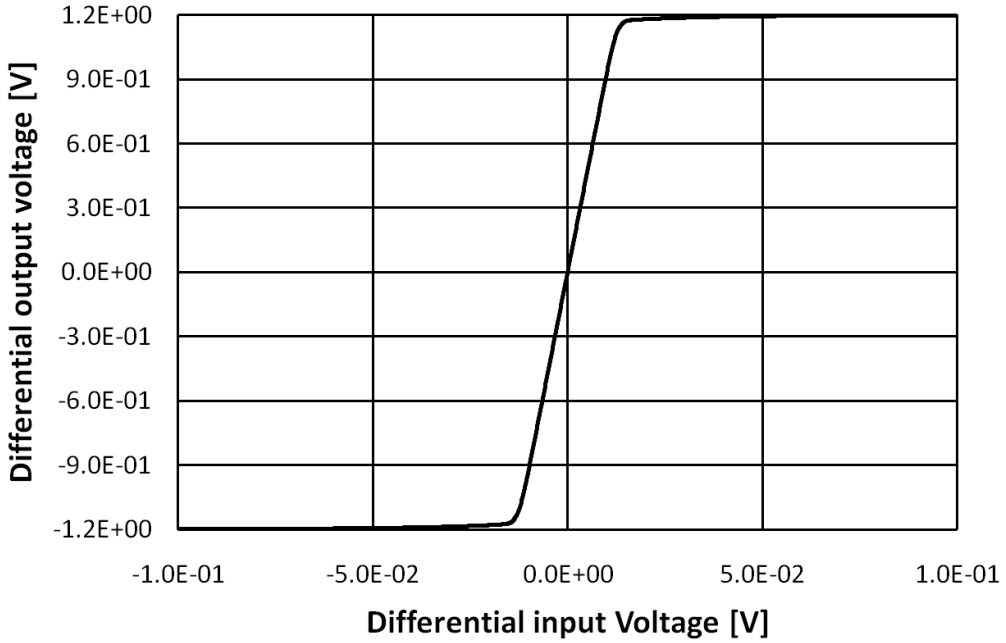

Figure 5.17: First-order opamp RC filter using four-stage multiple feed-forward operational amplifier - differential DC characteristics

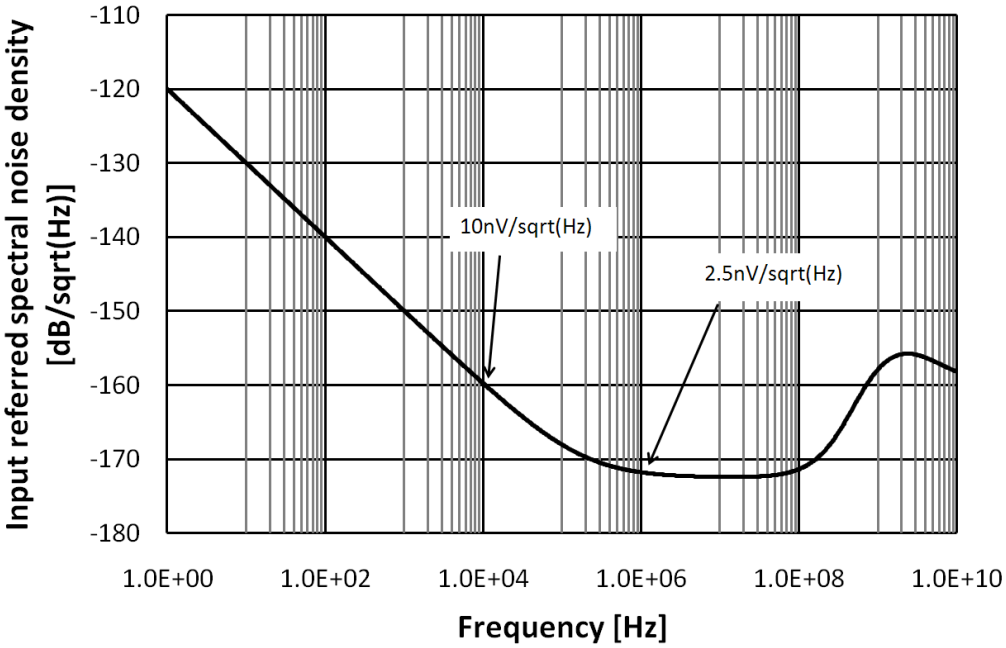

Figure 5.18: First-order opamp RC filter using four-stage multiple feed-forward operational amplifier - spectral input referred noise density

a sinusoidal input signal of 100 kHz. The THD of -40 dB of the output signal occurs

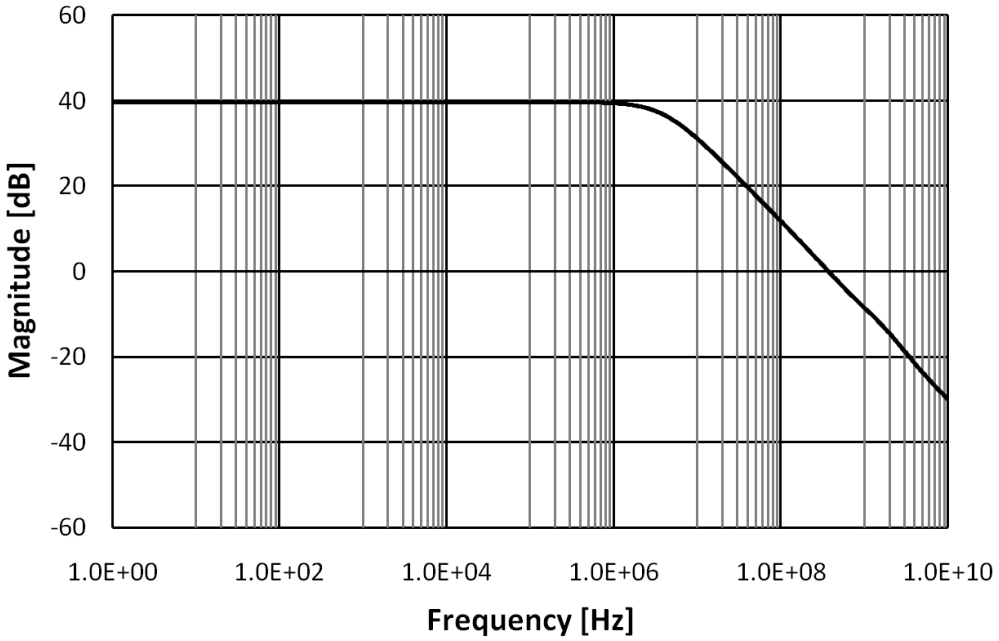

(a) Amplitude response

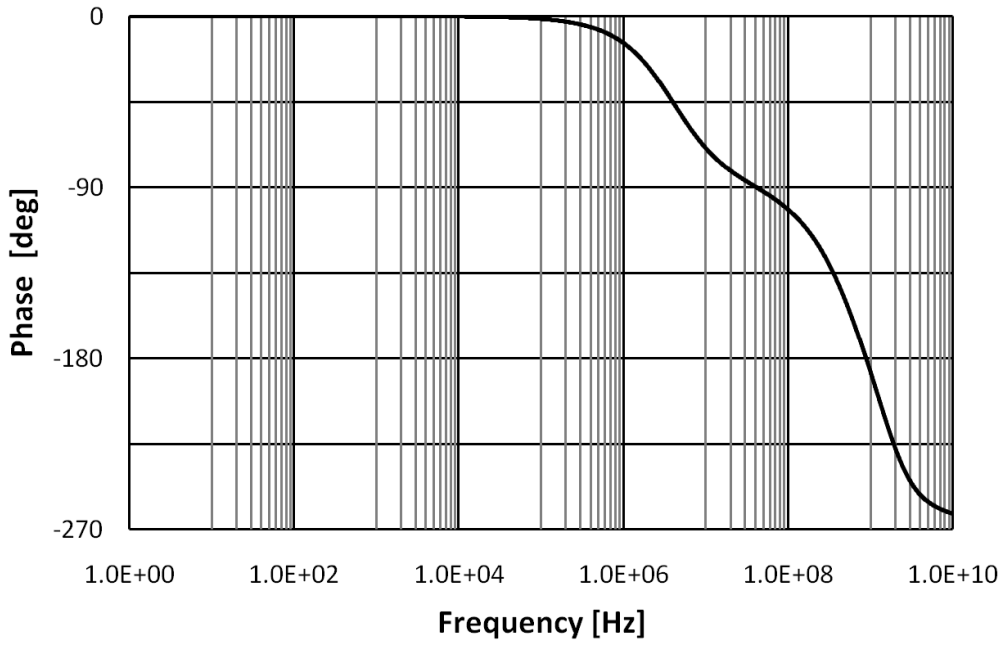

(b) Phase response

Figure 5.19: Four-stage multiple feed-forward operational amplifier - differential frequency response

at a differential input signal amplitude of 11.48 mV_p. The in-band intermodulations are determined by using two-tones at 1 MHz and 1.2 MHz. A differential input signal

Table 5.5: First-order opamp RC low-pass filter using the 4-stage multiple feed-forward opamp - performance summary

Technology	65 nm CMOS
Supply voltage	1.2 V
Power consumption	11.5 mW
DC gain	40 dB
3 dB cut-off frequency	4 MHz
Load	$2 \times 1.5\,\mathrm{pF}||5\,\mathrm{k}\Omega$
DR	62.7 dB
FOM_{Filter}	54744

amplitude of 7.2 mV_p causes IM3 of -40 dB. The filter has a DR of 62.7 dB and a FOM_{Filter} of 54744. A performance summary is given in table 5.5.

5.7.5 Three-Stage High-Voltage Operational Amplifier in 65 nm CMOS at 2.5 V Supply Voltage

An operational amplifier is implemented in 65 nm CMOS technology, which is appropriate for a 2.5 V supply voltage, although the nominal supply voltage of the digital CMOS process is only 1.2 V. The higher supply voltage enables a higher output voltage swing and, hence, avoids clipping at large input signals. Furthermore higher drain-source voltages of the transistors can be provided due to the high supply voltage. Thus lower distortions and intermodulation products occur [HS03a]. Applying a supply voltage outside specification is a challenging issue. Nanometer CMOS transistors with their thin gate oxide are vulnerable to high electrical fields. Hence, V_{GS} and V_{DS} must remain within the specified limits. Exceeding these limits leads to reliability problems up to immediate electrical damage. To avoid those breakdowns, additional transistors are inserted between the supply rails. They ensure a proper voltage dividing and additionally they operate as cascodes which enhance speed and gain [PP04, SS99].

The schematic of the operational amplifier is shown in figure 5.20. The opamp is organized in three stages, the input stage, the high-gain stage, and the output stage. A feed-forward from the input-stage to the output stage is implemented as well. The input stage is realized with two differential pairs. The load of the NMOS differential pair is substituted by the PMOS differential pair. The NMOS current source is split into two parts, M_{1a} having a fixed bias, and M_{2a}, which is used for the common-mode feedback. The current source is cascoded with M_{3a}. M_{9a} and M_{8a} are used for proper voltage division. The common-mode regulation is realized with a cascoded PMOS differential pair. The actual value of the common-mode voltage is determined by R_{1a} and R_{2a}, and C_{1a} and C_{2a}. The set point is V_{cma}. The common-mode regulation is closed by M_{2a}.

The high-gain stage uses a PMOS differential pair (M_{3b} and M_{4b}). The current source is again split into a fixed part (M_{6b}) and a variable part (M_{7b}) for a fast common-mode regulation. The current source is cascoded by M_{5b} and the load transistors M_{1b} and M_{2b} are constantly biased.

The output stage is simultaneously the summing stage for the high-gain branch and the feed-forward branch. The feed-forward signal is amplified and added to the output signal by the transistors M_{5c} and M_{6c}. The high-gain signal is amplified and added to the output signal by M_{1c} and M_{2c}. M_{3c} and M_{4c} are cascode transistors and M_{7c} and M_{8c} are current sources. The common-mode feedback is realized with an NMOS differential pair. The regulation is closed by the current source transistor M_{7b} of the high-gain stage.

The compensation is done by nested Miller compensation [PP02]. The compensation network is R_{C1}, R_{C2}, and C_{C1} to C_{C4}.

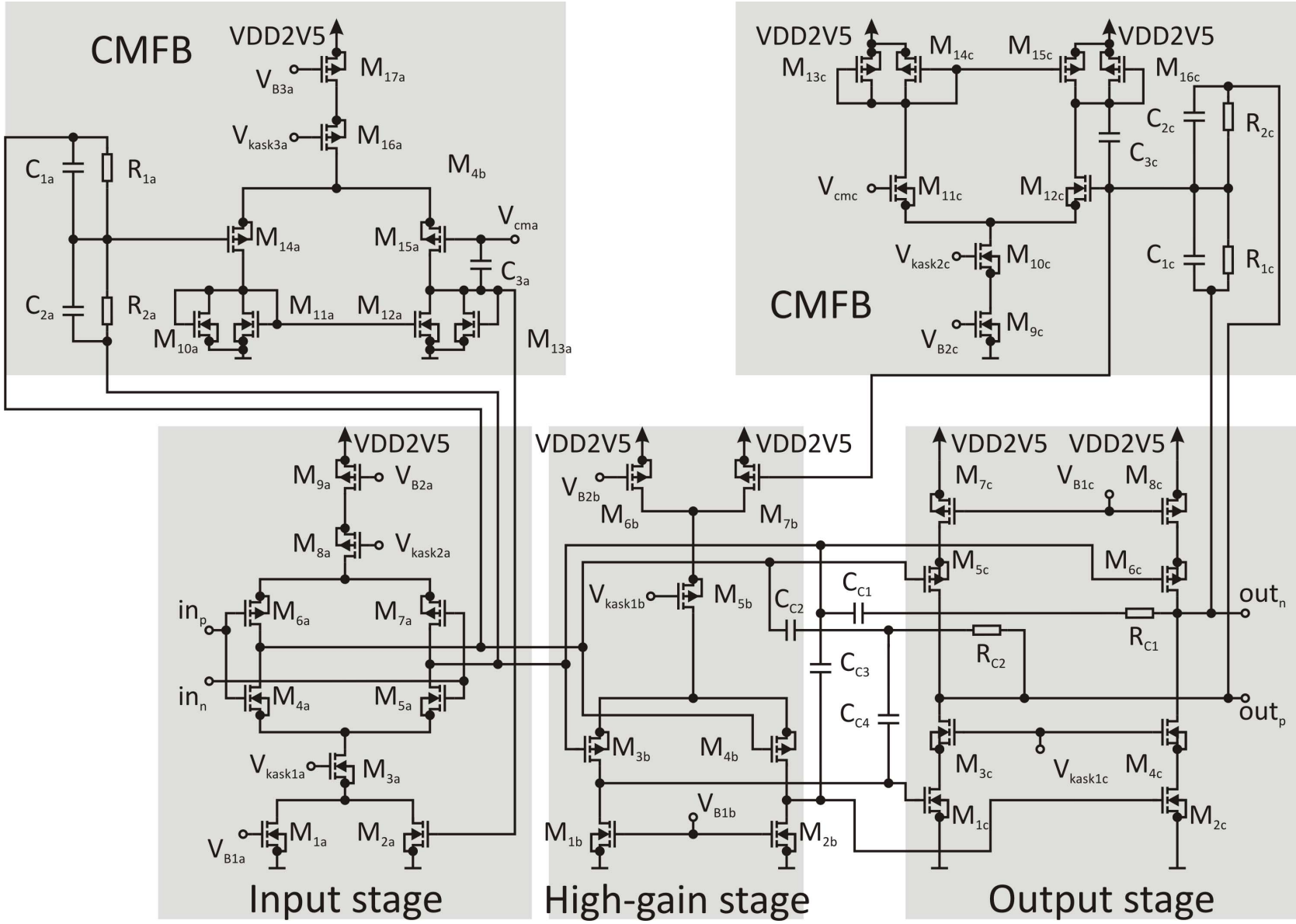

Figure 5.20: Three-stage high-voltage operational amplifier - schematics

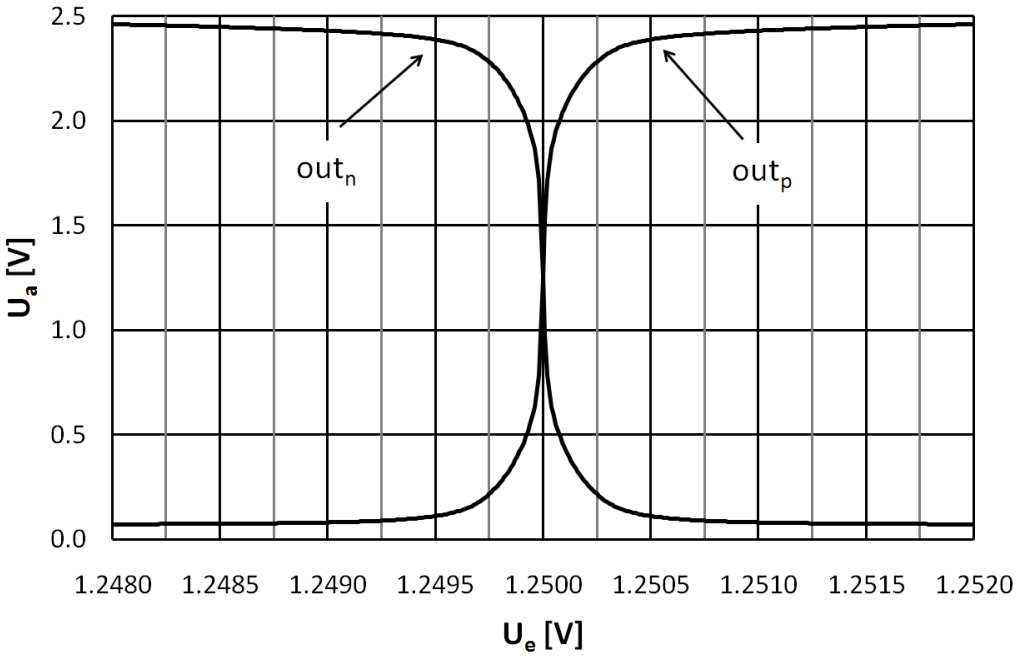

Figure 5.21: Three-stage high-voltage operational amplifier - DC characteristics

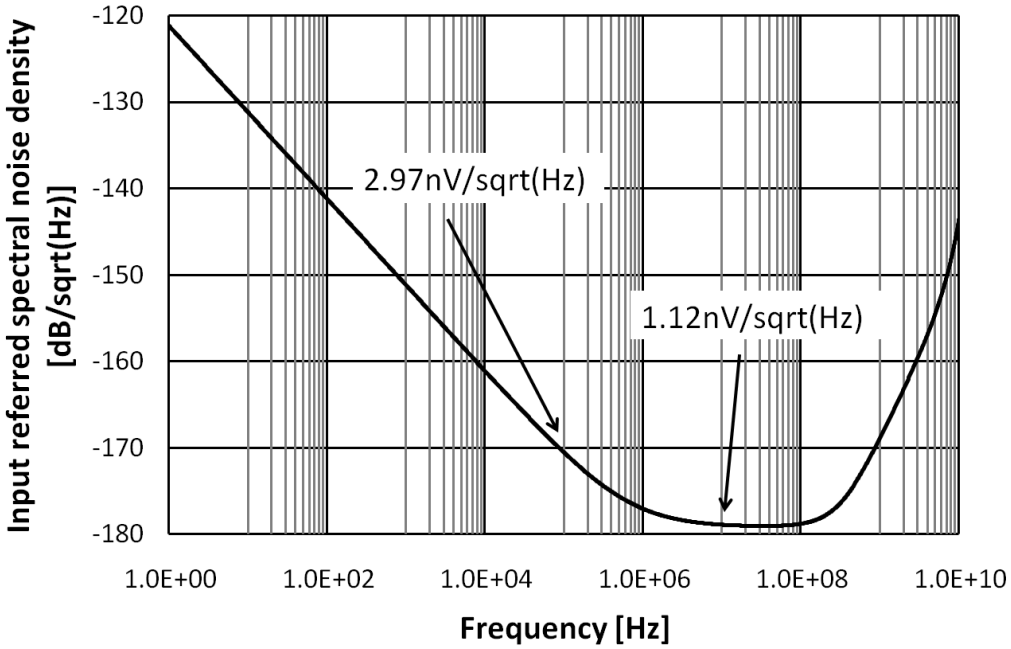

Figure 5.22: Three-stage high-voltage operational amplifier - input referred spectral noise density

Simulation results The operational amplifier has a supply voltage of 2.5 V and a current consumption of 5.85 mA. The opamp drives a load of 1 pF at each output pin.

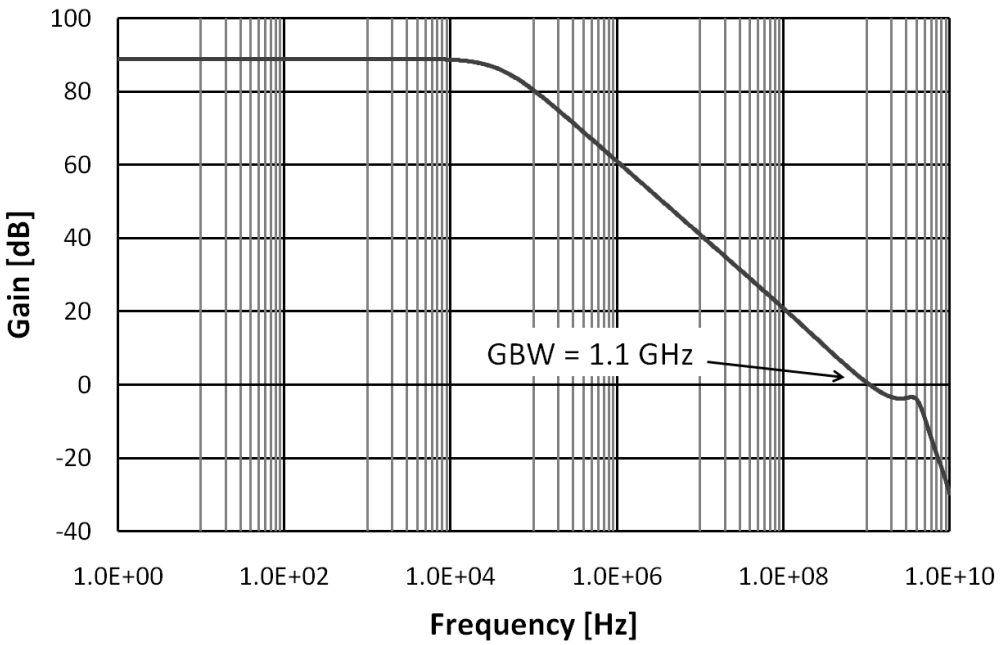

(a) Amplitude response

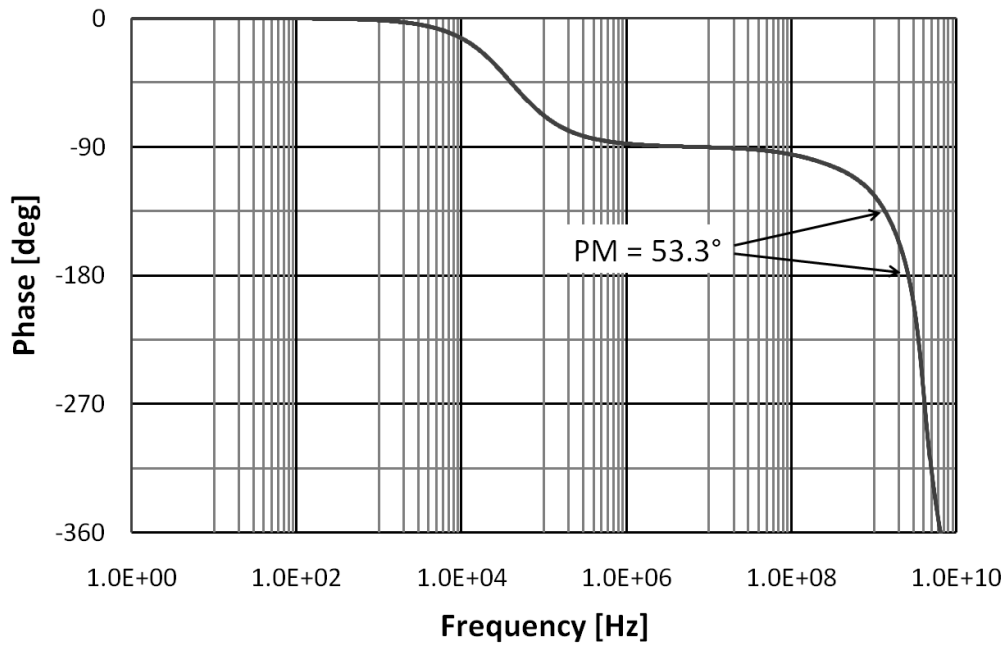

(b) Phase response

Figure 5.23: Three-stage high-voltage operational amplifier - frequency response

The DC characteristics are depicted in figure 5.21. The output range is between 0.1 V and 2.4 V. The common-mode output voltage is 1.25 V.

The input referred spectral noise density is depicted in figure 5.22. At 100 kHz the input referred noise density is $1.97\,\mathrm{nV}/\sqrt{\mathrm{Hz}}$ and at 10 MHz $2.12\,\mathrm{nV}/\sqrt{\mathrm{Hz}}$. The average input referred integrated noise density is $1.71\,\mathrm{nV}/\sqrt{\mathrm{Hz}}$ between the integration limits of 500 Hz and 4 MHz.

The AC characteristics are given in figure 5.23. The amplitude response in figure 5.23(a) shows a DC gain of 89 dB and a gain-bandwidth product of 1.1 GHz. The phase response in figure 5.23(b) has a PM of 53.3°. The $\mathrm{PSRR}_{\mathrm{VSS}}$ is 107 dB and $\mathrm{PSRR}_{\mathrm{VDD}}$ is 108 dB. The operational amplifier has a FOM_{Opamp} of 376 $\frac{MHz \cdot pF}{mA}$. The performance summary is given in table 5.6.

Table 5.6: Three-stage high-voltage operational amplifier - performance summary

Technology	65 nm CMOS
Supply voltage	2.5 V
Current consumption	5.85 mA
DC gain	89 dB
GBW	1.1 GHz
Load	2×1 pF
PM	53.3°
FOM_{Opamp}	376 $\frac{MHz \cdot pF}{mA}$

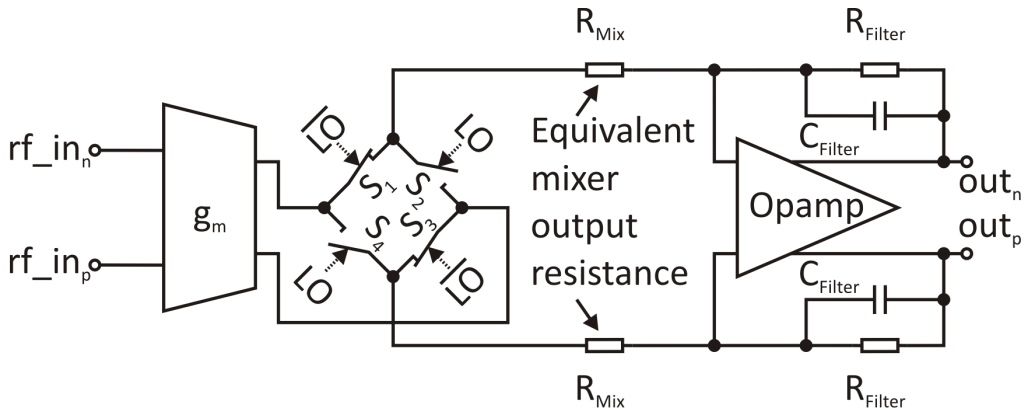

Figure 5.24: Mixer filter combination

5.7.6 Mixer and Filter Combination Using the Three-Stage High-Voltage Operational Amplifier

The high-voltage operational amplifier is inserted in a mixer-filter combination of a direct conversion receiver architecture [UDK+10]. The mixer and the filter is depicted in figure 5.24. The mixer is a four transistor switching network including a g_m-cell for signal amplification, working in the 2.5 V domain as well. The passive mixer is used because of the lower 1/f noise especially in narrow band channels. Passive mixers have no inherent 1/f noise [Hoo94] and additional bias networks are not necessary. A better power efficiency can be achieved. The g_m-cell and the passive mixer was provided by Infineon. The mixer operation principle is described in [PJZM09]. The mixer-filter operates in the UHF (ultra high frequency) band in the frequency range from 470 MHz to 862 MHz, which is divided in 48 channels.

Simulation results The first-order low-pass filter is realized by using the equivalent output resistance R_{Mix} of the passive mixer. The filter transfer function is

$$H_{Filter} = \frac{R_{Filter}}{R_{Mix}} \frac{1}{1 + sR_{Filter}C_{Filter}}. \tag{5.7}$$

C_{Filter} denotes the filter capacitance and is 23 pF. R_{Filter} is the filter resistor with a value of 2 kΩ. The mixer output resistance is 100 Ω. C_{Filter} and R_{Filter} are set for a mixer-filter gain of 24 dB and a -3 dB cut-off frequency of 4 MHz. The clock frequency f_{LO} is set to 666 MHz. 666 MHz is the carrier frequency of the 45th DVB-T channel which is in the middle of the UHF band. The average integrated input referred noise density, integrated from 500 Hz to 4 MHz, results in 2.96 nV/$\sqrt{\text{Hz}}$. The noise figure NF is 16.1 dB. The mixer-filter combination consumes 12.7 mA at a supply voltage of 2.5 V.

Table 5.7: Performance summary

Technology	65 nm CMOS
Supply voltage	2.5 V
Frequency	666 MHz
Bandwidth (base-band)	4 MHz
Gain	24 dB
NF	16.1 dB
Average integrated noise density	$2.96\,\mathrm{nV}/\sqrt{\mathrm{Hz}}$
IIP3	+10 dBm
Current consumption	12.7 mA

The out-of-band IIP3 is determined by applying two sinusoidal signals of 658 MHz and 663 MHz, hence the IM3 is at 2 MHz in the pass-band. The 1 dB compression point is determined by a input signal of 668 MHz, 2 MHz in the pass-band as well and results in 0 dBm. The 3rd-order input intercept point of +10 dBm is achieved. A performance summary of the mixer-filter combination is given in table 5.7 [UDK+10].

Comparison of the mixer-filter combination The comparison to similar mixer filter combinations is difficult, because only complete analog front-ends are mostly published. A mixer-filter architecture in 0.13 μm CMOS for a ultra-wide band receiver is presented in [LXHH08]. The front-end has an in-phase and a quadrature-phase branch, which consists of one g_m-cell, two mixers, and two transimpedance amplifiers. The -3 dB cut-off frequency is 250 MHz at a clock frequency range from 3.1 to 4.7 GHz. The minimum noise figure is 3.3 dB and the IIP3 is -14 dBm. A direct comparison is difficult, due to different specifications in bandwidth and rf frequency range.

5.8 Comparison to State-of-the-Art of Operational Amplifiers

A comparison to the state-of-the-art of operational amplifiers is given in table 5.8. The publications are sorted chronologically. It needs to be kept in mind, that regarding (5.4) higher values of FOM_{Opamp} are better.

The operational amplifier in [VGS01] is simulated in 0.8 μm CMOS and has a gain of 106 dB. A good FOM_{Opamp} of 1111 $\frac{MHz \cdot pF}{mA}$ is reached due to the ultra low-power design (6.75 μW). The opamp has only a moderate GBW of 1 MHz at a PM of 47° and 5 pF load capacitance. An operational amplifier in 0.13 μm CMOS with 50 dB gain and 3.2 MHz GBW is realized in [MPHS02]. Simulation results without any C_L are given, hence no FOM_{Opamp} is available. A high-speed opamp (0.18 μm CMOS) with a GBW of 2.6 GHz is presented in [HW02]. Only a moderate FOM_{Opamp} of 367 $\frac{MHz \cdot pF}{mA}$ is achieved due to the small load capacitance and 4 mA current consumption at 1.8 V supply.

The opamp in [SDZ03] can drive a large C_L of 10 pF at 1.2 V supply voltage and 1.8 mA power consumption. The GBW of 46 MHz (PM = 66°) allows only a moderate FOM_{Opamp} of 256 $\frac{MHz \cdot pF}{mA}$. A medium-speed opamp in 0.18 μm CMOS is realized in [SKF04]. Despite the use of cascodes a power of 12 mW is needed to drive a 2 pF load (post layout simulations). The PM (73°) is high, however only a moderate FOM_{Opamp} (118 $\frac{MHz \cdot pF}{mA}$) is achieved. A high-speed opamp with a GBW of 1.5 GHz is published in [SZ04] in 120 nm CMOS technology. The gain is only 40 dB but the FOM_{Opamp} of 1048 $\frac{MHz \cdot pF}{mA}$ is good, 9.16 mA at 1.2 V supply is needed to drive a load of 3.2 pF twice. The high-gain opamp (120 dB) in 120 nm CMOS technology, presented in [SDZ04], consumes much power (27.5 mW). The GBW is high (886 MHz) at a load of 3.5 pF twice and a PM of 36° but the FOM_{Opamp} of 265 $\frac{MHz \cdot pF}{mA}$ is only moderate.

A 0.35 μm CMOS technology is used in [CC05]. Cascoding, which is only possible with sufficient supply voltage allows a low power consumption and a huge load capacitance of 100 pF. A current consumption of 0.666 mA at 3.3 V supply voltage and a low GBW of 7.8 MHz (PM = 67°) results in a good FOM_{Opamp} (1171 $\frac{MHz \cdot pF}{mA}$). An excellent FOM_{Opamp} of 1492 $\frac{MHz \cdot pF}{mA}$ is achieved in [LMYY05], although the GBW (280.5 MHz) is only mid-range (PM = 48°). The current consumption is low (0.94 mA) due to a folded cascode structure at 2.5 V supply voltage ($C_L = 5$ pF). Three operational amplifiers in 0.18 CMOS technology (supply voltage 1.8 V) are compared in [HS05]. The first one has a GBW of 2.4 GHz ($C_L = 8.6$ pF), a gain of 66 dB, a current consumption of 35 mA, and a medium FOM_{Opamp} of 560 $\frac{MHz \cdot pF}{mA}$. The second opamp has a GBW of 4.8 GHz ($C_L = 2 \times 7.4$ pF), a DC gain of only 27.1 dB, and needs 40 mA. Despite of the enormous power consumption a good FOM_{Opamp} (1776 $\frac{MHz \cdot pF}{mA}$) is reached. The remaining high-gain opamp with 111 dB DC gain and a current consumption of 45 mA (GBW = 1.27 GHz) has no given load capacitance, hence no FOM_{Opamp} is available. Two ultra low-power opamps at only 1 V

supply voltage (0.18 μm CMOS) are presented in [AFS06]. Both reach only moderate FOM_{Opamp} of 238 $\frac{MHz \cdot pF}{mA}$ (C_L = 5 pF, GBW = 26.2 MHz, 0.55 mA current consumption) and 162 $\frac{MHz \cdot pF}{mA}$ (C_L = 5 pF, GBW = 1.3 MHz, 0.04 mA current consumption). No C_L is given in the low-power opamp design (1.8 mW, 0.13 μm CMOS, GBW = 10 MHz) in [KLSK06], hence no FOM_{Opamp} is calculable. A three-stage operational amplifier in 120 nm CMOS is proposed in [YZ06] with 73 dB DC gain, 4.4 MHz GBW, and 1.2 mA current consumption at 1.5 V. A C_L of 5 pF leads to a poor FOM_{Opamp} of 18.3 $\frac{MHz \cdot pF}{mA}$. A low-power 0.35 μm CMOS opamp at only 1 V supply voltage is presented in [CTPD07]. A GBW of 8.1 MHz and a power dissipation of 385 μW together with the load capacitance of 17 pF results in a medium FOM_{Opamp} of 385 $\frac{MHz \cdot pF}{mA}$. An opamp in 0.35 μm CMOS technology at 3 V is presented in [LK07]. Despite of the cascoded circuitry the power consumption is high (48 mW), the GBW is 135 MHz, and the FOM_{Opamp} of 58 $\frac{MHz \cdot pF}{mA}$ is poor.

A 135 MHz GBW opamp at C_L of 15 pF in 0.12 μm CMOS is introduced in [YZ07]. A DC gain of 76.3 dB, a current consumption of 11.5 mA at 1.5 V supply lead to a medium FOM_{Opamp} of 176 $\frac{MHz \cdot pF}{mA}$. Two opamps in 0.35 μm CMOS with a high GBW (570 MHz and 350 MHz) are published in [DNDR08]. The high power consumption (both: 15.84 mW) and the low load capacitance (both: 1.4 pF) disallow a good FOM_{Opamp} (166 $\frac{MHz \cdot pF}{mA}$ and 102 $\frac{MHz \cdot pF}{mA}$). A low voltage (1 V) operational amplifier in 0.12 μm CMOS with a power dissipation of 1.4 mW is presented in [YKZ08b]. A GBW of 40.2 MHz (PM = 62°), a C_L of 500 pF, and a DC gain of 108 dB allow an excellent FOM_{Opamp} of 14357 $\frac{MHz \cdot pF}{mA}$. An operational amplifier in 65 nm CMOS is presented in [YKZ08a] with an open-loop gain of 100 dB, a GBW of 40 MHz (PM = 64°) and a load of 15 pF. A power consumption of 0.72 mW at 1 V supply voltage results in a good FOM_{Opamp} of 833 $\frac{MHz \cdot pF}{mA}$. A high-gain opamp is introduced in [WRZW09] in 0.6 μm technology. A GBW of 11.9 MHz and a PM of 53° are achieved. No C_L and no power consumption are reported. Two operational amplifiers in 90 nm CMOS with a high GBW (1.014 GHz and 539.4 MHz) are realized in [dCdRG+09]. The PM (7.7°) of the second opamp is extremely small. No further information is provided. A high GBW operational amplifier (2.3 GHz) in 0.18 μm CMOS is introduced in [GB10] and reaches a moderate FOM_{Opamp} of 331 $\frac{MHz \cdot pF}{mA}$ due to the small load capacitance (2 pF) and the high power consumption (13.9 mA at 1.8 V supply voltage). A low-power (107 μW) and low supply voltage (0.7 V) opamp with a GBW of 0.97 MHz is presented in [SWKH10], but [SWKH10] does not provide the C_L for a FOM_{Opamp} calculation. Unfortunately only a few operational amplifier designs in nanometer CMOS technology were available at this time.

The operational amplifiers presented in the work at hand [USSZ09, UZ09b, UDK+10] are implemented in 65 nm CMOS technology. A low supply voltage (1.2 V) and high threshold voltages of the transistors disallow the application of cascodes. There is the tendency of high power consumption at high operational amplifier gain and high GBW at the same time. A high GBW of 1 GHz and a high load capacitance enable a good

FOM_{Opamp} ($1052\,\frac{MHz \cdot pF}{mA}$ and $833\,\frac{MHz \cdot pF}{mA}$). The opamp at 2.5 V is optimized for a large output signal swing and uses extensive cascoding. A high gain of 89 dB is realized. The output stage of the opamp is optimized for an on-chip design, hence only small load capacitances are taken into account. A small C_L and the high power consumption result in a moderate FOM_{Opamp} of $367\,\frac{MHz \cdot pF}{mA}$.

Table 5.8: Comparison to the state-of-the-art of operational amplifiers

Citation	CMOS Technology	Supply voltage	Power consumption	Gain	GBW	PM	Load	FOM_{Opamp}
State-of-the-art								
[VGS01]	0.8 μm	1.5 V	6.75 μW	106 dB	1 MHz	47°	5 pF	1111 $\frac{MHz \cdot pF}{mA}$
[MPHS02]	0.13 μm	1.5 V	4.65 mW	50 dB	3.2 MHz	44°	n.a.†	n.a.†
[HW02]	0.18 μm	1.8 V	7.2 mW	50 dB	2.6 GHz	35°	2×0.3 pF||1 kΩ	367 $\frac{MHz \cdot pF}{mA}$
[SDZ03]	0.12 μm	1.2 V	2.16 mW	86 dB	46 MHz	66°	10 pF||750 kΩ	256 $\frac{MHz \cdot pF}{mA}$
[SKF04]	0.18 μm	1.8 V	12 mW	86 dB	392 MHz	73°	2pF	118 $\frac{MHz \cdot pF}{mA}$
[SZ04]	0.12 μm	1.2 V	10.99 mW	40.4 dB	1.5 GHz	45°	2×3.2 pF	1048 $\frac{MHz \cdot pF}{mA}$
[SDZ04]	0.12 μm	1.2 V	27.5 mW	120 dB	866 MHz	36°	2×3.5 pF	265 $\frac{MHz \cdot pF}{mA}$
[CC05]	0.35 μm	3.3 V	2.2 mW	60 dB	7.8 MHz	67°	100 pF	1171 $\frac{MHz \cdot pF}{mA}$
[LMYY05]	0.25 μm	2.5 V	2.35 mW	76 dB	280.5 MHz	48°	5 pF	1492 $\frac{MHz \cdot pF}{mA}$
[HS05]	0.18 μm	1.8 V	19.4 mW	66 dB	2.4 GHz	n.a.†	8.6 pF	560 $\frac{MHz \cdot pF}{mA}$
[HS05]	0.18 μm	1.8 V	72 mW	27.1 dB	4.8 GHz	n.a.†	2×7.4 pF	1776 $\frac{MHz \cdot pF}{mA}$
[HS05]	0.18 μm	1.8 V	81 mW	111 dB	1.27 GHz	n.a.†	n.a.†	n.a.†
[AFS06]	0.18 μm	1 V	550 μW	50.1 dB	26.2 MHz	n.a.†	5 pF||10 kΩ	238 $\frac{MHz \cdot pF}{mA}$
[AFS06]	0.18 μm	1 V	40 μW	53 dB	1.3 MHz	n.a.†	5 pF||10 kΩ	162 $\frac{MHz \cdot pF}{mA}$
[KLSK06]	0.13 μm	1.5 V	1.8 mW	63.16 dB	10 MHz	n.a.†	n.a.†	n.a.†
[YZ06]	0.12 μm	1.5 V	1.8 mW	73 dB	4.4 MHz	70°	5 pF	18.3 $\frac{MHz \cdot pF}{mA}$
[CTPD07]	0.35 μm	1 V	385 μW	76.2 dB	8.1 MHz	>60°	17 pF||1 MΩ	385 $\frac{MHz \cdot pF}{mA}$
[LK07]	0.35 μm	3 V	48.6 mW	93 dB	135 MHz	61°	7 pF	58 $\frac{MHz \cdot pF}{mA}$

† . . . not available

Table 5.8: Comparison to the state-of-the-art of operational amplifiers

Citation	CMOS Technology	Supply voltage	Power consumption	Gain	GBW	PM	Load	FOM_{Opamp}
[YZ07]	0.12 μm	1.5 V	17.5 mW	76.3 dB	135 MHz	51°	15 pF	176 $\frac{MHz \cdot pF}{mA}$
[DNDR08]	0.35 μm	3.3 V	15.84 mW	86.4 dB	570 MHz	85.6°	1.4 pF	166 $\frac{MHz \cdot pF}{mA}$
[DNDR08]	0.35 μm	3.3 V	15.84 mW	85.9 dB	350 MHz	56°	1.4 pF	102 $\frac{MHz \cdot pF}{mA}$
[YKZ08b]	0.12 μm	1 V	1.4 mW	108 dB	40.2 MHz	62°	500 pF	14357 $\frac{MHz \cdot pF}{mA}$
[YKZ08a]	65 nm	1 V	0.72 mW	100 dB	40 MHz	64°	15 pF	833 $\frac{MHz \cdot pF}{mA}$
[WRZW09]	0.6 μm	3 V	n.a.†	113.57 dB	11.9 MHz	56°	n.a.†	n.a.†
[dCdRG+09]	90 nm	n.a.†	n.a.†	52.37 dB	1.014 GHz	47.4°	n.a.†	n.a.†
[dCdRG+09]	90 nm	n.a.†	n.a.†	65.66 dB	539.4 MHz	7.7°	n.a.†	n.a.†
[GB10]	0.18 μm	1.8 V	25 mW	65 dB	2.3 GHz	58°	2 pF	331 $\frac{MHz \cdot pF}{mA}$
[SWKH10]	0.18 μm	0.7 V	107 μW	72.8 dB	0.97 MHz	70°	n.a.†	n.a.†
Own publications								
[USSZ09]	65 nm	1.2 V	11.4 mW	58 dB	1 GHz	62°	2×5 pF||10 kΩ	1052 $\frac{MHz \cdot pF}{mA}$
[UZ09b]	65 nm	1.2 V	11.52 mW	68 dB	1 GHz	60°	2×4 pF||10 kΩ	833 $\frac{MHz \cdot pF}{mA}$
[UDK+10]	65 nm	2.5 V	14.63 mW	89 dB	1.1 GHz	53.3°	2×1 pF	376 $\frac{MHz \cdot pF}{mA}$

† ... not available

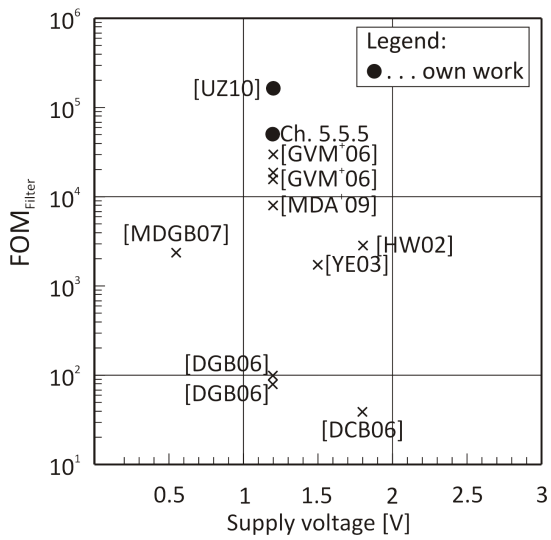

Figure 5.25: Comparison to the state-of-the-art - voltage-mode filters

5.9 Comparison to State-of-the-Art of Voltage-Mode Filters

A comparison to the state-of-the-art of voltage mode filters is given in table 5.9. The publications are sorted chronologically. It needs to keep in mind, that regarding (4.6) lower values of FOM_{Filter} are better. A plot of the FOM_{Filter}s against the supply voltage is depicted in figure 5.25.

The presented opamp in [HW02] is used in a 40 MHz to 350 MHz opamp RC filter. The 5th-order elliptic low-pass filter has a power dissipation of 25.2 mW at 1.8 V supply voltage. At the -3 dB cut-off frequency of 350 MHz the DR is moderate (52 dB) and the FOM_{Filter} is medium (2742). A low-power Butterworth filter at 1.5 V in 0.18 μm TSMC CMOS is introduced in [YE03]. The -3 dB cut-off frequency is tunable from 13 to 80 kHz. At 50 kHz a good DR of 75 dB is reached, but the low -3 dB cut-off frequency results in a medium FOM_{Filter} of 1527. A 90 nm CMOS elliptic low-pass filter design is published in [ECBS05], which has a cut-off frequency of 1, 10, and 100 MHz. The gain is variable from 13.5 to 67.5 dB. No distortion and noise performance are reported, hence no DR and FOM_{Filter} is available. A filter for UMTS and WLAN with -3 dB cut-off frequencies of 2.11 MHz and 11 MHz is realized in [DGB06]. Both filters in 0.13 μm CMOS at 1.2 V have a good DR of 81 dB and a good FOM_{Filter} of 97 and 77, respectively. Three filters for the application in WLAN, UMTS, and Bluetooth in 0.13 μm CMOS are presented in [GVM$^+$06]. Hence the -3 dB cut-off frequencies are 11 MHz, 2.5 MHz, and 1 MHz, respectively. The filters at 1.2 V supply voltage achieve a medium DR from 55 dB to 58.2 dB. The FOM_{Filter}s are moderate from 12146 to 34258. The given active area is big, but includes the area for the DAC. A 4th-order Bessel filter is realized in [DCB06]. In

0.18 μm CMOS at 1.8 V the filter consumes 2.28 mA and has a bandwidth of 10 MHz. A very good DR of 79 dB and a very good FOM_{Filter} of only 39 is achieved. A low-voltage active g_m-RC Butterworth filter in 0.13 μm CMOS is realized in [MDGB07]. At a supply voltage of 550 mV and a -3 dB cut-off frequency of 11.3 MHz a medium DR of 60 dB and a medium FOM_{Filter} of 2270 are achieved. A cascade of two opamp RC cells in 65 nm CMOS forms a 4th-order wideband filter in [MDA+09]. The filter has a gain of 32 dB, a moderate DR of 52 dB, and a moderate FOM_{Filter} of 7934 at a -3 dB cut-off frequency of 7.8 MHz. The multiple standard 3rd-order Butterworth filter in [LHI09] has a tuning range from 500 kHz to 20 MHz. The power consumption depends on the filter bandwidth and the supply voltage is only 1.2 V in 0.18 μm CMOS technology. The distortions are missing in [LHI09], hence no DR and FOM_{Filter} are available. A 2nd-order Butterworth filter with low power consumption of only 384.44 μW is introduced in [FM10]. The filter gain is 38 dB and the -3 dB cut-off frequency is 24 MHz. The noise as well as the distortions are not reported. DR and FOM_{Filter} cannot be determined.

The 65 nm CMOS filters designed in this work ([UZ10] and Sec. 5.7.4) have only a moderate FOM_{Filter} despite of the medium DR of 57.2 dB and 62 dB. A main reason is the system inherent filter-order and the filter gain in combination with distortions. The receiver front-end is designed to have a passive mixer and a following 1st-order Butterworth operational amplifier RC low-pass filter. The opamp RC filter does the output signal conversion from the passive mixer, the first signal amplification, and the bandwidth selection of the DVB-H channel. A 1st-order Butterworth low-pass filter is used instead of a higher-order filter in order to save power dissipation in the overall direct conversion receiver. The high filter gain in conjunction with the filter order is reason why the filter design comes off badly. The target -3 dB cut-off frequency of the filter is 4 MHz and the gain is 38 dB or 40 dB. Any modulation products appear in the 4 MHz channel bandwidth and disturb the desired in-band signal. Low distortions and intermodulations are achievable by a large GBW and a sufficient gain of the opamp. These constraints lead to a complex and power consuming opamp that deteriorates the FOM_{Filter} of the 1st-order Butterworth operational amplifier RC low-pass filter.

Table 5.9: Comparison to the state-of-the-art of voltage-mode filters

Citation	CMOS Technology	Supply voltage	Power consumption	Gain	Filter order	-3 dB cut-off frequency	Active area	DR	FOM_{Filter}
State-of-the-art									
[HW02]‡	0.18 μm	1.8 V	25.2 mW	0 dB	5	40-350 MHz	0.5 mm^2	52 dB	2742
[YE03]‡	0.18 μm	1.5 V	240 μW	n.a.†	3	13-80 kHz	0.113 mm^2	75 dB	1527
[ECBS05]	90 nm	1.4 V	13.5 mW	13.5-67.5 dB	6	1-100 MHz	0.55 mm^2	n.a.†	n.a.†
[DGB06]‡	0.13 μm	1.2 V	3.4 mW	4 dB	4	2.11 MHz	0.9 mm^2	81 dB	97
[DGB06]‡	0.13 μm	1.2 V	14.2 mW	4 dB	4	11 MHz	0.9 mm^2	81 dB	77
[GVM+06]‡	0.13 μm	1.2 V	5.6 mW	8 dB	4	11 MHz	0.7 mm^2	55 dB	12146
[GVM+06]‡	0.13 μm	1.2 V	3 mW	8 dB	4	2.5 MHz	0.8 mm^2	58 dB	14349
[GVM+06]‡	0.13 μm	1.2 V	3 mW	8 dB	4	1 MHz	0.7 mm^2	58 dB	34258
[DCB06]‡	0.18 μm	1.8 V	4.1 mW	-3.5 dB	4	10 MHz	0.26 mm^2	79 dB	39
[MDGB07]‡	0.13 μm	0.55 V	3.4 mW	0 dB	4	11.3 MHz	0.45 mm^2	60 dB	2270
[MDA+09]‡	65 nm	1.2 V	1.3 mW	32 dB	4	7.8 MHz	n.a.†	52 dB	7934
[LHI09]	0.18 μm	1.2 V	4.1-11.1 mW	0 dB	3	0.5-20 MHz	0.23 mm^2	n.a.†	n.a.†
[FM10]‡	0.18 μm	1.8 V	384.44 μW	38 dB	2	24 MHz	n.a.†	n.a.†	n.a.†

† ... not available; ‡ ... plotted in figure 5.25

Table 5.9: Comparison to the state-of-the-art of voltage-mode filters

Citation	CMOS Technology	Supply voltage	Power consumption	Gain	Filter order	-3 dB cut-off frequency	Active area	DR	FOM_{Filter}
Own publications									
[UZ10]‡	65 nm	1.2 V	10 mW	38 dB	1	3.5-4.5 MHz	0.104 mm^2	57 dB	143945
Sec. 5.7.4‡	65 nm	1.2 V	11.5 mW	40 dB	1	4 MHz	n.a.†	62 dB	54744

† ... not available; ‡ ... plotted in figure 5.25

Chapter 6

Conclusion

This thesis examines analog filter design in digital nanometer CMOS technology. Major drive developing analog circuits in digital CMOS technology is the idea of system on chip. In a system on chip all important parts of a system are integrated onto one chip. Although the main parts of such a system on chip are digital function blocks, some blocks remain analog like DAC, ADC, and rf-frontends. Hence, analog design is still necessary in a digital optimized CMOS technology.

Two different filter structures are introduced for different applications. The first is a current-mode filter for a transmit path in a software defined radio system. The filters are based on cross-coupled current-mode integrators and low-pass filters. Three 3rd-order current-mode Butterworth filters are designed with the focus on chip-area saving techniques. A capacitance multiplication strategy for fully differential current-mode low-pass filters is developed and an enlargement of 30% of the effective capacitance is achieved. In a comparison to the state-of-the-art it is shown, that the three filter designs are competitive to existing current-mode filters in literature.

The second filter design is part of a receiving path of DVB-H devices. It is a 1st-order operational amplifier RC low-pass filter having a gain of 40 dB. Three different multi-stage operational amplifiers with feed-forward are presented. High gain-bandwidth products are achieved at a respectable load capacitance. The comparison to the state-of-the-art gives good figures of merit of the presented operational amplifiers despite of limiting factors in nanometer CMOS technology. The first-order Butterworth low-pass filters in the DVB-H receiver are built using the introduced operational amplifiers. The resulting filter performance is moderate because of the power consuming high gain-bandwidth product operational amplifiers. They are needed to reduce the distortions and intermodulations in the filter base-band. A mixer-filter combination is also presented by using the last operational amplifier. The characteristic of the design is the supply voltage of 2.5 V in 65 nm CMOS technology, which is essential for low non-linearities. The operational amplifier uses cascoding to ensure the voltage limits of the transistors.

Bibliography

[Abi95] Asad A. Abidi. Direct-Conversion Radio Transceivers for Digital Communications. *IEEE Journal of Solid-State Circuits*, 30(12):1399 – 1410, December 1995.

[AFS06] Herve Facpong Achigui, Christian Jesus B. Fayomi, and Mohamad Sawan. 1-V DTMOS-Based Class-AB Operational Amplifier: Implementation and Experimental Results. *IEEE Journal of Solid-State Circuits*, 41(11):2440 – 2448, November 2006.

[All91] David J. Allstot. Current-Mode Analog Signal Processing: a Tutorial. *IEEE Pacific Rim Conference on Communications, Computers and Signal Processing*, 2:815 – 818, May 1991.

[ANvLT05] Anne-Johan Annema, Bram Nauta, Ronald van Langevelde, and Hans Tuinhout. Analog Circuits in Ultra-Deep-Submicron CMOS. *IEEE Journal of Solid-State Circuits*, 40(1):132 – 143, Jan. 2005.

[BAB+04] P. Bai, C. Auth, S. Balakrishnan, M. Bost, R. Brain, V. Chikarmane, R. Heussner, M. Hussein, J. Hwang, D. Ingerly, R. James, J. Jeong, C. Kenyon, E. Lee, S.-H. Lee, N. Lindert, M. Liu, Z. Ma, T. Marieb, A. Murthy, R. Nagisetty, S. Natarajan, J. Neirynck, A. Ott, C. Parker, J. Sebastian, R. Shaheed, S. Sivakumar, J. Steigerwald, S. Tyagi, C. Weber, B. Woolery, A. Yeoh, K. Zhang, and M. Bohr. A 65nm Logic Technology Featuring 35nm Gate Lengths, Enhanced Channel Strain, 8 Cu Interconnect Layers, Low-k ILD and 0.57 μm^2 SRAM Cell. *International Electron Devices Meeting*, pages 657 – 660, December 2004.

[Bah96] Hussein Baher. *Microelectronic Switched-Capacitor Filters: with ISICAP: a Computer-Aided-Design Package.* John Wiley and Sons, 1996.

[Bes08] Robert Bestak. Evolution of Mobile Networks. *International Conference on Systems, Signals and Image Processing*, pages 29 – 32, June 2008.

[Bul00] Klaas Bult. Analog Design in Deep Sub-Micron CMOS. *European Solid-State Circuits Conference*, pages 126 – 132, Sept. 2000.

[CC05] C.-L. Chen and Y.-C. Chang. Self-Biased Cross-Coupled Low-Cost Fully-Differential CMOS Operational Amplifier. *Electronics Letters*, 41(9):512 – 514, April 2005.

[CCC+08] Mi-Chang Chang, Chih-Sheng Chang, Chih-Ping Chao, Ken-Ichi Goto, Meikei Ieong, Lee-Chung Lu, and Carlos H. Diaz. Transistor- and Circuit-Design Optimization for Low-Power CMOS. *IEEE Transactions on Electron Devices*, 55(1):84 – 95, January 2008.

[CMRB95] Rinaldo Castello, Federico Montecchi, Francesco Rezzi, and Andrea Baschirotto. Low-Voltage Analog Filters. *IEEE Transactions on Circuits and Systems I: Fundamental Theory and Applications*, 42(11):827 – 840, Nov 1995.

[CSB92] Anantha P. Chandrakasan, Samuel Sheng, and Robert W. Brodersen. Low-Power CMOS Digital Design. *IEEE Journal of Solid-State Circuits*, 27(4):473 – 484, Apr. 1992.

[CTPD07] Juan M. Carrillo, Guido Torelli, Raquel Perez-Aloe, and J. Francisco Duque-Carrillo. 1-V Rail-to-Rail CMOS OpAmp with Improved Bulk-Driven Input Stage. *IEEE Journal of Solid-State Circuits*, 42(3):508 – 517, March 2007.

[DBD08] E. Doicaru, M. Bodea, and C. Dan. A CMOS Fifth-Order Low-Pass Continuous-Time Filter for Low-Voltage Applications. *International Biennial Baltic Electronics Conference*, pages 135 – 138, October 2008.

[DCB06] Stefano D'Amico, Matteo Conta, and Andrea Baschirotto. A 4.1 mW 10 MHz Fourth-Order Source-Follower-Based Continuous-Time Filter with 79 dB DR. *IEEE Journal of Solid-State Circuits*, 41(12):2713 – 2719, December 2006.

[dCdRG+09] Sherlyn C. dela Cruz, Mark-Gerard T. delos Reyes, Terence C. Gaffud, Tanya Vanessa Abaya, Maria Theresa A. Gusad, and Marc D. Rosales. Design and Implementation of Operational Amplifiers with Programmable Characteristics in a 90nm CMOS Process. *European Conference on Circuit Theory and Design*, pages 209 – 212, August 2009.

[DGB06] Stefano D'Amico, Vito Giannini, and Andrea Baschirotto. A 4th-Order Active-Gm-RC Reconfigurable (UMTS/WLAN) Filter. *IEEE Journal of Solid-State Circuits*, 41(7):1630 – 1637, July 2006.

[Dia04] Carlos H. Diaz. CMOS Technology for MS/RF SoC. *IEEE Workshop on Microelectronics and Electron Devices*, pages 24 – 27, September 2004.

[DL01] Yuanying Deng and Edward K.F. Lee. Design of a 1V 250MHz Current-Mode Filter in Conventional CMOS Process. *IEEE International Symposium on Circuits and Systems*, 1:236 – 239, May 2001.

[DNDR08] Jose-Angel Diaz-Madrid, Harald Neubauer, Gines Domenech-Asensi, and Ramon Ruiz. Comparative Analysis of Two Operational Amplifier Topologies for a 40MS/s 12-bit Pipelined ADC in 0.35 μm CMOS. *IEEE International Conference on Integrated Circuit Design and Technology and Tutorial*, pages 121 – 124, June 2008.

[DSF99] Theodore L. Deliyannis, Yichuang Sun, and J. Kel Fidler. *Continuous-Time Active Filter Design.* CRC-Press, 1999.

[ECBS05] Mostafa Elmala, Brent Carlton, Ralph Bishop, and Krishnamurthy Soumyanath. A Highly Linear Filter and VGA Chain with Novel DC-Offset Correction in 90 nm Digital CMOS Process. *Symposium on VLSI Circuits Digest of Technical Papers*, pages 302 – 303, June 2005.

[FM10] Mohammed Mehdi Farhad and Sattar Mirzakuchaki. A Second-Order Gm-C Continuous Time Tilter in Mobile Radio Receiver Architecture. *International Conference on Education Technology and Computer*, 5:V5–170 – V5–173, June 2010.

[Fot99] Daniel Foty. Taking a Deep Look at Analog CMOS. *IEEE Circuits and Devices Magazine*, 15(2):23 – 28, Mar. 1999.

[GB10] Daibashish Gangopadhyay and T.K. Bhattacharyya. A 2.3 GHz gm-Boosted High Swing Class-ab Ultra-Wide Bandwidth Operational Amplifier in 0.18 μm CMOS. *IEEE International Midwest Symposium on Circuits and Systems*, pages 713 – 716, Augst 2010.

[GD05] Georges Gielen and Wim Dehaene. Analog and Digital Circuit Design in 65nm CMOS: End of the Road? *Design, Automation and Test in Europe*, 1:37 – 42, Mar. 2005.

[GGH97] Ricardo Gonzalez, Benjamin M. Gordon, and Mark A. Horowitz. Supply and Threshold Voltage Scaling for Low Power CMOS. *IEEE Journal of Solid-State Circuits*, 32(8):1210 – 1216, Aug. 1997.

[GHLM01] Paul R. Gray, Paul J. Hurst, Stephen H. Lewis, and Robert G. Meyer. *Analysis and Design of Analog Integrated Circuits.* John Wiley and Sons, Inc, New York, 2001.

[Gil68] Barrie Gilbert. A New Wide-Band Amplifier Technique. *IEEE Journal of Solid-State Circuits*, 3(4):353 – 365, December 1968.

[GVM+06] Nicola Ghittori, Andrea Vigna, Piero Malcovati, Stefano D'Amico, and Andrea Baschirotto. 1.2 V Low-Power Multi-Mode DAC+Filter Blocks for Reconfigurable (WLAN/UMTS, WLAN/Bluetooth) Transmitters. *IEEE Journal of Solid-State Circuits*, 41(9):1970 – 1982, September 2006.

[Ham03] Hesham F.A. Hamed. A low voltage digitally programmable current-mode filter. *International Conference on Microelectronics*, pages 413 – 416, December 2003.

[Hau96] John R. Hauser. Extraction of Experimental Mobility Data for MOS Devices. *IEEE Transactions on Electron Devices*, 43(11):1981 – 1988, November 1996.

[HBHK95] Bedrich J. Hosticka, Werner Brockherde, Dirk Hammerschmidt, and Rainer Kokozinski. Low-Voltage CMOS Analog Circuits. *IEEE Trans-*

actions on Circuits and Systems I: Fundamental Theory and Applications, 42(11):864 – 872, Nov. 1995.

[HCLS06] Y.-S. Hwang, J.-J. Chen, J.-H. Lai, and P.-W. Sheu. Fully Differential Current-Mode Third-Order Butterworth VHF G_m-C Filter in 0.18μm CMOS. *IEE Proceedings - Circuits, Devices and Systems*, 153(6):552 – 558, December 2006.

[HH08] Nor Zaidi Haron and Said Hamdioui. Why is CMOS Scaling Coming to an END? *International Design and Test Workshop*, pages 98 – 103, December 2008.

[Hoo94] F.N. Hooge. 1/f Noise Sources. *IEEE Transactions on Electron Devices*, 41(11):1926 – 1935, November 1994.

[HS03a] Bjornar Hermes and Trond Saether. *Design Criteria for Low Distortion in Feedback Opamp Circuits*. Kluwer Academic Publishers, 2003.

[HS03b] Bjørnar Hernes and Trond Sæther. *Design Criteria for Low Distortion in Feedback Opamp Circuits*. Kluwer Academic Publishers, 2003.

[HS05] Bjørnar Hernes and Willy Sansen. Distortion in Single-, Two- and Three-Stage Amplifiers. *IEEE Transactions on Circuits and Systems I: Regular Papers*, 52(5):846 – 856, May 2005.

[HW02] J. Harrison and N. Weste. 350 MHz Opamp-RC Filter in 0.18 μm CMOS. *Electronics Letters*, 38(6):259 – 260, March 2002.

[HY96] Jai-Sop Hyun and Kwang S. Yoon. Design of a 3V - 50 MHz Analog CMOS Current-Mode NRL Filter. *IEEE International Symposium on Circuits and Systems*, 1:129 – 132, May 1996.

[IF04] Vadim V. Ivanov and Igor M. Filanovsky. *Operational Amplifier Speed and Improvement*. Kluwer Academic Publishers, 2004.

[Iwa06] Hiroshi Iwai. Recent Status on Nano CMOS and Future Direction. *International Workshop on Nano CMOS*, pages 1 – 5, February 2006.

[JXC+09] F. Ji, J.P. Xu, J.J. Chen, H.X. Xu, C.X. Li, and P.T. Lai. A Compact Threshold-Voltage Model of MOSFETs with Stack High-k Gate Dielectric. *IEEE International Conference of Electron Devices and Solid-State Circuits*, pages 236 – 239, December 2009.

[KKH98] Marko Kosunen, Kimmo Koli, and Kari Halonen. A 50 MHz 5th-order Elliptic LP-Filter Using Current-Mode Gm-C Topology. *IEEE International Symposium on Circuits and Systems*, 1:512 – 515, May 1998.

[KLSK06] Jeongwook Koh, Jung-Eun Lee, Chun-Deok Suh, and Hoon-Tae Kim. A 1/f-Noise Reduction Architecture for an Operational Amplifier in a 0.13 μm Standard Digital CMOS Technology. *IEEE Asian Solid-State Circuits Conference*, pages 179 – 182, November 2006.

[KM07] Michael Kornfeld and Gunther May. DVB-H and IP Datacast - Broadcast to Handheld Devices. *IEEE Transactions on Broadcasting*, 53(1):161 – 170, March 2007.

[KR03] J. Veerendra Kumar and K. Radhakrishna Rao. A Low-Voltage Low-Power CMOS Companding Filter. *International Conference on VLSI Design*, pages 309 – 314, January 2003.

[KYZ08] Robert Kolm, Weixun Yan, and Horst Zimmermann. Current-Mode Filter in 65nm CMOS for a Software-Radio Application. *IEEE International Symposium on Circuits and Systems*, pages 3130 – 3133, May 2008.

[KZ07] Robert Kolm and Horst Zimmermann. 3rd-Order Current-Input/Output Filter with Virtual Ground in 65nm CMOS. *Proc. of Austrochip 2007 conference*, pages 35 – 38, 2007.

[Lam79] Harry Y-F. Lam. *Analog and Digital Filters: Design and Realization.* Prentice Hall, Inc, 1979.

[LHI09] Tien-Yu Lo, Chung-Chih Hung, and Mohammed Ismail. A Wide Tuning Range Gm-C Filter for Multi-Mode CMOS Direct-Conversion Wireless Receivers. *IEEE Journal of Solid-State Circuits*, 44(9):2515 – 2524, September 2009.

[LK07] B. Lipka and U. Kleine. Design of a Cascoded Operational Amplifier with High Gain. *Proc. Mixed Design of Integrated Circuits and Systems*, pages 260 – 261, June 2007.

[LKC+06] Jeong-Hyun Lee, Sang-Yun Kim, Ilhyun Cho, Sungbo Hwang, and Jong-Ho Lee. 1/f Noise Characteristics of Sub-100 nm MOS Transistors. *Journal of Semiconductor Technology and Science*, 6(1):38 – 42, 2006.

[LMYY05] Zhiyuan Li, Jianguo Ma, Mingyan Yu, and Yizheng Ye. Low-Noise Operational Amplifier Design with Current Driving Bulk in 0.25 μm CMOS Technology. *International Conference on ASIC*, 2:630 – 634, October 2005.

[LP08] C. Laoudias and C. Psychalinos. Low-Voltage CMOS Current-Mode Filters Using Current Mirrors: Two Alternative Approaches. *IEEE Mediterranean Electrotechnical Conference*, pages 435 – 440, May 2008.

[LSE+04] Z. Luo, A. Steegen, M. Eller, R. Mann, C. Baiocco, P. Nguyen, L. Kim, M. Hoinkis, V. Ku, V. Klee, F. Jamin, P. Wrschka, P. Shafer, W. Lin, S. Fang, A. Ajmera, W. Tan, D. Park, R. Mo, J. Lian, D. Vietzke, C. Coppock, A. Vayshenker, T. Hook, V. Chan, K. Kim, A. Cowley, S. Kim, E. Kaltalioglu, B. Zhang, S. Marokkey, Y. Lin, K. Lee, H. Zhu, M. Weybright, R. Rengarajan, J. Ku, T. Schiml, J. Sudijono, I. Yang, and C. Wann. High Performance and Low Power Transistors Integrated in 65nm Bulk CMOS Technology. *International Electron Devices Meeting*, pages 661 – 664, 2004.

[LXHH08] Weinan Li, Lingli Xia, Yumei Huang, and Zhiliang Hong. A 0.13 μm CMOS UWB Receiver Front-End Using Passive Mixer. *IEEE Asia Pacific Conference on Circuits and Systems*, pages 288 – 291, Dec. 2008.

[LYWM09] Lanny L. Lewyn, Trond Ytterdal, Carsten Wulff, and Kenneth Martin. Analog Circuit Design in Nanoscale CMOS Technologies. *Proceedings of the IEEE*, 97(10):1687 – 714, October 2009.

[LZAL91] Sang-Soo Lee, Rajesh H. Zele, David J. Allstot, and Guojin Liang. A Continuous-Time Current-Mode Integrator. *IEEE Transactions on Circuits and Systems*, 38(10):1236 – 1238, October 1991.

[LZAL93] Sang-Soo Lee, Rajesh H. Zele, David J. Allstot, and Guojin Liang. CMOS Continuous-Time Current-Mode Filters for High-Frequency Applications. *IEEE Journal of Solid-State Circuits*, 28(3):323 – 329, March 1993.

[McP07] J.W. McPherson. Reliability Trends with Advanced CMOS Scaling and the Implications for Design. *IEEE Custom Integrated Circuits Conference*, pages 405 – 412, September 2007.

[MDA+09] M. De Matteis, S. D'Amico, P. Andriulo, G. Cocciolo, and A. Baschirotto. A 4th-Order CMOS 65 nm Wideband Low-Power Analog Filter for Wireless Receivers. *IEEE International Conference on Electronics, Circuits, and Systems*, pages 191 – 194, December 2009.

[MDGB07] Marcello De Matteis, Stefano D'Amico, Vito Giannini, and Andrea Baschirotto. A 550mV 8dBm IIP3 4th Order Analog Base Band Filter for WLAN Receivers. *Proc. European Solid-State Circuits Conference*, pages 504 – 507, September 2007.

[MJC+04] Shigenobu Maeda, You-Seung Jin, Jung-A Choi, Sun-Young Oh, Hyun-Woo Lee, Jae-Yoon Yoo, Min-Chul Sun, Ja-Hum Ku, Kwon Lee, Su-Gon Bae, Sung-Gun Kang, Jeong-Hwan Yang, Young-Wug Kim, and Kwang-Pyuk Suh. Impact of Mechanical Stress Engineering on Flicker Noise Characteristics. *Symposium on VLSI Technology*, pages 102 – 103, June 2004.

[MJR+04] A. Mercha, W. Jeamsaksiri, J. Ramos, S. Jenei, S. Decoutere, D. Linten, and P. Wambacq. Impact of Scaling on Analog/RF CMOS Performance. *IEEE Solid-State and Integrated Circuits Technology*, 1:147 – 152, October 2004.

[Mot07] Motorola, Inc. Long Term Evolution (LTE). White Paper, 2007.

[MPHS02] H. Maarefi, A. Parsa, H. Hatamkhani, and D. Shiri. A Wide Swing 1.5 V Fully Differential Opamp Using a Rail-to-Rail Analog CMFB Circuit. *Midwest Symposium on Circuits and Systems*, 1:105 – 108, August 2002.

[Nin00] Tak H. Ning. CMOS in the New Millennium. *IEEE 2000 Custom Integrated Circuits Conference*, pages 49 – 56, 2000.

[OCA06] A. Otin, S. Celma, and C. Aldea. A Design Strategy for VHF Filters with Digital Programmability. *IEEE International Symposium on Circuits and Systems*, pages 1059 – 1062, 2006.

[PFE96] Dominique Python, Rafael Fried, and Christian C. Enz. A 1.2V Companding Current-Mode Integrator for Standard Digital CMOS Processes. *IEEE International Conference on Electronics, Circuits, and Systems*, 1:231 – 234, October 1996.

[PJZM09] Zhaolin Pan, Peichen Jiang, Li Zhang, and Cui Mao. Low Flicker Noise and High Linearity Passive Mixer in 0.18 μm CMOS for Direct Conversion Receiver. *Asia Pacific Conference on Postgraduate Research in Microelectronics and Electronics*, pages 21 – 24, January 2009.

[PKH91] Hong-June Park, Ping Keung Ko, and Chenming Hu. A Charge Sheet Capacitance Model of Short Channel MOSFETs for SPICE. *IEEE Transactions on Computer-Aided Design of Integrated Circuits and Systems*, 10(3):376 – 389, March 1991.

[PP02] Gaetano Palumbo and Salvatore Pennisi. Design Methodology and Advances in Nested-Miller Compensation. *IEEE Transactions on Circuits and Systems I: Fundamental Theory and Applications*, 49(7):893 –903, July 2002.

[PP04] Vladislav Y. Potanin and Elena E. Potanina. High-Voltage-Tolerant Power Supply in a Low-Voltage CMOS Technology. *IEEE International Symposium on Circuits and Systems (ISCAS)*, 1:393 – 396, May 2004.

[Rap96] Juha Rapeli. UMTS - A Path to 3rd Generation Mobile Communications of the 21st Century. *IEEE International Conference on Personal Wireless Communications*, pages 58 – 67, February 1996.

[RDB+09] Francois Rivet, Yann Deval, Jean-Babtiste Begueret, Dominique Dallet, Philippe Cathelin, and Didier Belot. From Software-Defined to Software Radio: Analog Signal Processor Features. *IEEE Radio and Wireless Symposium*, pages 348 – 351, January 2009.

[RH04] P. Rickert and B. Haroun. SoC Integration in Deep Submicron CMOS. pages 653 – 656, December 2004.

[RP03] John Rogers and Calvin Plett. *Radio Frequency Integrated Circuit Design.* Artech House, 2003.

[RS89] G.W. Roberts and A.S Sedra. All Current-Mode Frequency Selective Circuits. *Electronics Letters*, 25(12):759 – 761, 8 1989.

[San98] Willy Sansen. Mixed Analog-Digital Design Challenges. *IEE Colloquium on Systems on a Chip*, pages 1/1 – 1/6, Sept. 1998.

[San06] Willy M.C. Sansen. *Analog Design Essentials.* Springer-Verlag, 2006.

[SDR10] Wireless innovation forum. http://www.wirelessinnovation.org, 2010.

[SDZ03] Franz Schlögl, Horst Dietrich, and Horst Zimmermann. 120 nm CMOS Operational Amplifier with High Gain Down to ±0.3 V Supply. *IEEE International Systems-on-Chip Conference*, pages 121 – 124, September 2003.

[SDZ04] Franz Schlögl, Horst Dietrich, and Horst Zimmermann. High-Gain High-Speed Operational Amplifier in Digital 120 nm CMOS. *IEEE International SOC Conference*, pages 316 – 319, September 2004.

[SKF04] Boaz Shem-Tov, Müchahit Kozak, and Eby G. Friedman. A High-Speed CMOS Opamp Design Technique Using Negative Miller Capacitance. *IEEE International Conference on Electronics, Circuits and Systems*, pages 623 – 626, December 2004.

[SMS+06] Thomas Strasser, Ingomar Müller, Christoph Sünder, Oliver Hummer, and Heimo Uhrmann. Modeling of Reconfiguration Control Applications Based on the IEC 61499 Reference Model for Industrial Process Measurement and Control Systems. *Distributed Intelligent Systems: Collective Intelligence and Its Applications*, pages 127 – 132, June 2006.

[SS96] Sterling L. Smith and Edgar Sanchez-Sinencio. Low Voltage Integrators for High-Frequency CMOS Filters Using Current-Mode Techniques. *IEEE Transactions on Circuits and Systems II: Analog and Digital Signal Processing*, 43(1):39 – 48, January 1996.

[SS99] Gajendra P. Singh and Raoul B. Salem. High-Voltage-Tolerant Power I/0 Buffers with Low-Voltage CMOS Process. *IEEE Journal of Solid-States Circuits (JSSC)*, 34(11):1512 – 1525, Nov. 1999.

[SUZ09] Kurt Schweiger, Heimo Uhrmann, and Horst Zimmermann. Low-Voltage Low-Power Double Bulk Mixer for Direct Conversion Receiver in 65 nm CMOS. *Proc. Design and Diagnostics of Electronic Circuits and Systems*, pages 74 – 77, April 2009.

[SWKH10] Meng-Hung Shen, Yi-Shuan Wu, Guan-Hung Ke, and Po-Chiun Huang. A 0.7 V CMOS Operational Transconductance Amplifier with Bulk-Driven Technique. *International SoC Design Conference*, pages 392 – 395, November 2010.

[SZ03] Franz Schlögl and Horst Zimmermann. Opamp with 106 dB DC Gain in 120 nm Digital CMOS. *European Solid-State Circuits Conference*, pages 381 – 384, September 2003.

[SZ04] Franz Schlögl and Horst Zimmermann. 1.5 GHz OPAMP in 120 nm Digital CMOS. *European Solid-State Circuits Conference*, pages 239 – 242, September 2004.

[TBE+03] B. Tavel, M. Bidaud, N. Emonet, D. Barge, N. Planes, H. Brut, D. Roy, J.C. Vildeuil, R. Difrenza, K. Rochereau, M. Denais, V. Huard, P. Llinares, S. Bruyere, C. Parthasarthy, N. Revil, R. Pantel, F. Guyader, L. Vishnubotla, K. Barla, F. Arnaud, P. Stolk, and M. Woo. Thin Oxynitride

Solution for Digital and Mixed-Signal 65nm CMOS Platform. *International Electron Devices Meeting*, pages 643 – 646, December 2003.

[TCG+05] Scott E. Thompson, Robert S. Chau, Tahir Ghani, Kaizad Mistry, Sunit Tyagi, and Mark. T. Bohr. In Search of "Forever," Continued Transistor Scaling One New Material at a Time. *IEEE Transactions on Semiconductor Manufacturing*, 18(1):26 – 36, February 2005.

[TLC89] C. Toumazou, F.J. Lidgey, and P.Y.K. Cheung. Current-Mode Analogue Signal Processing Circuits-a Review of Recent Developments. *IEEE International Symposium on Circuits and Systems*, 3:1572 – 1575, May 1989.

[TMG02] Chris Toumazou, George Moschytz, and Barrie Gilbert, editors. *Trade-Offs in Analog Circuit Design*. Kluwer Academic Publishers, 2002.

[TS02] Ulrich Tieze and Christoph Schenk. *Halbleiter Schaltungstechnik*. Springer, 2002.

[Tsi94] Yannis Tsividis. Integrated Continuous-Time Filter Design - An Overview. *IEEE Journal of Solid-State Circuits*, 29(3):166 – 176, Mar 1994.

[Tsi01] Yannis Tsividis. Continuous-Time Filters in Telecommunications Chips. *IEEE Communications Magazine*, 39(4):132 – 137, Apr 2001.

[Tut99] Walter H.W. Tuttlebee. Software-Defined Radio: Facets of a Developing Technology. *IEEE Personal Communications*, 6(2):38 – 44, April 1999.

[UDK+10] Heimo Uhrmann, Lukas Dörrer, Franz Kuttner, Kurt Schweiger, and Horst Zimmermann. A Mixer-Filter Combination of a Direct Conversion Receiver for DVB-H Applications in 65 nm CMOS. *Proc. Design and Diagnostics of Electronic Circuits and Systems*, pages 209 – 212, April 2010.

[UGZ08] Heimo Uhrmann, Wolfgang Gaberl, and Horst Zimmermann. A Low-Noise Current Preamplifier in 120 nm CMOS Technology. *Advances in Radio Science*, pages 213 – 217, 2008.

[USSZ09] Heimo Uhrmann, Franz Schlögl, Kurt Schweiger, and Horst Zimmermann. A 1 GHz-GBW Operational Amplifier for DVB-H Receivers in 65 nm CMOS. *Proc. International Symposium on Design and Diagnostics of Electronic Circuits and Systems*, pages 182 – 185, April 2009.

[UZ07a] Heimo Uhrmann and Horst Zimmermann. A 3rd-Order Current-Mode Continuous-Time Filter in 65 nm CMOS. *Proc. Norchip*, pages 1 – 4, November 2007.

[UZ07b] Heimo Uhrmann and Horst Zimmermann. A Low-Noise Current Preamplifier in 120 nm CMOS Technology. *Proc. Mixed Design of Integrated Circuits and Systems*, pages 199 – 202, June 2007.

[UZ08a] Heimo Uhrmann and Horst Zimmermann. A 1V Current-Mode Filter in 65nm CMOS Using Capacitance Multiplication. *Proc. International Symposium on System-on-Chip*, pages 1 – 4, November 2008.

[UZ08b] Heimo Uhrmann and Horst Zimmermann. A Chip Area Saving Current-mode Integrator for Low-Pass Filters in Software Defined Radio. *Proc. Austrochip*, pages 25 – 28, 2008.

[UZ08c] Heimo Uhrmann and Horst Zimmermann. A Current-Mode Filter for Wireless Systems in 65 nm CMOS Technology. *Proc. Mixed Design of Integrated Circuits and Systems*, pages 165 – 168, June 2008.

[UZ09a] Heimo Uhrmann and Horst Zimmermann. A Current-Mode Continuous-Time Filter for Software Defined Radio Solutions. *Analog Integrated Circuits and Signal Processing*, 58:27 – 33, 2009.

[UZ09b] Heimo Uhrmann and Horst Zimmermann. A Fully Differential Operational Amplifier for a Low-pass Filter in a DVB-H Receiver. *Proc. Mixed Design of Integrated Circuits and Systems*, pages 197 – 200, June 2009.

[UZ10] Heimo Uhrmann and Horst Zimmermann. A First-Order Operational Amplifier RC Low-Pass Filter for DVB-H. *Proc. Austrochip*, pages 182 – 185, October 2010.

[VGS01] Volney C. Vincence, Carlos Galup-Montoro, and Marcio C. Schneider. Low-Voltage Class AB Operational Amplifier. *Symposium on Integrated Circuits and Systems Design*, pages 207 – 211, 2001.

[Vit90] Eric A. Vittoz. Future of Analog in the VLSI Environment. *IEEE International Symposium on Circuits and Systems*, 2:1372 – 1375, May 1990.

[vLTH+00] R. van Langevelde, L.F. Tiemeijer, R.J. Havens, M.J. Knitel, R.F.M. Roes, P.H. Woerlee, and D.B.M. Klaassen. RF-Distortion in Deep-Submicron CMOS Technologies. *International Electron Devices Meeting*, pages 807 – 810, December 2000.

[WP97] H. Wong and M.C. Poon. Approximation of the Length of Velocity Saturation Region in MOSFET's. *IEEE Transactions on Electron Devices*, 44(11):2033 – 2036, November 1997.

[WRZW09] Zhao Wu, Fu Rui, Zhang Zhi-Yong, and Cheng Wei-Dong. Design of a Rail-to-Rail Constant-gm CMOS Operational Amplifier. *World Congress on Computer Science and Information Engineering*, 6:198 – 201, April 2009.

[YE03] Uroschanit Yodprasit and Christian C. Enz. A 1.5 V 75 dB Dynamic Range Third-Order Gm-C Filter Integrated in a 0.18 μm Standard Digital CMOS Process. *IEEE Journal of Solid-State Circuits*, 38(7):1189 – 1197, July 2003.

[YHCH03] Z. Yang, T. Hinck, H.I. Cohen, and A.E. Hubbard. Current-Mode Integrator for Voltage-Controllable Low Frequency Continuous-Time Filters. *Electronics Letters*, 39(12):883 – 884, June 2003.

[YKZ08a] Weixun Yan, Robert Kolm, and Horst Zimmermann. A Low-Voltage Low-Power Fully Differential Rail-to-Rail Input/Output Opamp in 65 nm

CMOS. *IEEE International Symposium on Circuits and Systems*, pages 2274 – 2277, May 2008.

[YKZ08b] Weixun Yan, Robert Kolm, and Horst Zimmermann. Efficient Four-Stage Frequency Compensation for Low-Voltage Amplifiers. *IEEE International Symposium on Circuits and Systems*, pages 2278 – 2281, May 2008.

[Yua06a] Fei Yuan. Low-Voltage CMOS Current-Mode Circuits: Topology and Characteristics. *IEE Proceedings - Circuits, Devices and Systems*, 153(3):219 – 230, June 2006.

[Yua06b] Fei Yuan. Low-Voltage CMOS Current-Mode Preamplifier: Analysis and Design. *IEEE Transactions on Circuits and Systems I: Regular Papers*, 53(1):26 – 39, January 2006.

[YZ06] Weixun Yan and Horst Zimmermann. A 120 nm CMOS Fully Differential Rail-to-Rail I/O Opamp with Highly Constant Signal Behavior. *IEEE International SOC Conference*, pages 3 – 6, September 2006.

[YZ07] Weixun Yan and Horst Zimmermann. Speed Enhancement and Linearity Analysis for a Rail-to-Rail Input Opamp in 120 nm CMOS. *Proc. Mixed Design of Integrated Circuits and Systems*, pages 344 – 348, June 2007.

[ZA96] Rajesh H. Zele and David J. Allstot. Low-Power CMOS Continuous-Time Filters. *IEEE Journal of Solid-State Circuits*, 31(2):157 – 168, February 1996.

[ZLA93] Rajesh H. Zele, Sang-Soo Lee, and David J. Allstot. A 3V-125MHz CMOS Continuous-Time Filter. *IEEE International Symposium on Circuits and Systems*, 2:1164 – 1167, May 1993.

Curriculum Vitae

Personal details

Name	Dipl.Ing. Heimo Uhrmann
Date of Birth	2nd January, 1978
Place of Birth	St. Johann/T - Austria
Nationality	Austrian
Martial status	Married

Address information	Landstraße 3
	A-2003 Leitzersdorf
Mail address	heimo.uhrmann@tuwien.ac.at

Education

BRG Schützengasse 31, 1030 Wien 1988 – 1992

BRG Wiedner Gürtel 68, 1040 Wien 1992 – 1997

Studies

Electrical Engineering

at Vienna University of Technology 1998-2005

Graduate degree with excellent success 11/2005

Diploma thesis: "Unterbrechungsfreie Rekonfiguration von IEC 61499-basierten Abtastregelkreisen im laufenden Betrieb"

Supervisor: Univ.Prof. DI Dr.techn. Bernard Favre-Bulle

Military service

Jägerregiment 3 / Korneuburg

Sept 1997 – May 1998

since 12/2005 Doctoral study at the Institute of Electrodynamics, Microwave and Circuit Engineering

List of Own Publications

Heimo Uhrmann and Horst Zimmermann. A Low-Noise Current Preamplifier in 120 nm CMOS Technology. *Proc. Mixed Design of Integrated Circuits and Systems*, pages 199 – 202, June 2007

Heimo Uhrmann, Wolfgang Gaberl, and Horst Zimmermann. A Low-Noise Current Preamplifier in 120 nm CMOS Technology. *Advances in Radio Science*, pages 213 – 217, 2008

Heimo Uhrmann and Horst Zimmermann. A Current-Mode Continuous-Time Filter for Software Defined Radio Solutions. *Analog Integrated Circuits and Signal Processing*, 58:27 – 33, 2009

Heimo Uhrmann and Horst Zimmermann. A 3rd-Order Current-Mode Continuous-Time Filter in 65 nm CMOS. *Proc. Norchip*, pages 1 – 4, November 2007

Heimo Uhrmann and Horst Zimmermann. A Current-Mode Filter for Wireless Systems in 65 nm CMOS Technology. *Proc. Mixed Design of Integrated Circuits and Systems*, pages 165 – 168, June 2008

Heimo Uhrmann and Horst Zimmermann. A Chip Area Saving Current-mode Integrator for Low-Pass Filters in Software Defined Radio. *Proc. Austrochip*, pages 25 – 28, 2008

Heimo Uhrmann and Horst Zimmermann. A 1V Current-Mode Filter in 65nm CMOS Using Capacitance Multiplication. *Proc. International Symposium on System-on-Chip*, pages 1 – 4, November 2008

Heimo Uhrmann, Franz Schlögl, Kurt Schweiger, and Horst Zimmermann. A 1 GHz-GBW Operational Amplifier for DVB-H Receivers in 65 nm CMOS. *Proc. International Symposium on Design and Diagnostics of Electronic Circuits and Systems*, pages 182 – 185, April 2009

Heimo Uhrmann and Horst Zimmermann. A First-Order Operational Amplifier RC Low-Pass Filter for DVB-H. *Proc. Austrochip*, pages 182 – 185, October 2010

Heimo Uhrmann and Horst Zimmermann. A Fully Differential Operational Amplifier for a Low-pass Filter in a DVB-H Receiver. *Proc. Mixed Design of Integrated Circuits and Systems*, pages 197 – 200, June 2009

Heimo Uhrmann, Lukas Dörrer, Franz Kuttner, Kurt Schweiger, and Horst Zimmermann. A Mixer-Filter Combination of a Direct Conversion Receiver for DVB-H Applications in 65 nm CMOS. *Proc. Design and Diagnostics of Electronic Circuits and Systems*, pages 209 – 212, April 2010

Thomas Strasser, Ingomar Müller, Christoph Sünder, Oliver Hummer, and Heimo Uhrmann. Modeling of Reconfiguration Control Applications Based on the IEC 61499 Reference Model for Industrial Process Measurement and Control Systems. *Distributed Intelligent Systems: Collective Intelligence and Its Applications*, pages 127 – 132, June 2006

Kurt Schweiger, Heimo Uhrmann, and Horst Zimmermann. Low-Voltage Low-Power Double Bulk Mixer for Direct Conversion Receiver in 65 nm CMOS. *Proc. Design and Diagnostics of Electronic Circuits and Systems*, pages 74 – 77, April 2009